REPORT NUMBER 151
SEPTEMBER 1964

ESTIMATED DYNAMIC STAB ICS

REPORT NUMBER 151
SEPTEMBER 1964

ESTIMATED DYNAMIC STABILITY CHARACTERISTICS

[illegible] FLIGHT RESEARCH AIRCRAFT PROGRAM

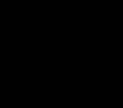

[illegible] ELECTRIC

DDC AVAILABILITY NOTICES

1. Distribution of thid document is unlimited.

2. This document is subject to special report controls and each transmittal to foreign governments or foreign nationals may be made only with prior approval of US Army Aviation Materiel Laboratories, Fort Eustis, Virginia 23604.

3. In addition to security requirements which must be met, this document is subject to special export controls and each transmittal to foreign governments or foreign nationals may be made only with prior approval of USAAVLABS, Fort Eustis, Virginia 23604.

4. Each transmittal of this document outside the agencies of the US Government must have prior approval of US Army Aviation Materiel Laboratories, Fort Eustis, Virginia 23604.

5. In addition to security requirements which apply to this document and must be met, each transmittal outside the agencies of the US Government must have prior approval of US Army Aviation Materiel Laboratories, Fort Eustis, Virginia.

6. Each transmittal of this document outside the Department of Defense must have prior approval of US Army Aviation Materiel Laboratories, Fort Eustis, Va.

7. In addition to security requirements which apply to this document and must be met, each transmittal outisde the Department of Defense must have prior approval of US Army Aviation Materiel Laboratories, Fort Eustis, Virginia 23604.

8. This document may be further distributed by any holder only with specific prior approval of US Army Aviation Materiel Laboratories, Fort Eustis, Va. 23604.

9. In addition to security requirements which apply to this document and must be met, it may be further distributed by the holder only with specific prior approval of US Army Aviation Materiel Laboratories, Fort Eustis, Virginia 23604.

DISCLAIMER

10. The findings in this report are not to be construed as an official Department of the Army position unless so designated by other authorized documents.

11. When Government drawings, specifications, or other data are used for any purpose other than in connection with a definitely related Government procurement operation, the United States Government thereby incurs no responsibility nor any obligation whatsoever; and the fact that the Government may have formulated, furnished, or in any way supplied the said drawings, specifications, or other data is not to be regarded by implication or otherwise as in any manner licensing the holder or any other person or corporation, or conveying any rights or permission, to manufacture, use, or sell any patented invention that may in any way be related thereto.

12. Trade names cited in this report do not constitute an official endorsement or approval of the use of such commercial hardware of software.

DISPOSITION INSTRUCTIONS

13. Destroy this report when no longer needed. Do not return it to originator.

14. When this report is no longer needed, Department of the Army organizations will destroy it in accordance with the procedures given in AR 380-5. Navy and Air Force elements will destroy it in accordance with applicable directions. Department of Defense contractors will destroy the report according to the requirement of Section 14 of the Industrial Security Manual for Safeguarding Classified Information. All others will return the report to US Army Aviation Materiel Laboratories, Fort Eustis, Virginia 23604.

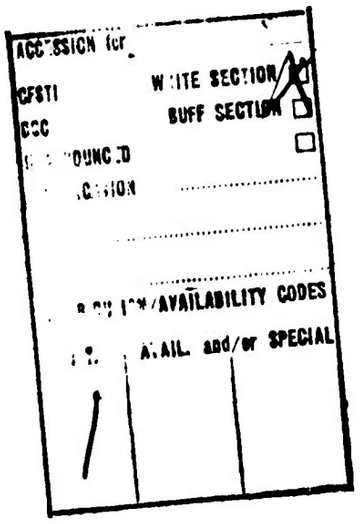

REPORT NUMBER 151

Estimated Dynamic Stability Characteristics

XV-5A Lift Fan

Flight Research Aircraft Program

September 1964

VB

Advanced Engine and Technology Department
General Electric Company
Cincinnati, Ohio 45215

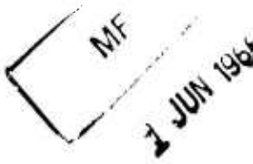

CONTENTS

LIST OF FIGURES

LIST OF FIGURES (Continued)

LIST OF FIGURES (Continued)

LIST OF FIGURES (Continued)

LIST OF TABLES

1.0 SUMMARY

This report presents the dynamic stability characteristics of the U. S. Army XV-5A lift fan research aircraft based on theoretical and empirical estimates of dynamic stability derivatives and static aerodynamic characteristics derived from scale model wind tunnel tests. Except for a presentation of the lift fan natural damping contributions to flight in the lift fan mode, the report is restricted to analysis of conventional flight characteristics.

Investigation shows that the dynamic stability characteristics of the aircraft are satisfactory for the research objectives within the examined flight envelope.

Aerodynamic stability data are presented for the entire structural flight envelope of the aircraft, (to Mach 0.9), however, conventional flight dynamic stability investigations have been limited to Mach 0.8. This has been selected as the maximum usable flight Mach number for the aircraft in the present configuration. Small scale wind tunnel test results show that large reductions in control effectiveness, and decreases in static stability occur at higher speeds. Test results also show a gradual deterioration in longitudinal static stability above Mach 0.7 at the higher lift coefficients corresponding to high normal load factors, due to a loss in tail effectiveness. Near Mach 0.8 at the higher lift coefficients, an abrupt loss in static stability is shown, indicating a pitch-up tendency. Therefore, caution should be exercised during initial flight testing above Mach 0.7, particularly at the higher altitudes.

Longitudinal dynamic response to control input may become sluggish at high altitudes, or at low speeds, due to a low natural frequency of the short period mode. The short period natural frequency at high altitude, or low speed, does not meet the requirements of the XV-5A Flying Qualities Specification. However, the short period mode is well damped and no unusual flight characteristics are anticipated which might affect the utility of the aircraft for its intended use.

Freeing the controls reduces to a slight degree the speed-altitude range, wherein the short period requirements of the Flying Qualities

Specification are satisfied, because of a small reduction in natural frequency and increase in damping ratio. In the conventional flight landing configuration, the longitudinal short period requirements of the Flying Qualities Specification are satisfied at all flight conditions. Longitudinal static stability in the landing configuration becomes marginal at high angles of attack. The flight characteristics, however, have been evaluated, using the XV-5A flight simulator and are estimated to be satisfactory, primarily due to a high level of pitch damping.

The estimated characteristics of the conventional flight, longitudinal phugoid mode satisfy the damping requirements of the Flying Qualities Specification for all flight conditions investigated in both the clean configuration, and landing configuration, including the effects of aeroelasticity and free controls.

The dutch roll damping and roll/slip ratio in the clean airplane configuration meet the requirements of the Flying Qualities Specification at all speeds less than 0.8 Mach number below 25,000 feet altitude. The dutch roll oscillation becomes more pronounced at altitudes above 25,000 feet at speeds less than 0.7 Mach number, but is not expected to be objectionable below 35,000 feet.

The dutch roll characteristics in the conventional flight landing configuration meet the requirements of the Flying Qualities Specification at all speeds above about 120 knots at sea level. The dutch roll damping is estimated to be only slightly less than the requirement between 95 and 120 knots.

The characteristics of the conventional flight spiral mode are considered satisfactory for all flight conditions investigated.

Pitch-yaw aerodynamic coupling is calculated to produce excessive vertical and lateral load factors during rapid, 360 degree rolling maneuvers developed at speeds above Mach 0.6, with more than one-half of full lateral control displacement and rudder and elevator fixed. The effects of pitch-yaw coupling at speeds below Mach 0.6 have not been determined at the present time.

Procedures for estimating the contributions of the wing fans to vertical lift damping, roll and yaw damping, and the contributions of the nose fan to pitch damping, are illustrated and checked with theory, wherever possible. These results indicate that the fan contributions are small, even at low speeds, compared with the damping attributed to the normal aircraft surfaces.

2.0 INTRODUCTION

This report presents an estimate of the dynamic stability characteristics of the U.S. Army XV-5A Lift Fan Research Aircraft. The XV-5A was designed and built by the Ryan Aeronautical Company for flight evaluation of the General Electric X353-5 Lift Fan Propulsion System. It is a V/STOL aircraft capable of conventional operation at high subsonic speeds.

The conventional flight configuration airframe and control surface dynamic stability derivatives were derived by theoretical and empirical methods, and are presented herein with the source references from which these methods were obtained. The effects of aeroelasticity on the stability derivatives are presented for several selected flight conditions representative of the areas of greatest aeroelastic effects.

The longitudinal and lateral-directional dynamic response characteristics of the aircraft were derived for trimmed, level flight conditions, for small perturbations. The effects of aeroelasticity and free controls on the dynamic stability characteristics of the conventional flight configuration are presented along with estimates for the rigid airframe.

The fan damping characteristics in the lift fan flight mode are also included herein, and were obtained using equations derived from application of theory and from wind tunnel test data. All investigations of the aircraft dynamic flight characteristics in the lift fan flight mode were performed on the Ryan Flight Simulator. The results of this fan flight simulation work will be given in subsequent flying qualities and flight simulation reports now in preparation.

3.0 CONVENTIONAL FLIGHT CHARACTERISTICS

The airframe and control surface dynamic stability derivatives presented in this section were estimated by standard theoretical and empirical methods contained in reference literature. The methods employed in evaluating many of the dynamic derivatives required the use of static aerodynamic data such as wing lift curve slope, etc. In those cases, experimental data derived from static wind tunnel tests, presented in Reference 1, were used.

The rigid airframe dynamic stability derivatives have been evaluated for the complete flight envelopes of the airplane in the clean configuration (flaps, gear retracted) and in the landing configuration. The effects of elasticity of structure on the dynamic stability derivatives are presented for several selected flight conditions.

Calculation of the dynamic response characteristics of the aircraft was performed using small perturbation analysis procedures, and the calculations were made for trimmed, level flight conditions. In addition, the usual assumption was made that the longitudinal and lateral-directional modes are uncoupled. Dynamic stability investigations were accomplished with the use of a digital computer program which solved for the roots of the characteristic equation derived from longitudinal and lateral-directional equations of motion. In either solution, three degrees of freedom were involved with controls fixed. The equations of motion used for the controls fixed case are derived in Reference 4. Analysis of the controls free cases required additional equations to express the control surface motion. The complete equations of motion for controls fixed and free are presented in the Appendix.

Dynamic stability investigations have effectively covered the speed-altitude envelope of the airplane. A speed of Mach 0.8 was chosen as a maximum for conventional flight studies. Mach 0.8 was selected since aerodynamic characteristics indicated that the maximum usable Mach number for the original configuration would not significantly exceed this value. Some of the effects include:

a) Canopy and wing ($\alpha = 0$) critical Mach number of approximately 0.73 resulting in reduced engine performance and possible aerodynamic buffeting,

b) Reduced longitudinal stability and possible pitch-up above Mach 0.8 at moderately low angles of attack due to loss in tail effectiveness,

c) Large reductions in lateral-directional stability between Mach 0.8 and 0.9,

d) Large reductions in control effectiveness for all axes between Mach 0.8 and 0.9.

No flying qualities restrictions are foreseen in demonstrating the XV-5A maximum speed objective of 450 knots (Mach 0.66) at hot day, 2,500 feet altitude condition.

The results of an interim flight simulation investigation of the XV-5A in conventional flight are presented in Reference 2.

3.1 LONGITUDINAL DYNAMIC STABILITY DERIVATIVES

The longitudinal dynamic stability derivatives for a rigid airframe are presented in Figures 3.1 through 3.12 for the conventional flight configuration. In general, the derivatives for the complete configuration were determined by simple addition of the individual contributions of the M-T and the tail. Since the dynamic stability derivatives are functions of the aircraft static aerodynamic and geometric characteristics, the compressibility effects for the airplane in its clean configuration ($\delta_f = 0°$) were determined by using wind tunnel test derived static data at the appropriate Mach number from Reference 1.

The M-T contribution to the pitching velocity derivatives C_{L_q} and C_{m_q} was calculated by the method presented in Reference 3. However, the equation presented in Reference 3 for C_{m_q} was modified slightly in order to reflect experimental values of the M-T lift curve slope, C_{L_α}. This was done by replacing those terms which represent the theoretical lift curve slope in Reference 3 by the test based values from Reference 1. The final modified equation thus used to calculate C_{m_q} for flaps up or down was as follows:

$$C_{m_{q_{M-T}}} = -C_{L_{\alpha_{M-T}}} \left[\frac{1}{2}\left(\frac{\chi_{ac}}{\bar{c}}\right) + 2\left(\frac{\chi_{ac}}{\bar{c}}\right)^2 + \frac{1}{8}\left(\frac{A + 2\cos\Lambda}{A}\right) + \frac{A^2}{24}\left(\frac{A + 2\cos\Lambda}{A + 6\cos\Lambda}\right)\tan^2\Lambda \right]$$

The variation of axial force with pitching velocity was assumed to be zero.

The vertical acceleration derivatives $C_{L_{\dot{\alpha}}}$ and $C_{m_{\dot{\alpha}}}$ are primarily attributed to the lag in change of downwash at the horizontal tail due to the rate of change of wing angle of attack. Since there is no known reliable method to predict the M-T contribution to these derivatives, only the downwash lag effect was considered.

The variation of axial force with vertical acceleration was assumed to be zero.

The contribution of the horizontal tail to the longitudinal dynamic derivatives, which is discussed in detail in Reference 4, was calculated from the following equations:

$$C_{L_{q_t}} = 2C_{L_{\alpha_t}} \eta_t \frac{S_t}{S} \frac{\ell_t}{\bar{c}}$$

$$C_{m_{q_t}} = -C_{L_{q_t}} \frac{\ell_t}{\bar{c}}$$

$$C_{L_{\dot{\alpha}_t}} = 2C_{L_{\alpha_t}} \eta_t \frac{S_t}{S} \frac{\ell_t}{\bar{c}} \frac{\partial \epsilon}{\partial \alpha}$$

$$C_{m_{\dot{\alpha}_t}} = -C_{L_{\dot{\alpha}_t}} \frac{\ell_t}{\bar{c}}$$

The low speed, flaps down derivatives for the complete model are shown as a function of angle of attack up to the stall. Ordinarily, these derivatives do not vary below the stall angle of attack for an aircraft with linear static aerodynamic characteristics. The variation with α that is shown arises from the nonlinear variation of horizontal tail dynamic pressure ratio (η_t) with α, nonlinearities in C_{L_α} and C_{m_α} of the M-T, highly nonlinear variation of downwash with angle of attack and variation of the horizontal tail moment arm with α due to its high location. The methods available from reference literature for evaluating the M-T dynamic

derivatives are generally limited to angles of attack well within the linear lift range. The data presented herein for angles of attack above 12° to 13° are therefore questionable and are presented only to indicate a probable trend.

The flaps up, clean airplane derivatives are presented as functions of Mach number and independent of angle of attack. This is possible because the clean airplane static characteristics do not exhibit the rather large nonlinearities in η_t, downwash, etc., as is the case when the flaps are down. However, as is true for the flaps down configuration, the clean airplane dynamic derivatives are not valid at high angles of attack approaching the stall.

The remaining airframe dynamic derivatives are those which are velocity dependent, and the drag terms. These derivatives were not calculated explicitly since they were computed for a given trim flight condition by digital computer which was used to solve the equations of motion. The computer program is discussed elsewhere in this section. Neglecting the drag due to elevator deflection, the remaining complete model derivatives were computer calculated from the following equations:

$$C_{L_{u_{CM}}} = \frac{M}{2}\left[\frac{\partial C_{L_{\alpha_{CM}}}}{\partial M}\left(\alpha_{TR} - \alpha_{OL_{CM}}\right) - C_{L_{\alpha_{CM}}}\left(\frac{\partial \alpha_{OL_{CM}}}{\partial M}\right) + \frac{\partial C_{L_{\delta_e}}}{\partial M}\left(\delta_{e_{TR}}\right)\right]$$

$$C_{m_{u_{CM}}} = \frac{M}{2}\left[\frac{\partial C_{m_{O\alpha_{CM}}}}{\partial M} + \frac{\partial C_{m_{\alpha_{CM}}}}{\partial M}\left(\alpha_{TR}\right) + \frac{\partial C_{m_{\delta_e}}}{\partial M}\left(\delta_{e_{TR}}\right)\right]$$

$$C_{D_{u_{CM}}} = C_{L_{u_{CM}}}\left(\frac{\partial C_D}{\partial C_L}\right)_{CM} + \frac{M}{2}\left(\frac{\partial C_D}{\partial M}\right)_{CM}$$

$$C_{D_{\alpha_{CM}}} = C_{L_{\alpha_{CM}}}\left(\frac{\partial C_D}{\partial C_L}\right)_{CM}$$

As shown by the above equations, the velocity dependent derivatives arise from compressibility effects and are therefore zero for the flaps down configuration. The values of the above derivatives calculated by the digital computer program in the course of dynamic stability investigations are presented in Figures 3.9 through 3.11.

The conventional turbojet thrust characteristics are presented in Reference 5. For purposes of dynamic stability analysis, the thrust derivative, $\partial T/\partial u$, was taken as the slope of installed net thrust versus free-stream velocity at 100% turbojet rpm. The data used are presented in Figure 3.12.

The effects on the stability derivatives of elastic deformation of the airframe due to aerodynamic loads were derived during the airframe loads analysis summary in Reference 10 and only pertinent results are presented in this report.

The effect of aeroelasticity is expressed in terms of the ratio of the elastic airframe derivative to the rigid airframe value as illustrated by the following example:

$$\text{elastic/rigid ratio} = \frac{{}^{*}C_{L_\alpha}}{C_{L_\alpha}}$$

The asterisk denotes the elasticized value.

The elastic/rigid ratios, or more simply the elastic ratios, were obtained from Reference 10 for Mach numbers of 0.3, 0.6 and 0.8 at both sea level and 20,000 foot standard day altitudes. Due to the high dynamic pressures represented, these include the most severe conditions to be encountered from the standpoint of aeroelastic effects. The M-T elastic ratios were based on an elastic wing and rigid body while the empennage elastic ratios were based on an elastic empennage and elastic body. The elastic ratios used in this report are presented in Tables 3.1 and 3.2.

The following expressions illustrate the use of the elastic ratios to calculate the elastic airframe derivatives:

$${}^{*}\alpha_{OL_{M-T}} = \alpha_{OL_{M-T}} \left[\frac{{}^{*}\alpha_{OL}}{\alpha_{OL}} \right]_{M-T}$$

$$*C_{m_{OL_{M-T}}} = C_{m_{OL_{M-T}}} \left[\frac{*C_{m_{OL}}}{C_{m_{OL}}} \right]_{M-T}$$

$$*C_{L_{\alpha_{M-T}}} = C_{L_{\alpha_{M-T}}} \left[\frac{*C_{L_{\alpha}}}{C_{L_{\alpha}}} \right]_{M-T}$$

$$*C_{m_{\alpha_{M-T}}} = C_{m_{\alpha_{M-T}}} \left[\frac{*C_{m_{\alpha}}}{C_{m_{\alpha}}} \right]_{M-T}$$

$$*C_{L_{\alpha_t}} = C_{L_{\alpha_t}} \left[\frac{*C_{L_{\alpha}}}{C_{L_{\alpha}}} \right]_t$$

$$\frac{*x_{ac}}{\bar{c}} = - \left[\frac{*C_{m_{\alpha}}}{*C_{L_{\alpha}}} \right]_{M-T}$$

$$*C_{L_{\delta_e}} = C_{L_{\delta_e}} \left[\frac{*C_{L_{\delta_e}}}{C_{L_{\delta_e}}} \right]$$

$$*C_{m_{\delta_e}} = C_{m_{\delta_e}} \left[\frac{*C_{L_{\delta_e}}}{C_{L_{\delta_e}}} \right]$$

$$*C_{L_{\alpha_{CM}}} = *C_{L_{\alpha_{M-T}}} + *C_{L_{\alpha_t}} \eta_t \frac{S_t}{S} \left(1 - \frac{\partial \epsilon}{\partial \alpha} \right)$$

$$*C_{m_{\alpha_{CM}}} = *C_{m_{\alpha_{M-T}}} - *C_{L_{\alpha_t}} \eta_t \frac{S_t}{S} \frac{\ell_t}{\bar{c}} \left(1 - \frac{\partial \epsilon}{\partial \alpha}\right)$$

The elasticized longitudinal dynamic derivatives were determined by the same methods as the rigid airframe derivatives, but used the elastic static aerodynamic terms as obtained from the above expressions. The variation of airplane drag with lift and Mach number was assumed to be unaffected by aeroelastic considerations.

The elastic airframe static and dynamic stability derivatives were evaluated for Mach numbers of 0.6 and 0.8 at sea level and 20,000 feet altitudes. Flight conditions at lower dynamic pressures than these conditions will not be greatly affected by aeroelastic considerations. The values of the hand calculated derivatives and the velocity dependent derivatives calculated by the digital computer dynamic stability program are presented in Table 3.3, for the most aft cg at F.S. 246.0.

The greatest effect of aeroelasticity on the complete model derivatives is the reduction in the static stability margin dC_m/dC_L. This reduction is due to the large reduction in horizontal tail effectiveness since the M-T derivatives are not affected significantly by aeroelastic effects as evidenced by the elastic ratios in Table 3.3. At a nominal flight condition (Mach 0.8 at 20,000 feet) the static margin is reduced from about -0.06 to -0.035 for the most aft cg (F.S. 246.0). The static margin at the most forward cg location (F.S. 240.0) will then be about -0.085 including aeroelastic effects. This total range of static margin is considered good for normal flight conditions from the standpoint of frequency of the longitudinal, short period mode and gradient of stick force vs. normal load factor. At the most severe flight condition, (Mach 0.8 at sea level), the static margin at the most aft cg remains stable, but is reduced from about -0.06 to -0.01 due to aeroelastic effects. This is an extreme flight condition for the XV-5A and one not likely to be encountered, because it is in excess of the level flight speed capability at sea level.

The second most significant effect of aeroelastic considerations on the longitudinal stability derivatives is on pitch damping. The derivatives C_{m_q} and $C_{m_{\dot{\alpha}}}$ are both reduced approximately 25% at the condition of Mach 0.8 at sea level and about 13% at the nominal condition of Mach 0.8 at 20,000 feet. Inasmuch as the rigid airframe pitch damping is quite high, this reduction should not result in any serious deterioration in longitudinal stability.

3.2 LATERAL-DIRECTIONAL DYNAMIC STABILITY DERIVATIVES

The rigid airframe lateral-directional dynamic stability derivatives are presented in Figures 3.13 through 3.28 for the conventional flight configuration. These derivatives were estimated by standard theoretical and empirical methods from various references. Experimental static aerodynamic data from Reference 1 were used, where applicable, in the calculation of the dynamic derivatives.

The M-T contributions to the yawing velocity derivatives C_{n_r} and C_{ℓ_r} were estimated from Reference 6 for both the flaps up and flaps down configurations. Compressibility effects on C_{ℓ_r} were estimated from Reference 6 and from References 6 and 7 for C_{n_r}. The M-T contribution to C_{y_r} was estimated from the potential flow equation presented in Reference 3. C_{y_r} was determined to be negligible for small lift coefficients and the method is not valid for large lift coefficients. In addition, no information was available to predict compressibility effects on C_{y_r} of the M-T. Therefore, the M-T contribution was neglected.

The M-T contribution to the rolling velocity derivatives C_{y_p} and C_{ℓ_p} was estimated from Reference 6, including compressibility effects. The derivative C_{n_p} was estimated by the empirical method presented in Reference 8 for the low speed range. The "tip suction" effect discussed in Reference 8 was neglected, as recommended by that report. The method appeared to correlate quite well with dynamic test data shown in Reference 8, and permits a reasonable means of estimating C_{n_p} up to high angles of attack. The method is based primarily on the use of experimental lift and drag characteristics which were available in this case.

The only significant contribution of the horizontal tail to the lateral-directional dynamic derivatives is to the damping in roll, C_{ℓ_p}. This contribution was estimated in the same manner as the M-T contribution assuming an average $\eta_t = 0.90$. The horizontal tail term contributes approximately 3% of the complete model roll damping.

The contribution of the vertical tail to the lateral-directional dynamic derivatives was estimated from the following empirical relationships from Reference 12:

$$C_{y_{r_v}} = 2\,C_{n_\beta}$$

$$C_{y_{p_v}} = 2\,C_{\ell_{\beta_v}} + C_{y_{\beta_v}} \frac{\partial\sigma}{\partial\left(\frac{pb}{2V}\right)}$$

$$C_{n_{r_v}} = \frac{2C^{2}_{n_{\beta_v}}}{C_{y_{\beta_v}}}$$

$$C_{n_{p_v}} = \frac{2C_{n_{\beta_v}} C_{\ell_{\beta_v}}}{C_{y_{\beta_v}}} + C_{n_{\beta_v}} \frac{\partial\sigma}{\partial\left(\frac{pb}{2V}\right)}$$

$$C_{\ell_{r_v}} = \frac{2C_{n_{\beta_v}} C_{\ell_{\beta_v}}}{C_{y_{\beta_v}}}$$

$$C_{\ell_{p_v}} = \frac{2C^{2}_{\ell_{\beta_v}}}{C_{y_{\beta_v}}} + C_{\ell_{\beta_v}} \frac{\partial\sigma}{\partial\left(\frac{pb}{2V}\right)}$$

The vertical tail static derivatives used in the above equations were obtained from Reference 1 and were based on XV-5A scale model wind tunnel tests. The vertical tail sidewash due to rolling velocity was estimated from Reference 7 for flaps up and flaps down and is shown in Figure 3.25 herein. Since no compressibility effects on that term could be determined, the values shown in Figure 3.25 for flaps 0° were applied throughout the Mach number range.

The sidewash due to yawing velocity was omitted from the vertical tail yawing derivatives because virtually no information on this term was available in reference literature.

The effect on the lateral-directional derivatives of elasticity of structure was applied in much the same manner as for the longitudinal case discussed in Section 3.1. The elastic/rigid ratios were obtained from Reference 10 and are shown in Tables 3.1 and 3.2 herein. The only elasticized M-T contribution available was the damping in roll, C_{ℓ_p} and therefore all other M-T contributions to the lateral-directional derivatives were assumed independent of aeroelastic effects.

The following expression illustrates the method of calculating the elastic derivatives from the rigid airframe derivatives and elastic ratios.

$$*C_{\ell_{p_{M-T}}} = C_{\ell_{p_{M-T}}} \left[\frac{*C_{\ell_p}}{C_{\ell_p}} \right]_{M-T}$$

Where the term above in brackets is the elastic ratio shown in Tables 3.1 and 3.2.

Based on the equations presented previously, which were used to calculate the contribution of the vertical tail to the rigid airframe derivatives, the elasticized vertical tail contributions to the derivatives C_{y_β}, C_{n_β}, C_{ℓ_β}, C_{y_r}, C_{n_r}, C_{ℓ_r} and C_{ℓ_p} were obtained by multiplying the rigid airframe vertical tail contribution by the vertical tail elastic ratio $*C_{y_\beta}/C_{y_\beta}$ from Table 3.2. The vertical tail contribution to $*C_{y_p}$ and $*C_{n_p}$ were obtained from their respective elastic ratios shown in Table 3.2 which are slightly different than the C_{y_β} ratio. The elastic aileron and rudder effectiveness were calculated from the following expressions.

$$*C_{y_{\delta_r}} = C_{y_{\delta_r}} \left[\frac{*C_{y_{\delta_r}}}{C_{y_{\delta_r}}} \right]$$

$$*C_{n_{\delta_r}} = C_{n_{\delta_r}} \left[\frac{*C_{n_{\delta_r}}}{C_{n_{\delta_r}}} \right]$$

$$*C_{\ell_{\delta_r}} = C_{\ell_{\delta_r}} \left[\frac{*C_{\ell_{\delta_r}}}{C_{\ell_{\delta_r}}} \right]$$

$$*C_{\ell_{\delta_a}} = C_{\ell_{\delta_a}} \left[\frac{*C_{\ell_{\delta_a}}}{C_{\ell_{\delta_a}}} \right]$$

Elastic effects on the sideforce and yawing moment due to aileron deflection were not considered. The complete model elastic lateral-directional derivatives were evaluated for Mach 0.6 and 0.8 at both sea level and 20,000 feet, standard day altitudes. The derivatives are presented in Table 3.4 and are based on the angle of attack for trimmed level flight at the design gross weight of 9200 pounds.

The most significant effect of aeroelasticity on the lateral-directional derivatives is on the directional stability (C_{n_β}) and yaw damping (C_{n_r}). The other derivatives are affected to some degree, but where there is a significant percentage change, the magnitude of the derivative was so small that the change was not very important. For the most severe flight condition (Mach 0.8 at sea level) the complete model C_{n_β} was reduced about 35% and C_{n_r} about 14%. At a more reasonable flight condition at 20,000 feet and Mach 0.8, the respective reduction in C_{n_β} and C_{n_r} was 25% and 11%.

Although the reduction in directional stability and yaw damping due to aeroelastic effects appears to be quite significant in itself, it is shown in Section 3.4.2 that the effect on the over-all lateral-directional dynamic stability is small.

From a controls standpoint, rudder effectiveness $C_{n_{\delta_r}}$ was reduced by 18% and the aileron effectiveness $C_{\ell_{\delta_a}}$ by 27% at the worst aeroelastic

condition. The estimated reduction in aileron effectiveness was allowed for in the design of the lateral control system so as to meet the high speed roll performance requirements. Normally, the requirements placed on the rudder at high speed are small.

3.3 CONTROL SURFACE DYNAMIC DERIVATIVES

The control surface dynamic hinge moment derivatives were estimated as a prerequisite to investigation of control free stability. The equations used to calculate the derivatives for the elevator, rudder and aileron tab were derived from theoretical considerations, with the exception of the control surface rate derivatives which were estimated from Reference 9.

Derivatives are presented for the aileron tab rather than the aileron itself because only the tab is directly subject to external disturbances as the aileron itself is hydraulic powered and can only be disturbed through the aileron tab.

The following equations were used to calculate the elevator derivatives where the static aerodynamic terms were obtained from Reference 1.

$$C_{h_{e_\alpha}} = \left(1 - \frac{\partial \epsilon}{\partial \alpha}\right) C_{h_{e_{\alpha_t}}}$$

$$C_{h_{e_{\dot{\alpha}}}} = 2 \frac{\ell_t}{\bar{c}_e} \cdot \frac{\partial \epsilon}{\partial \alpha} \cdot C_{h_{e_{\alpha_t}}}$$

$$C_{h_{e_q}} = 2 \frac{\ell_t}{\bar{c}_e} C_{h_{e_{\alpha_t}}}$$

$C_{h_{e_{\dot{q}}}}$ = This term arises from elevator mass unbalance about the hinge line. Since the XV-5A elevator is mass balanced this derivative is zero.

$$C_{h_{e_u}} = \frac{1}{a_o}\left[\frac{\partial C_{h_{e_{\delta_e}}}}{\partial M}\left(\delta_{e_{TR}}\right) + \frac{\partial C_{h_{e_\alpha}}}{\partial M}\left(\alpha_{TR}\right)\right]$$

$$C_{h_{e_{\dot{\delta}_e}}} = -\frac{\bar{c}_t}{\bar{c}_e}\left[K_1 + K_2\, C_{L_{\alpha_t}}\right]$$

The constants K_1 and K_2 in the equation for the elevator damping derivative $C_{h_{e_{\dot{\delta}_e}}}$ are presented in Reference 9 as a function of the chordwise hinge position. The values of these constants for the XV-5A are:

$$K_1 = 1.06$$

$$K_2 = 0.06$$

The rudder dynamic derivatives are analogous to the elevator derivatives, and were calculated from the following equations:

$$C_{h_{r_{\dot{\beta}}}} = -\frac{2\ell_v}{\bar{c}_r}\left[\frac{\partial\sigma/\partial\beta}{1 + \partial\sigma/\partial\beta}\right] C_{h_{r_\beta}}$$

$$C_{h_{r_r}} = -\frac{2\ell_v}{\bar{c}_r}\,\frac{C_{h_{r_\beta}}}{1 + \partial\sigma/\partial\beta}$$

$$C_{h_{r_p}} = \frac{C_{h_{r_\beta}}}{1 + \frac{\partial\sigma}{\partial\beta}}\left[\frac{2Z_v}{\bar{c}_r} + \frac{b}{\bar{c}_r}\,\frac{\partial\sigma}{\partial\left(\frac{pb}{2V}\right)}\right]$$

$$C_{h_{r_{\dot{\delta}_r}}} = -\frac{\bar{c}_v}{\bar{c}_r}\left[K_3 - K_4\, C_{y_{\beta_v}}\,\frac{S}{S_v}\right]$$

$C_{h_{r_{\dot{r}}}}$, $C_{h_{r_{\dot{p}}}}$ — These derivatives arise from rudder mass unbalance about the hinge line which does not exist on the XV-5A. Therefore these terms are zero.

The rudder damping derivative $C_{h_{r_{\dot{\delta}_r}}}$ is similar to that for the elevator and likewise the constants K_3 and K_4 were obtained from Reference 9. The values of the rudder constants are:

$$K_3 = 0.75$$

$$K_4 = 0.05$$

All of the rudder static aerodynamic terms are presented in Reference 1 with the exception of $\partial\sigma/\partial\beta$. Since wind tunnel data yields the derivative $C_{h_{r_\beta}}$ and not $C_{h_{r_{\alpha_v}}}$, which is desired, an estimate of the sidewash factor was made for the purpose of evaluating the rudder dynamic derivatives. This was done by obtaining a theoretical estimate of the low speed vertical tail lift curve slope, $C_{L_{\alpha_v}}$, including the horizontal tail end plate effect from Reference 7 and compressibility effects from Reference 6. The vertical tail lift curve slope is shown in Figure 3.26. Utilizing the following definitions, the sidewash term can be calculated:

$$\alpha_v = -\beta - \sigma$$

$$\frac{\partial\sigma}{\partial\beta} = -\left[1 + \frac{C_{y_{\beta_v}}}{C_{L_{\alpha_v}}\left(\frac{S_v}{S}\right)}\right]$$

The sideforce derivative was obtained from Reference 1 which was based on wind tunnel test data. The estimated values of $\partial\sigma/\partial\beta$ are shown in Figures 3.27 and 3.28, and are rather small for the flight conditions for which rudder free stability was investigated (M = 0.6 and 0.8).

The aileron tab derivatives with respect to the tab hinge line were calculated from the following derived equations:

$$C_{h_{t_\beta}} = -2\Gamma\, C_{h_{t_\alpha}}$$

$$C_{h_{t_r}} = 8\frac{y_t}{\bar{c}_t}\, C_{h_{t_\alpha}}$$

$$C_{h_{t_p}} = -4 \frac{y_t}{\bar{c}_t} C_{h_{t_\alpha}}$$

$C_{h_{t_{\dot{\beta}}}}$, $C_{h_{t_{\dot{r}}}}$, $C_{h_{t_{\dot{p}}}}$ } These derivatives arise from mass unbalance about the tab hinge line which is zero for the XV-5A.

$$C_{h_{t_{\dot{\delta}_a}}} = 2 \frac{\chi_t}{\bar{c}_t} C_{h_{t_{\delta_a}}}$$

$$C_{h_{t_{\dot{\delta}_t}}} = -\frac{\bar{c}}{\bar{c}_t} \left[K_5 + K_6 \, C_{L_{\alpha_{M-T}}} \right]$$

The static derivatives, $C_{h_{t_{\delta_t}}}$ and $C_{h_{t_{\delta_a}}}$, were obtained from Reference 1 and $C_{h_{t_\alpha}}$ was estimated by the theoretical methods presented in References 16 and 17. The estimated value of $C_{h_{t_\alpha}}$ was +0.0344 per radian and was assumed invariant with Mach number.

The equation for the tab damping derivative, $C_{h_{t_{\dot{\delta}_t}}}$ was obtained from Reference 9 which gives the following values for the constants K_5 and K_6:

$$K_5 = 0.21$$

$$K_6 = 0.02$$

Compressibility effects on the dynamic hinge moment derivatives of all the control surfaces were accounted for by using the static aerodynamic terms from Reference 1 at the appropriate Mach number.

The investigation of control free stability has been limited to two Mach numbers, and the control surface dynamic derivatives have been evaluated only for those Mach numbers. The values for the rudder, elevator and aileron tab are presented in Table 3.5.

Aeroelastic effects on control surface hinge moments have not been estimated, and therefore, all of the dynamic hinge moment data presented in this report are based on a completely rigid control system.

3.4 DYNAMIC STABILITY INVESTIGATIONS

Investigations of the dynamic stability characteristics of the XV-5A conventional flight configuration were conducted so as to effectively span the speed-altitude envelope of the aircraft, with consideration of requirements for investigations per the XV-5A Flying Qualities Specification. Analysis of the flaps down landing configuration covered the speed range from 1.15 V_S to the flaps down limit speed of 180 knots at sea level. Investigation of the dynamic stability of the clean airplane configuration spanned the speed range from 1.15 V_S (flaps up) to Mach 0.8 at sea level, 20,000 feet and 40,000 feet. All of the results presented in this report were based on the design gross weight of 9200 pounds, most aft cg at F.S. 246.0 and the ARDC standard day atmosphere. The dynamic stability derivatives and aerodynamic data which were used are those contained in this report and in Reference 1. Miscellaneous constants such as moments of inertia are given in Table 3.6.

The effect of aeroelasticity and free controls on dynamic stability was investigated for the clean airplane configuration at Mach numbers of 0.6 and 0.8 at both sea level and 20,000 feet.

The results of dynamic stability investigations presented in this report were based on uncoupled longitudinal and lateral-directional modes. However, wind tunnel test data as reported in Reference 1, indicates some pitch-yaw coupling in the form of a negative pitching moment due to sideslip. Unpublished results of a five degree of freedom investigation of the effect of the pitch-yaw coupling at Mach 0.6 indicate that both the vertical and lateral limit load factors may be exceeded in rapid, 360 degree rolling maneuvers at high speed with the elevator and rudder fixed. The load factors developed in rolling maneuvers with not more than one half of full aileron throw are estimated to be small.

Solution of the longitudinal and lateral-directional equations of motion was performed by digital computer. The controls fixed equations of motion developed in Reference 4 have been expanded to include the effects

of free controls. The complete equations of motion solved by the computer are presented and briefly discussed in the Appendix to this report.

The computer program is written to extract the roots of the characteristic equation developed from the equations of motion and in addition to calculate the frequency, damping ratio, time to damp to half amplitude and the inverse of the cycles to damp to half amplitude for any oscillatory modes which exist. The roll/slip ratio, φ/v_e, is also calculated for the dutch roll oscillation. The computer results of all the cases investigated are presented in Tables 3.7 through 3.13.

3.4.1 Longitudinal Investigations

The longitudinal dynamic characteristics for the flaps down landing configuration are presented graphically in Figures 3.29 and 3.30 for the short period and phugoid modes respectively. The characteristics are presented in terms of the period and damping ratio of the oscillation in comparison with the requirements of the XV-5A Flying Qualities Specification, Reference 11.

The highest speed points in both Figures 3.29 and 3.30 show a consistent trend with decreasing velocity. The short period damping ratio and period both increase and the frequency decreases as speed decreases, while exactly the opposite is true for the phugoid or long period oscillation. Note in Figure 3.29 that no data are presented for the short period mode at the lowest flaps down speed point investigated (94.6 knots). The computer results obtained for the low speed point showed that one of the two usual longitudinal oscillatory modes had become aperiodic and convergent as evidenced by two negative real roots of the characteristic equation. The period of the oscillatory mode was 39.5 seconds which was much too long to classify it as the conventional "short period" mode. The appearance of the aperiodic modes is, in all probability, due to the fact that the static stability margin approaches zero at very low speeds as discussed in Reference 1. Since the frequency of the usual short period mode is heavily dependent on the static stability and decreases with decreasing stability, one would tend to believe that the usual short period oscillation was the one which became aperiodic.

The aperiodic modes are well damped with the times to damp to half amplitude being about 0.5 and 0.9 second. The short times to damp are probably due to the high level of pitch rate damping C_{m_q}. The very low speed range with zero static stability margin was investigated on the Ryan Flight Simulator and with the high level of pitch damping the flying qualities were found to be satisfactory, (Reference 2).

The longitudinal dynamic stability of the XV-5A in the landing configuration meets the requirements of the Flying Qualities Specification for all flight conditions investigated.

High speed, scale model wind tunnel tests of the clean airplane configuration have shown that at the higher Mach numbers, the static longitudinal stability decreases with increase in angle of attack. Figure 3.31, excerpted from Reference 1, shows the definable boundary for zero static longitudinal stability as a function of Mach number and complete model lift coefficient. Although the available data shows a gradual deterioration of static stability with increasing angle of attack, extreme caution should be exercised during flight test investigations when approaching the boundaries of the questionable high speed area. It is not likely that the higher speed boundary will be encountered in level flight, but will be in pull-up maneuvers or in dive recovery. The lower part of the questionable area will be encountered in level flight at altitudes at and above about 20,000 feet. The dynamic stability investigations in this report were based on linearized derivatives consistent with the assumption of small perturbations. The static stability values used are based on a value near the level flight lift coefficient.

The characteristics of the longitudinal short period mode for the clean airplane configuration are presented in Figure 3.32 for the rigid airframe with fixed controls. The short period characteristics are shown in terms of the natural frequency and damping ratio in comparison with the requirements of the XV-5A Flying Qualities Specification, (Reference 11). The characteristics of the XV-5A satisfy the requirements of Reference 11 for all conditions investigated, except at low speeds or altitudes above approximately 30,000 feet.

The low frequencies calculated for the low speed and the high altitude data points indicate that the response of the aircraft, at those flight conditions, will be rather slow or sluggish in longitudinal maneuvers. At more forward cg locations than that presented, the short period natural frequency increases, while the damping ratio decreases slightly which would improve the response characteristics for the low speed and/or high altitude cases. Although not specifically investigated, for the case of high speed flight at low altitude, the most forward cg location will probably cause these points to be outside the boundary on the high frequency side. This would give a sensitive and highly responsive aircraft which, depending on the actual magnitude of the frequency and damping ratio, would be susceptible to pilot induced oscillations. These high dynamic pressure characteristics are, however, greatly influenced by aeroelastic considerations, which will be discussed next. The rigid

airframe characteristics presented in Figure 3.32 for free stream dynamic pressures less than that at about 25,000 feet and Mach 0.5 will be only slightly affected by aeroelastic considerations.

The effect of aeroelasticity on the short period characteristics of the clean airplane are shown in Figure 3.33 for several flight conditions which are representative of the most severe aeroelastic conditions.

Aeroelastic considerations do not result in any unsatisfactory short period characteristics for any of the cases investigated. In light of the previous comments on more forward cg locations, the reduction in natural frequency and increase in damping ratio due to aeroelastic effects are actually favorable, because they will tend to bring the short period characteristics for more forward cg locations toward the center of the satisfactory boundary.

The large aeroelastic effects at Mach 0.8 at sea level tend to bring the short period damping ratio very close to the critical value of 1.0, with a correspondingly large reduction in frequency. This is probably due to the large reduction in static stability margin which was shown in Section 3.1 to be the major effect of aeroelasticity on the stability derivatives. A further reduction in static margin would cause the short period to be over-damped and hence become aperiodic. The same sort of situation existed for the flaps down, short period characteristics, where the reduction in static margin was due to nonlinear increasing downwash at high angles of attack.

The solution of the elevator free characteristic equation of motion yields an additional pair of complex roots which represent the elevator oscillatory motion. These roots are easily distinguished from the airframe roots, as they are very much larger. The elevator frequency varied from about 12 to 26 cycles per second for the flight conditions investigated, and the longest period, was about 0.08 seconds. The longest time to damp to half amplitude was 0.018 seconds.

The effect of a free elevator on the airframe short period characteristics is shown in Figure 3.33. The effects are not very large, but they do cause the natural frequency at Mach 0.6 at 20,000 feet to decrease very slightly below the lower limit of the satisfactory boundary of Reference 11. Note that no datum point is shown in Figure 3.33 for Mach 0.8 at sea level. As shown in Table 3.9, the short period mode became aperiodic with the elevator free, as evidenced by the two large real roots with times to damp to half amplitude of 0.12 and 0.23 seconds.

The characteristics of the conventional phugoid mode for the clean airplane are shown in Figure 3.34 compared with the requirements of Reference 11. These data are applicable to a rigid airframe with fixed controls. There was no unstable phugoid oscillation for any of the flight conditions investigated. At Mach 0.75 at all altitudes, and at Mach 0.8 at sea level, no phugoid oscillation existed as the mode was aperiodic in both cases. Of the aperiodic modes, one mild divergence existed at Mach 0.75 at 40,000 feet, wherein the time to double the amplitude was 55 seconds. It is not considered likely that the mild divergence should produce objectionable flying qualities.

The effects of aeroelasticity and a free elevator on the phugoid characteristics are presented in Figure 3.35. No data are shown for the cases at Mach 0.8 at sea level and 20,000 feet, as the modes were aperiodic for the elevator fixed or free. One divergent, aperiodic mode existed at both sea level and 20,000 feet and the times to damp to half amplitude were 37.5 and 21.0 seconds, respectively, for the elevator fixed and 42.5 and 20.6 seconds, respectively, for the elevator free. Generally speaking, the usual phugoid mode often becomes aperiodic in the super-critical Mach number range due to large variations in drag with speed (i.e., drag divergence). In the case of the XV-5A the negative variation of thrust with velocity shown in Figure 3.12 is such as to magnify this effect.

The effects of aeroelasticity and free elevator on the phugoid characteristics at Mach 0.6 at sea level and 20,000 feet shown in Figure 3.35 present a somewhat puzzling picture. There is a very large variation in period and damping ratio at sea level, while virtually no effect exists at 20,000 feet. The reason for the great difference can only be determined by more detailed analysis.

3.4.2 Lateral-Directional Investigations

The characteristics of the lateral-directional oscillatory or dutch roll mode for the flaps down landing configuration are presented in Figure 3.36, compared with the requirements of the XV-5A Flying Qualities Specification, Reference 11. The requirements are specified in terms of the inverse cyclic damping and the roll/slip ratio. The Reference 11 requirements are met at all speeds above about 120 knots, and the damping level is only slightly less than the satisfactory boundary for speeds down to 1.15 V_S or 94.6 knots.

The increasing roll/slip ratio as speed decreases is probably due to the rapidly increasing dihedral effect with angle of attack or lift coefficient. This trend is not an uncommon characteristic of low aspect ratio, swept wings.

The effect of a more forward cg location would be primarily to increase the inverse cyclic damping as a result of greater directional stability (C_{n_β}) and yaw damping (C_{n_r}). Therefore, at the most forward cg location, the dutch roll characteristics will probably lie entirely within the satisfactory area of Reference 11.

The spiral mode for the flaps down configuration is always convergent and the rolling mode is heavily damped which satisfies the requirements of Reference 11.

The dutch roll characteristics for the flaps up clean configuration are presented in Figure 3.37 for the rigid airframe with controls fixed. The requirements of Reference 11 are met at all speeds for altitudes below about 25,000 feet and for speeds above approximately Mach 0.7 for the higher altitudes. The deterioration in dutch roll characteristics at low speed and high altitude is probably due to the increasing dihedral effect at the high lift coefficients, similar to the low speed, flaps down case.

The effects of aeroelasticity and free rudder on the clean airplane dutch roll are shown in Figure 3.38 and the effect of free ailerons is shown in Figure 3.39. The effects are too minor to merit much discussion as to the detailed causes for the small variations which do occur.

The clean airplane exhibits a mild spiral divergence for all speeds at and above 0.6 Mach number for either the rigid or elastic airframe and with the controls fixed or free. The minimum time for the spiral divergence to double the amplitude in any of the cases investigated was about 55 seconds. Therefore, the spiral divergence should introduce no unsatisfactory flying qualities. The rolling mode is heavily damped under all flight conditions.

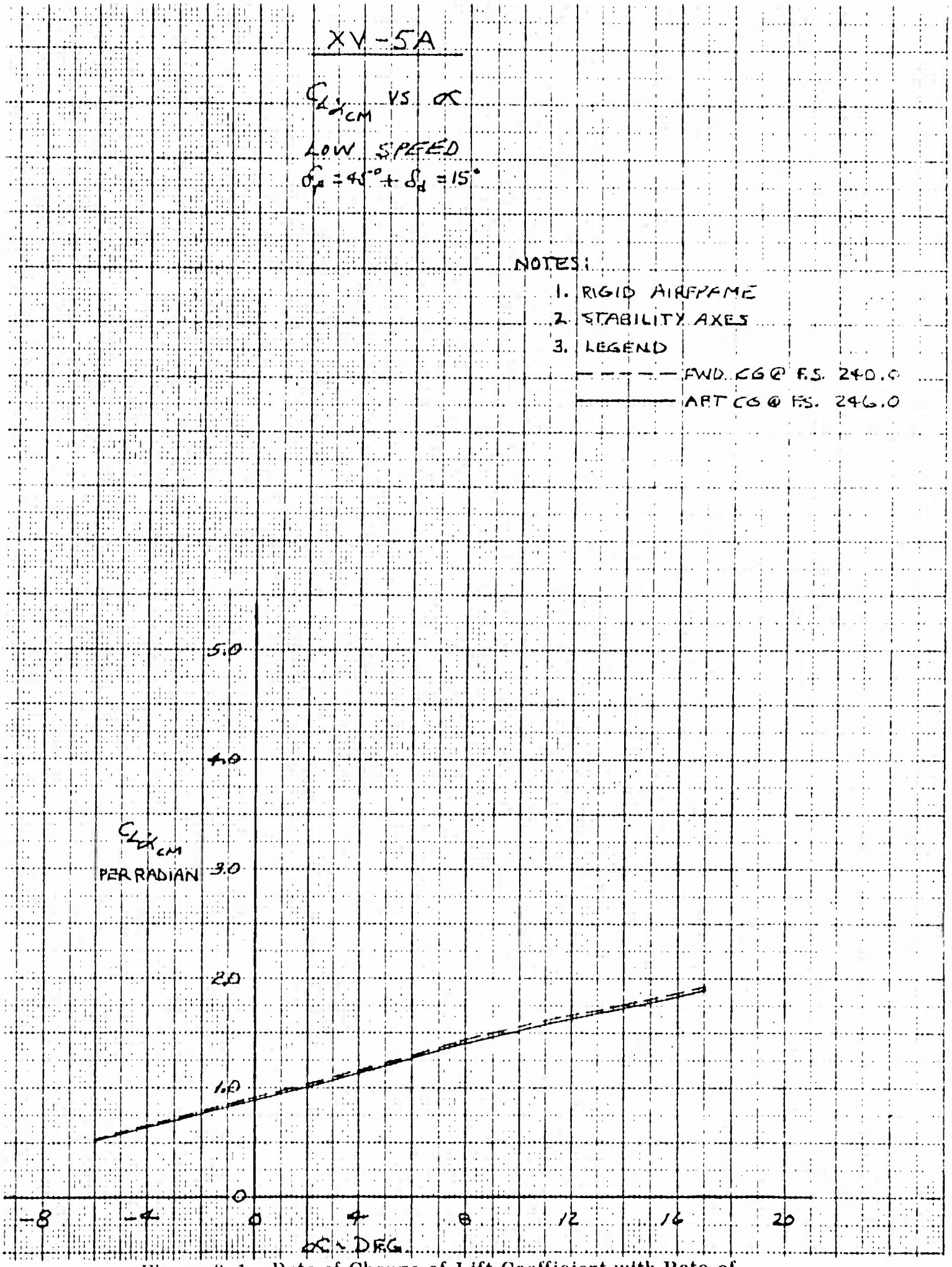

Figure 3.1 Rate of Change of Lift Coefficient with Rate of Change of Angle of Attack, $C_{L_{\dot{\alpha}_{CM}}}$, vs Angle of Attack.

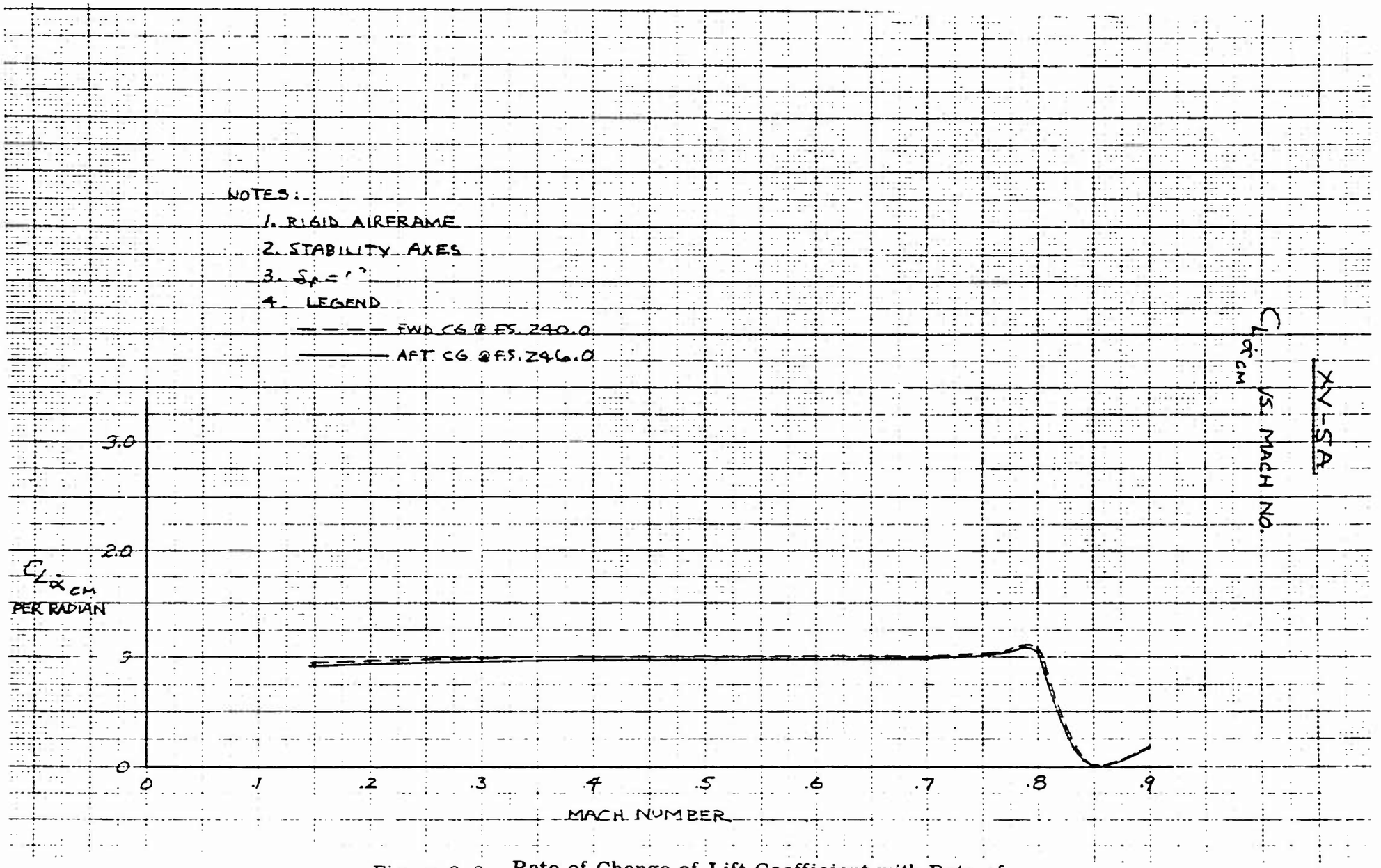

Figure 3.2 Rate of Change of Lift Coefficient with Rate of Change of Angle of Attack, $C_{L_{\dot{\alpha}_{CM}}}$, vs Mach No.

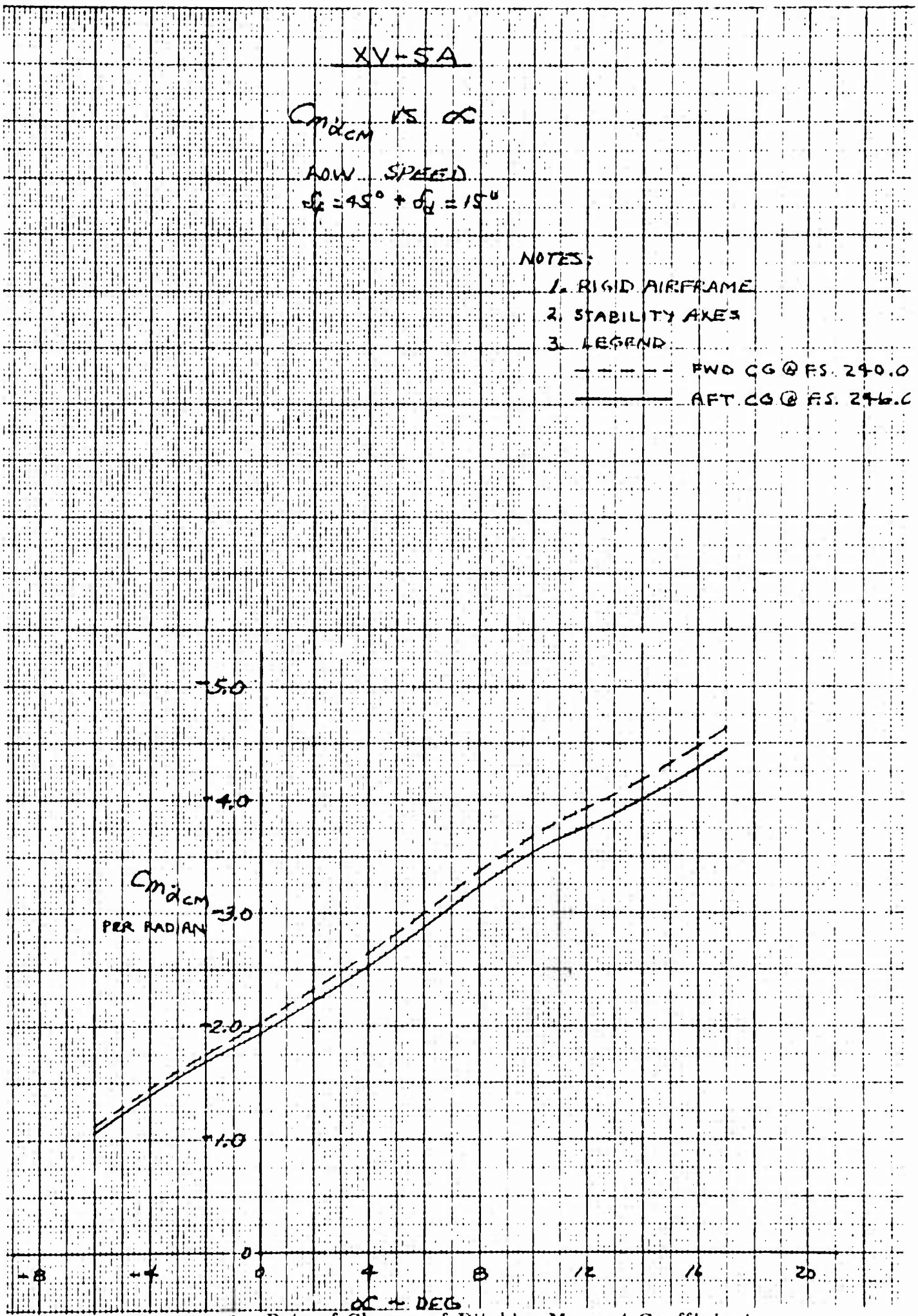

Figure 3.3 Rate of Change of Pitching Moment Coefficient with Rate of Change of Angle of Attack, $C_{m_{\dot{\alpha}_{CM}}}$, vs Angle of Attack.

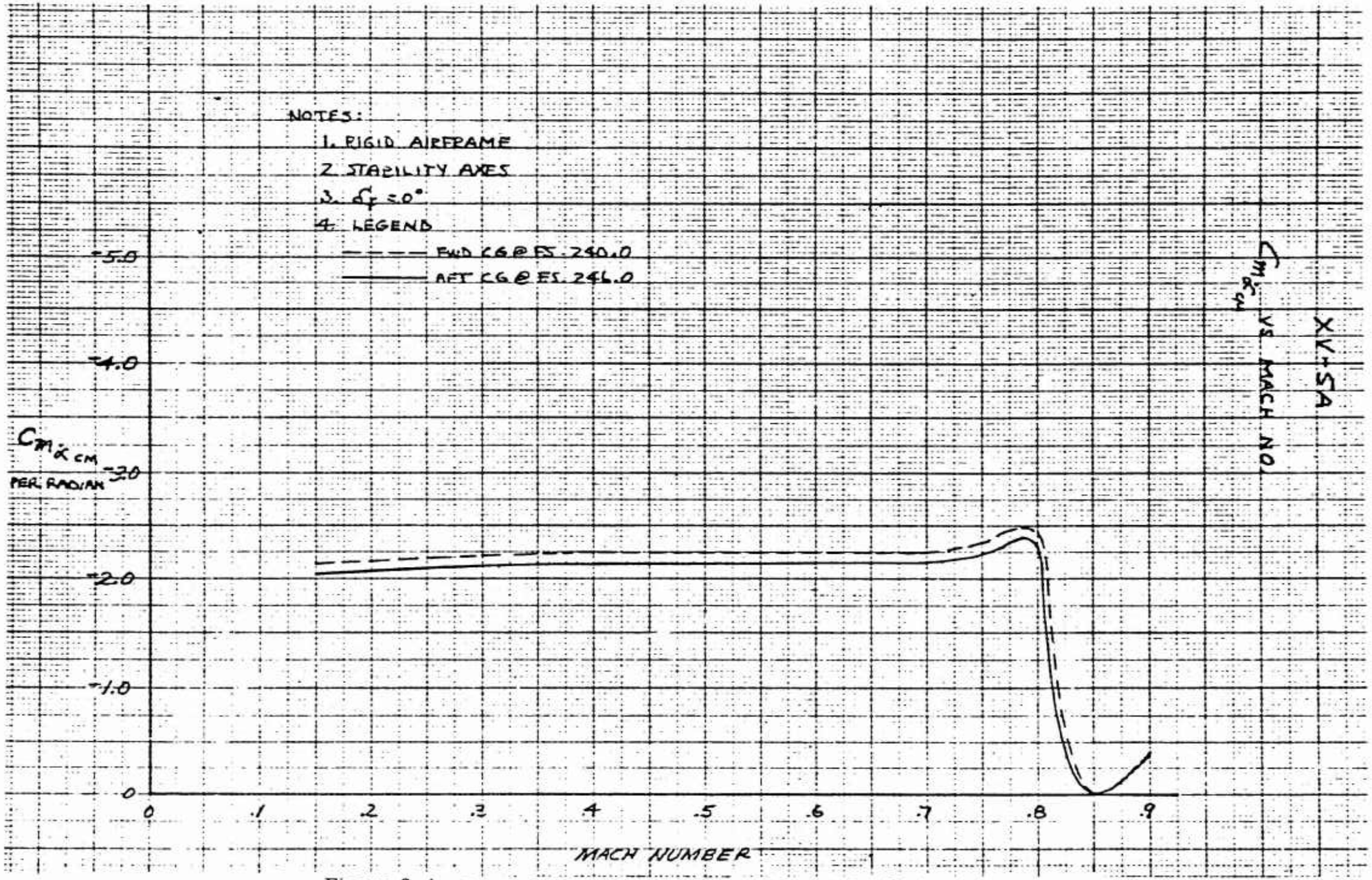

Figure 3.4 Rate of Change of Pitching Moment Coefficient with Rate of Change of Angle of Attack, $C_{m_{\dot{\alpha}_{CM}}}$, vs Mach No.

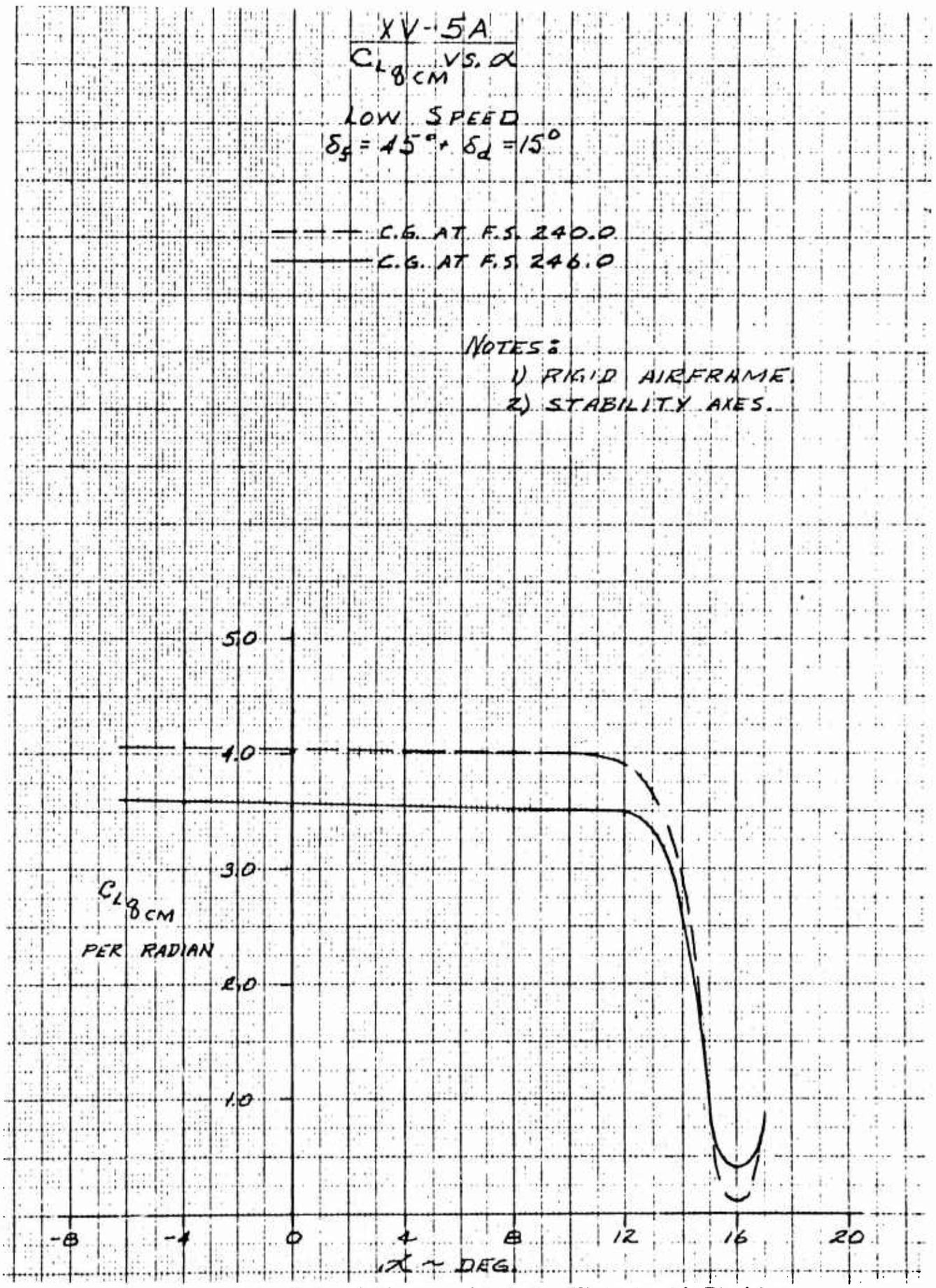

Figure 3.5 Rate of Change of Lift Coefficient with Pitching Velocity, $C_{L_{q_{CM}}}$, vs Angle of Attack.

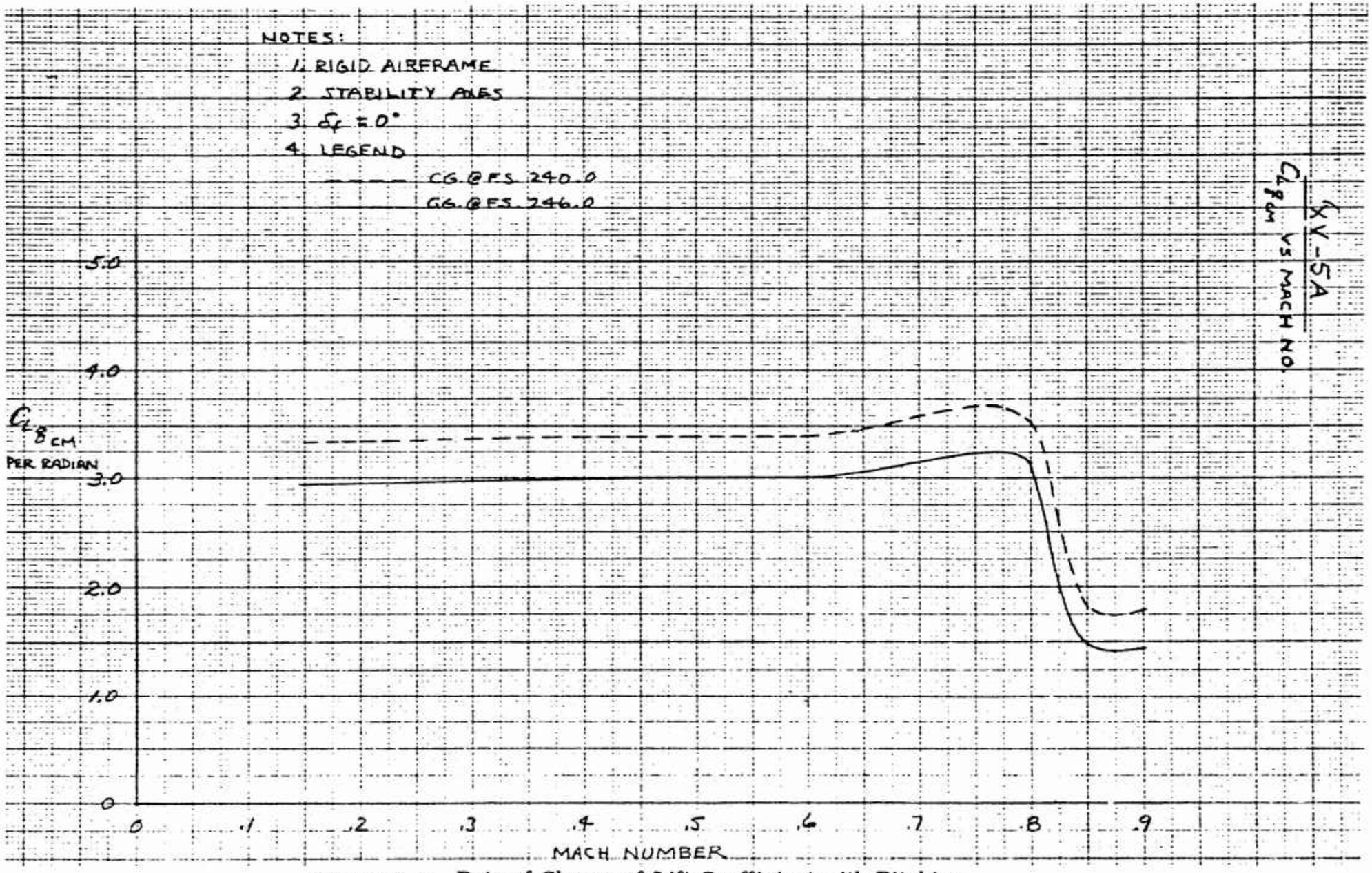

Figure 3.6 Rate of Change of Lift Coefficient with Pitching Velocity, $C_{L_{q_{CM}}}$, vs Mach No.

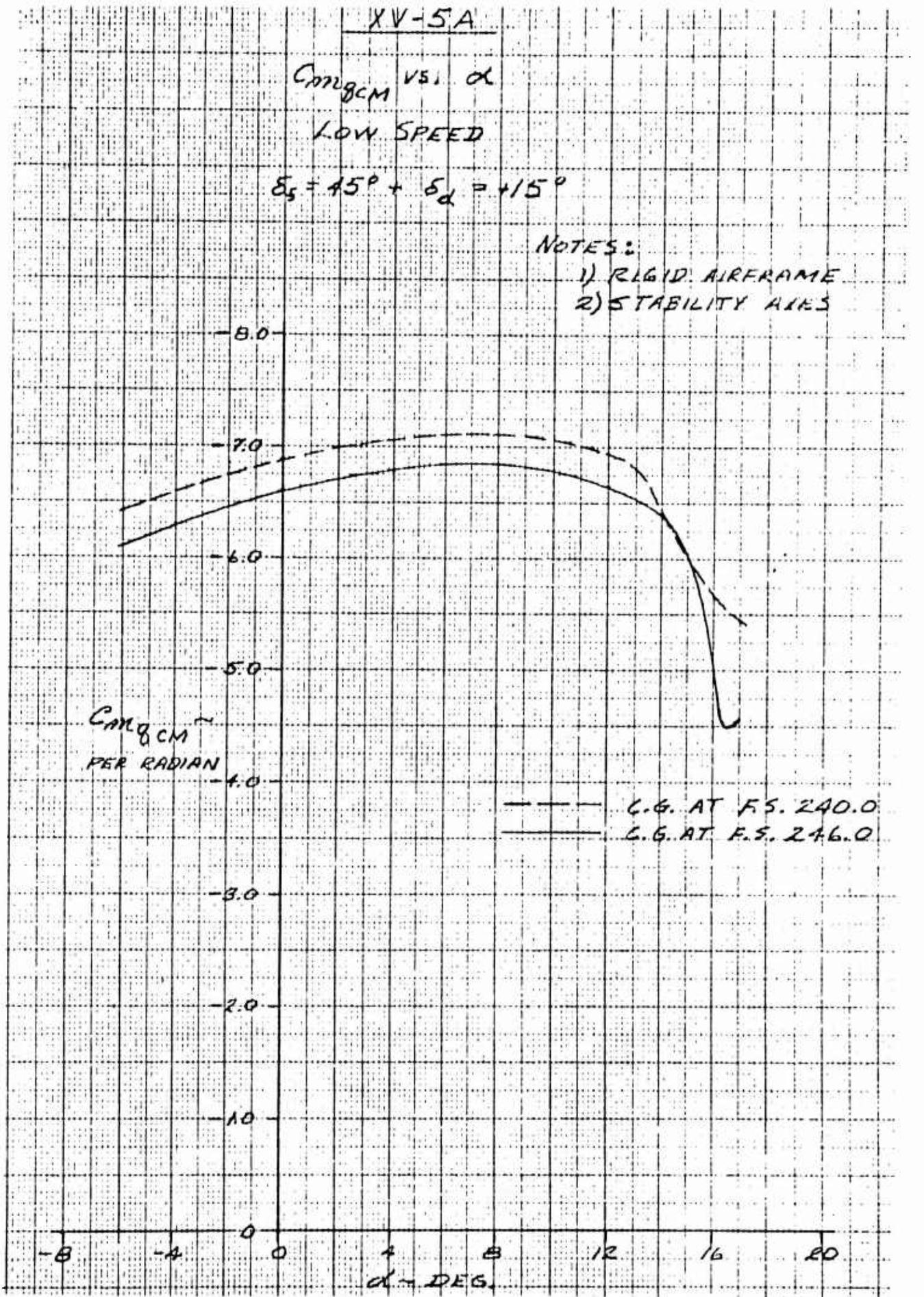

Figure 3.7 Rate of Change of Pitching Moment Coefficient with Pitching Velocity, $C_{m_{q_{CM}}}$, vs Angle of Attack.

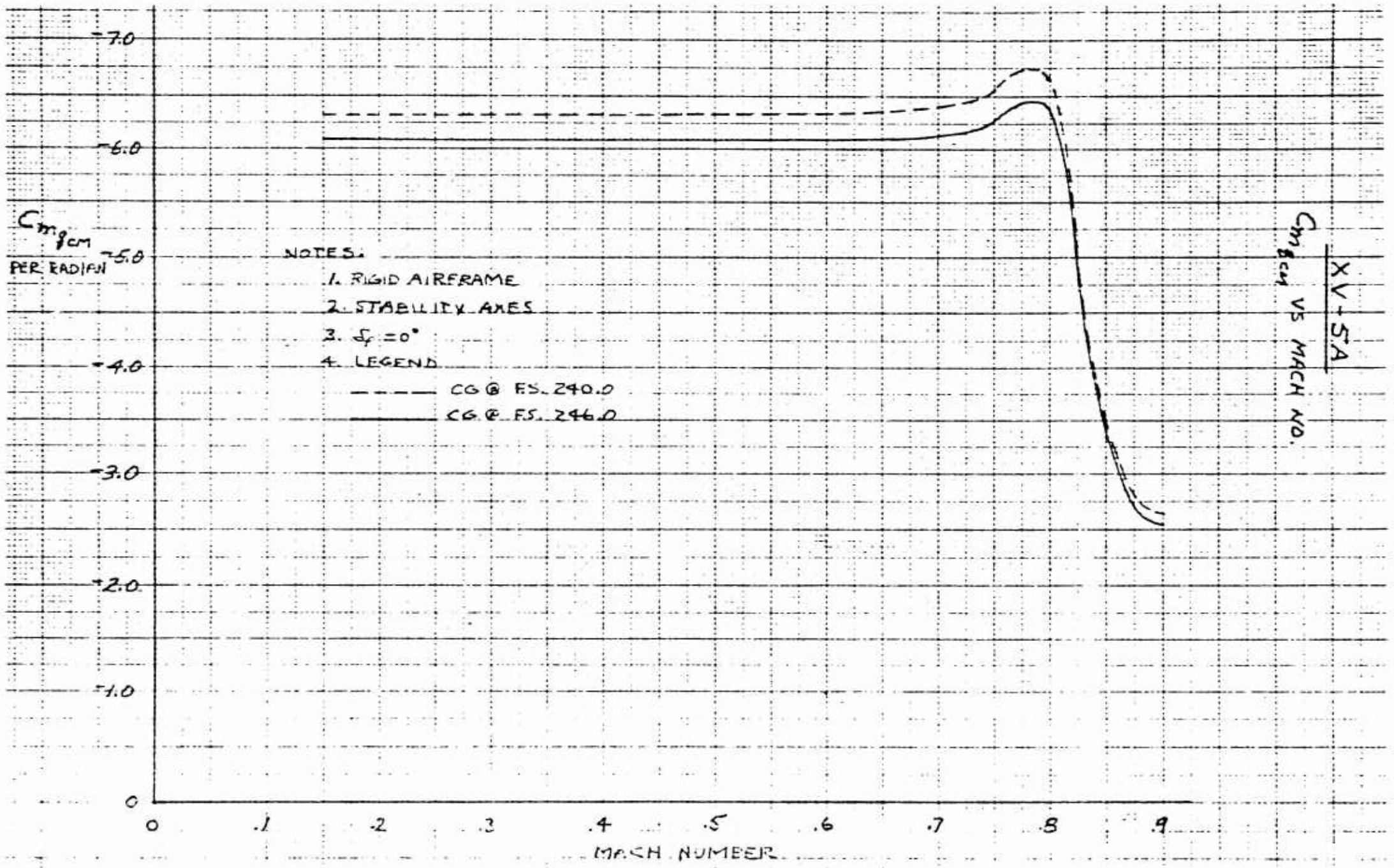

Figure 3.8 **Rate of Change of Pitching Moment Coefficient with Pitching Velocity, $C_{m_{q_{CM}}}$, vs Mach No.**

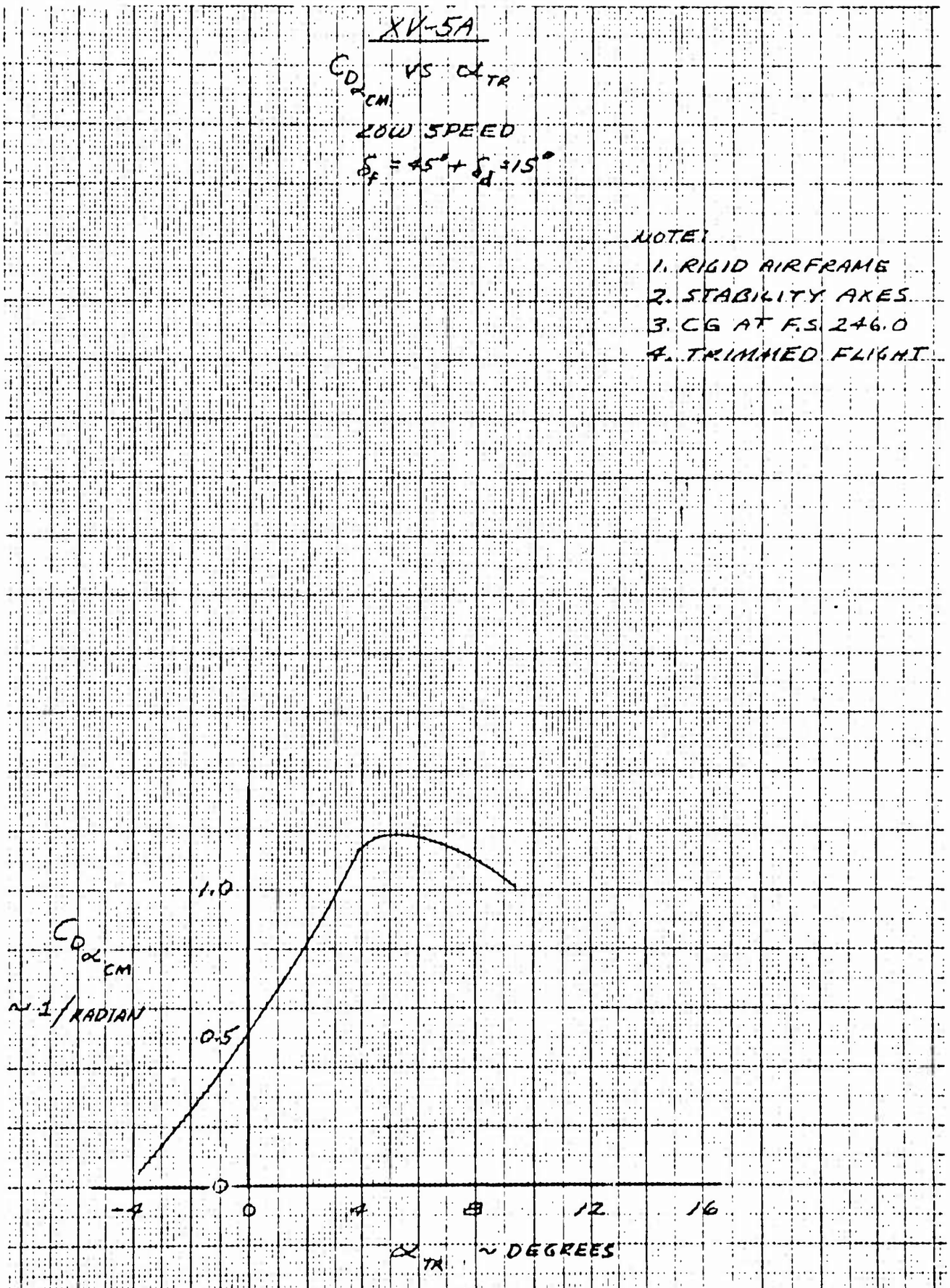

Figure 3.9 Rate of Change of Drag Coefficient with Angle of Attack, $C_{D_{\alpha_{CM}}}$, vs Angle of Attack.

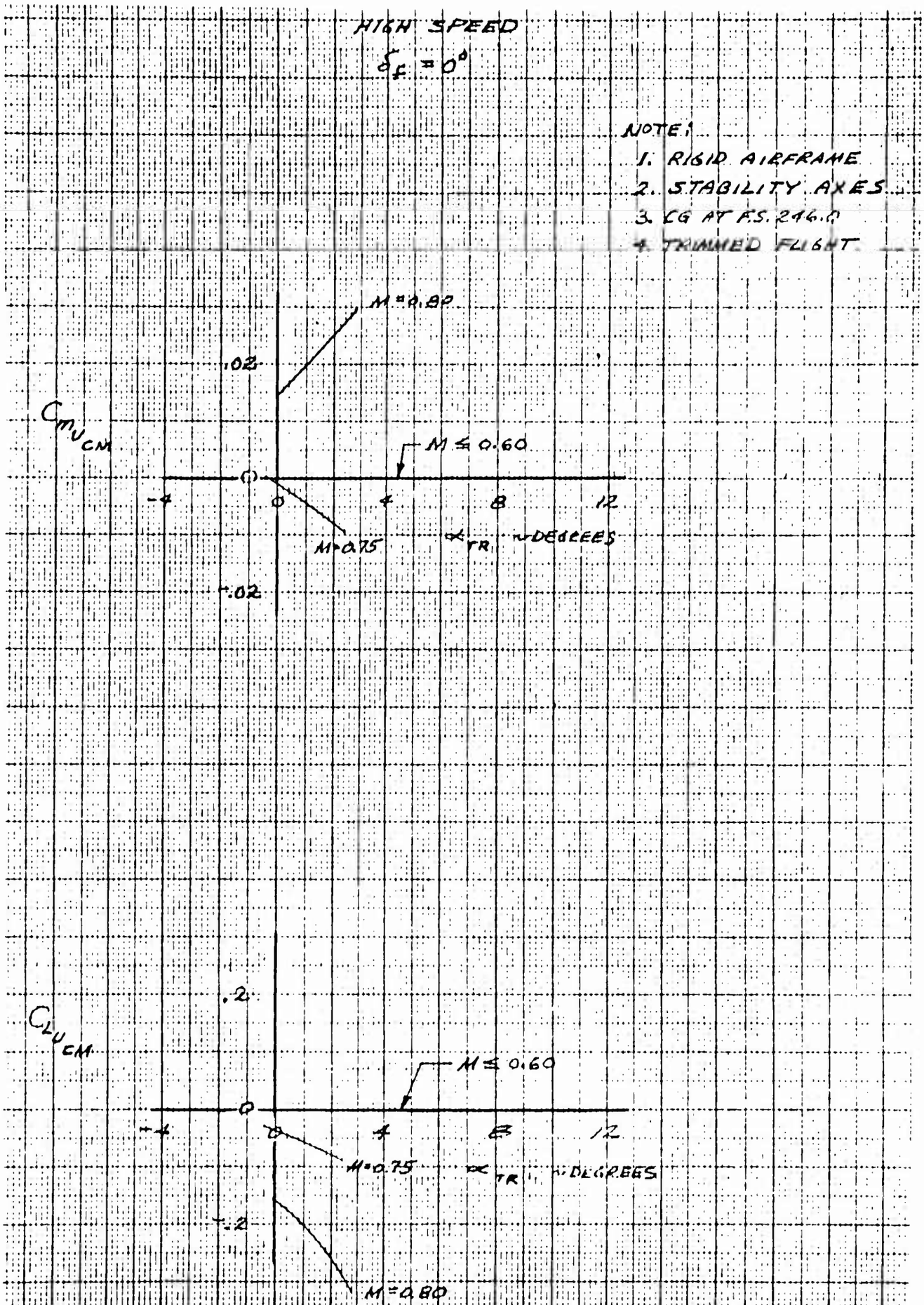

Firgure 3.10 Rate of Change of Lift Coefficient and Pitching Moment Coefficient with Forward Velocity, $C_{L_{u_{CM}}}$ and $C_{m_{u_{CM}}}$, vs Angle of Attack.

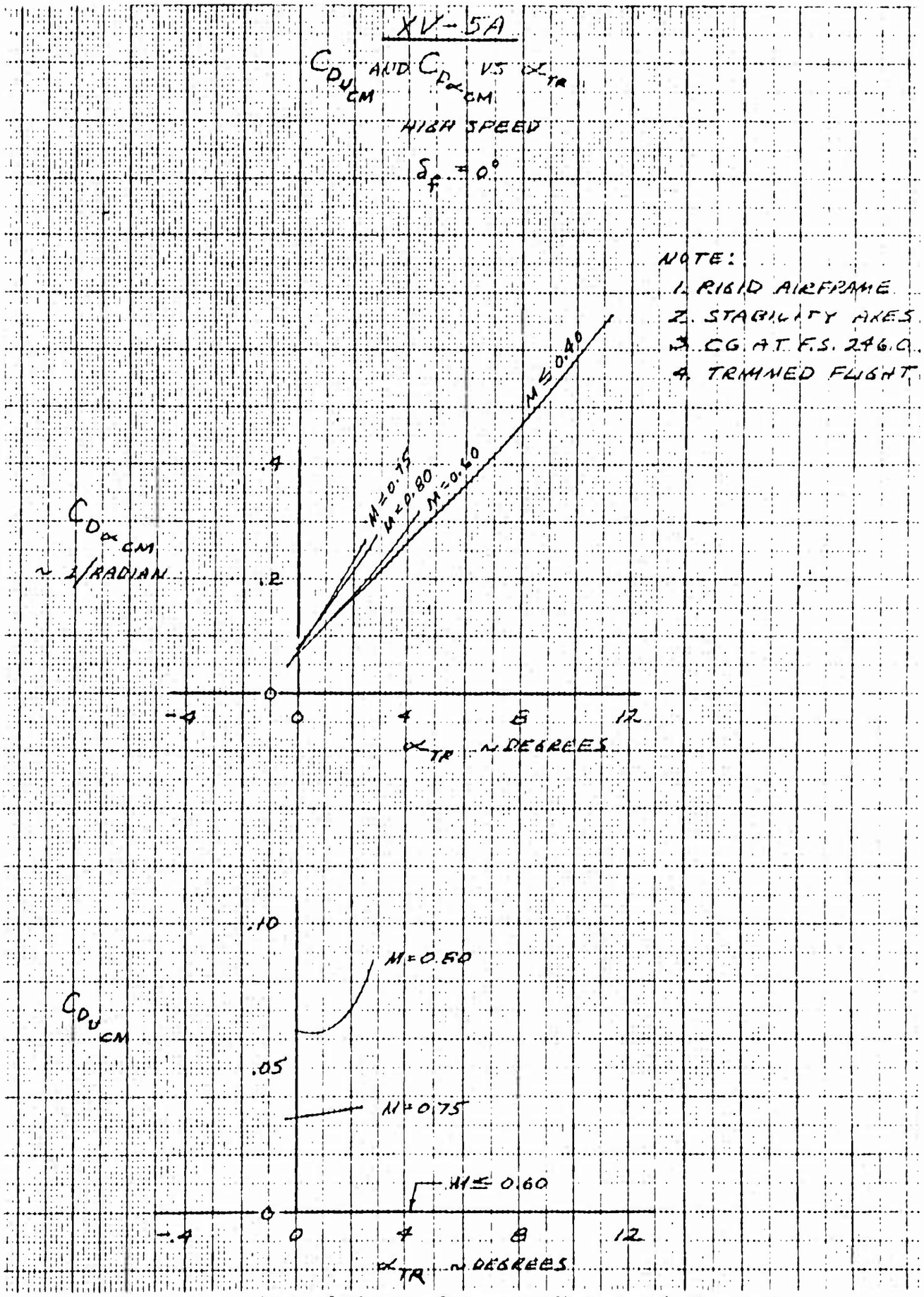

Figure 3.11 Rate of Change of Drag Coefficient with Forward Velocity and Angle of Attack, $C_{D_{u_{CM}}}$ and $C_{D_{\alpha_{CM}}}$, vs Angle of Attack.

NOTES:
1) ARDC STANDARD ATMOSPHERE.
2) TWO G.E.-X353-5B POWER PLANTS.
3) TURBOJET MODE.
4) 100% ENGINE R.P.M.

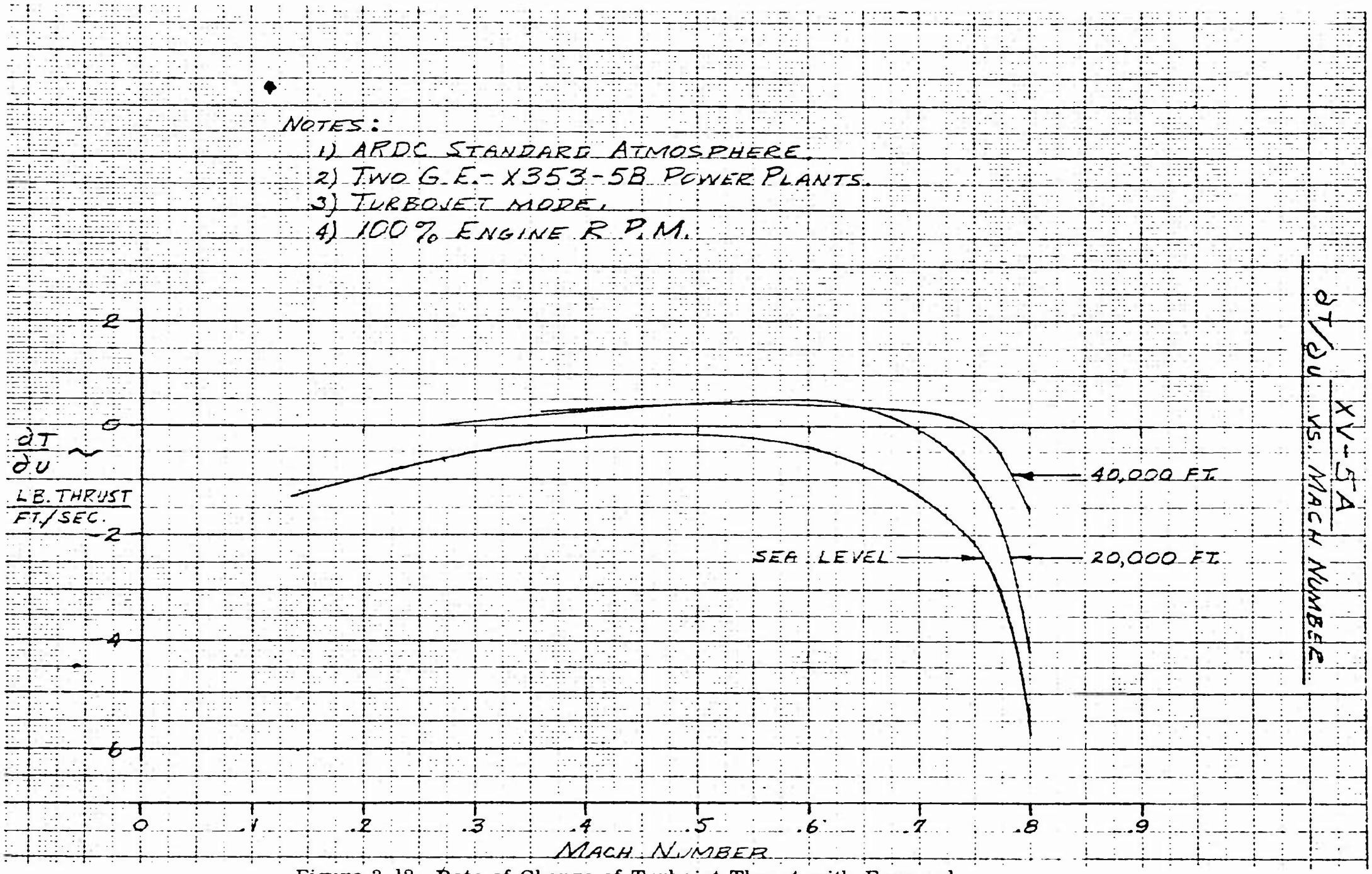

Figure 3.12 Rate of Change of Turbojet Thrust with Forward Velocity, $\partial T/\partial u$, vs Mach No.

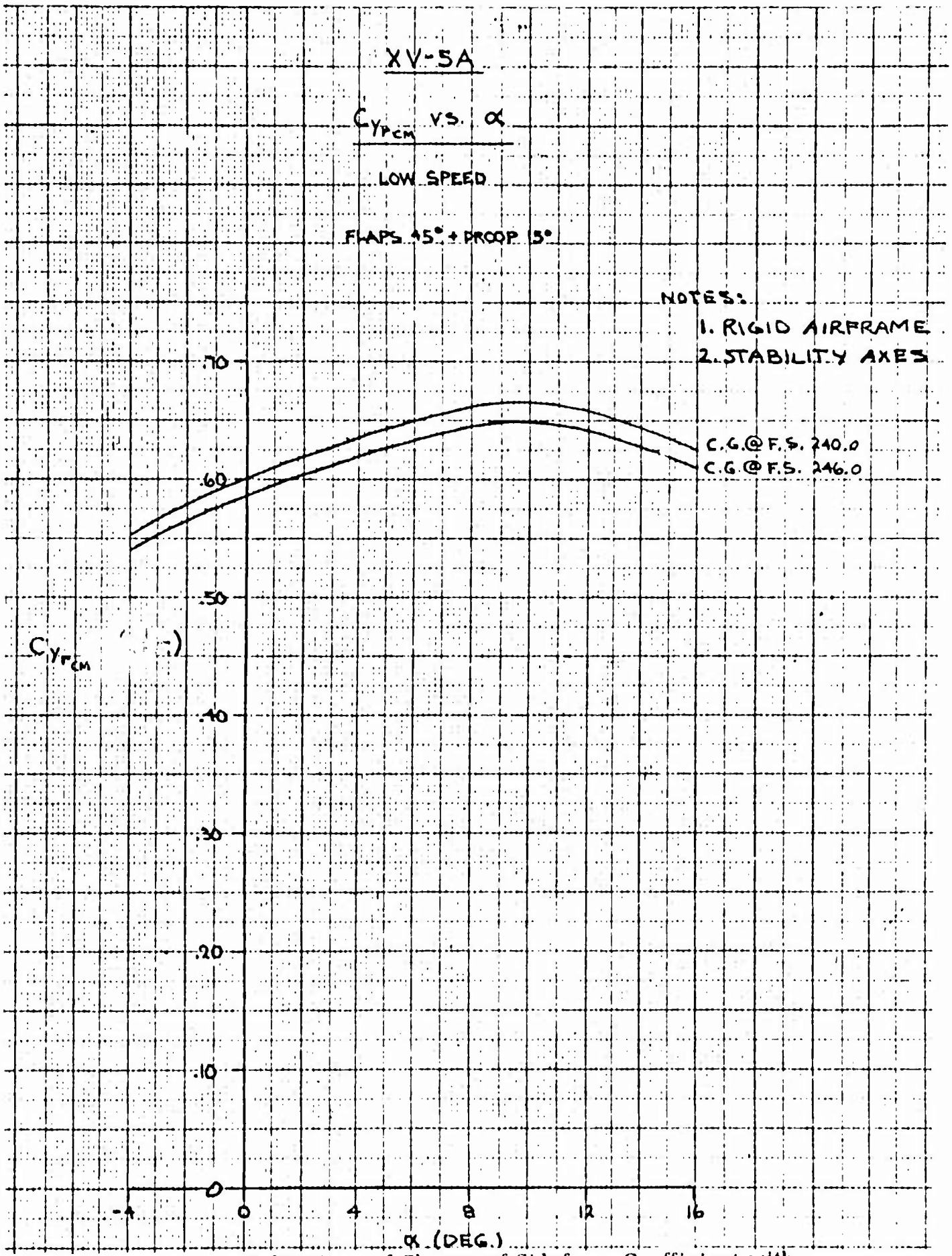

Figure 3.13 Rate of Change of Sideforce Coefficient with Yawing Velocity, $C_{y_{r_{CM}}}$, vs Angle of Attack.

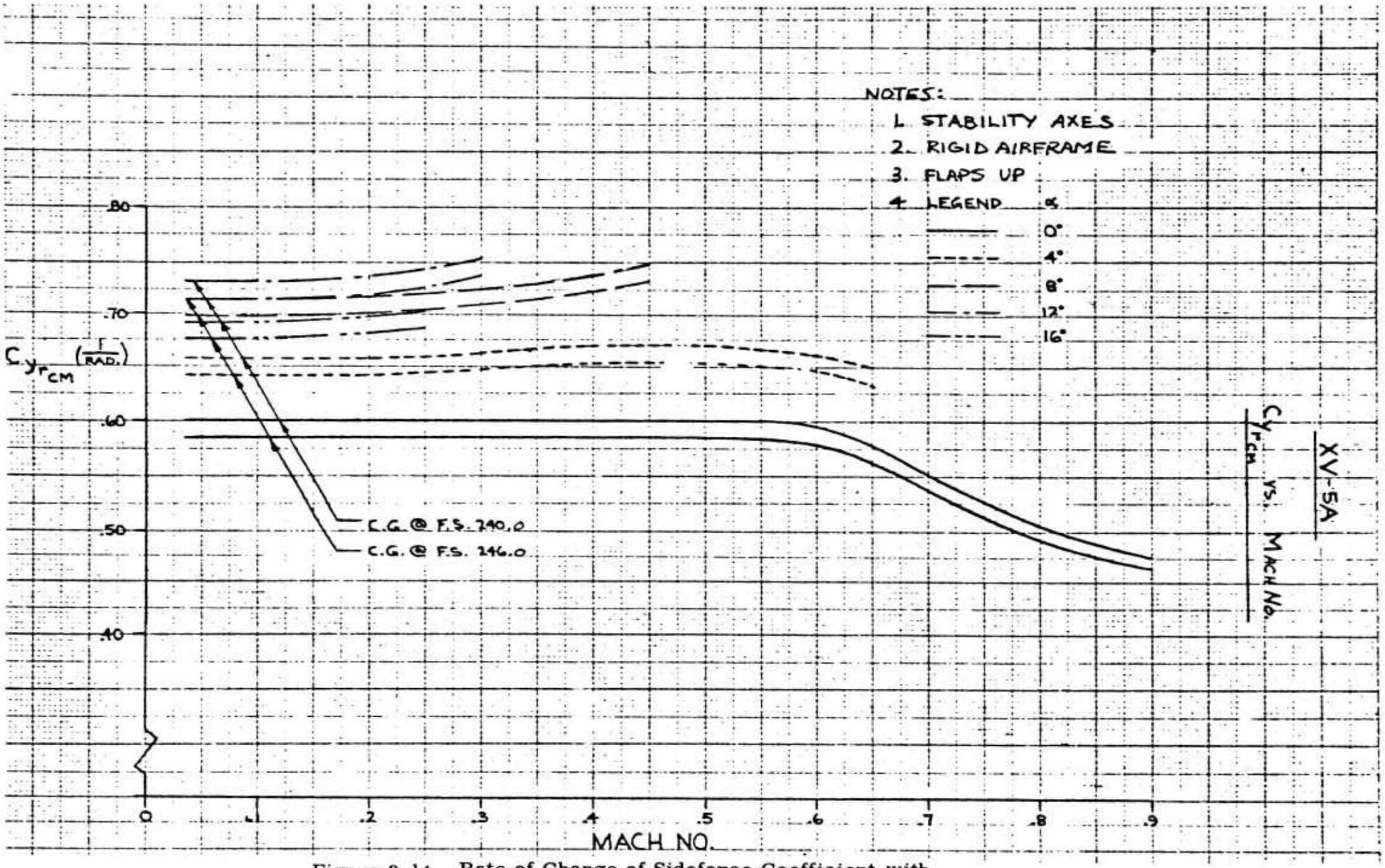

Figure 3.14 Rate of Change of Sideforce Coefficient with Yawing Velocity, $C_{y_{r_{CM}}}$, vs Mach No.

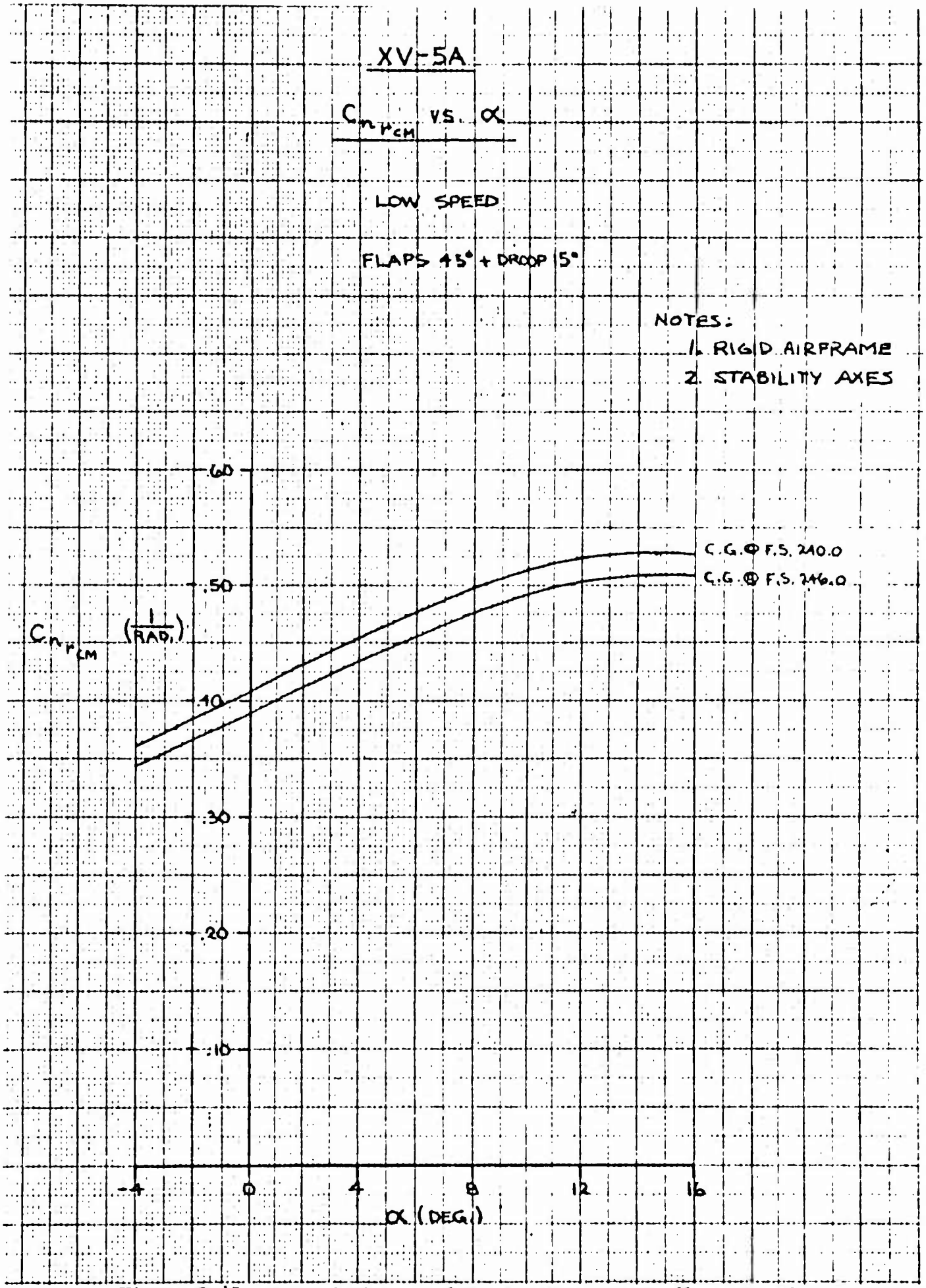

Figure 3.15 Rate of Change of Yawing Moment Coefficient with Yawing Velocity, $C_{n_{r_{CM}}}$, vs Angle of Attack.

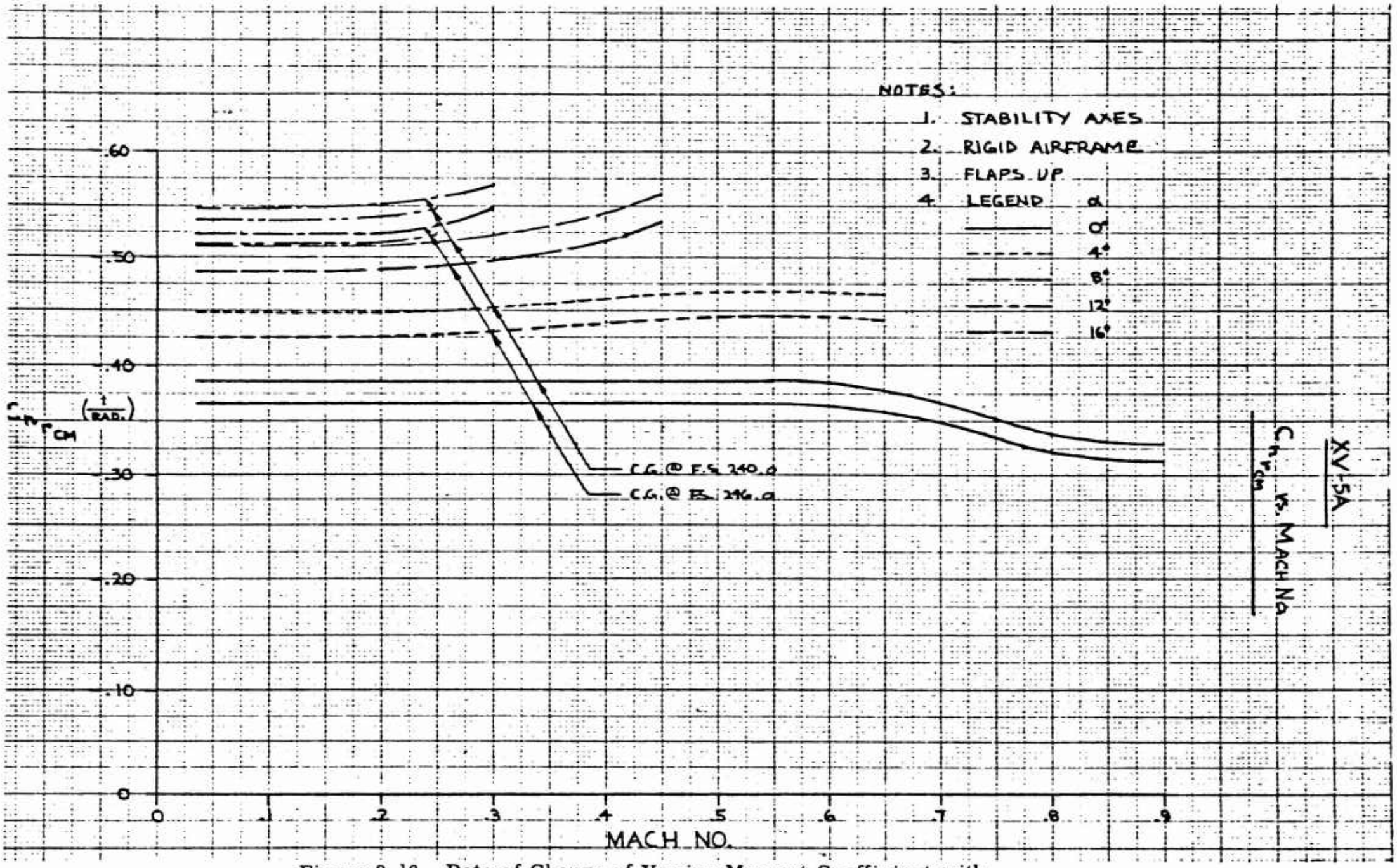

Figure 3.16 Rate of Change of Yawing Moment Coefficient with Yawing Velocity, $C_{n_{r_{CM}}}$, vs Mach No.

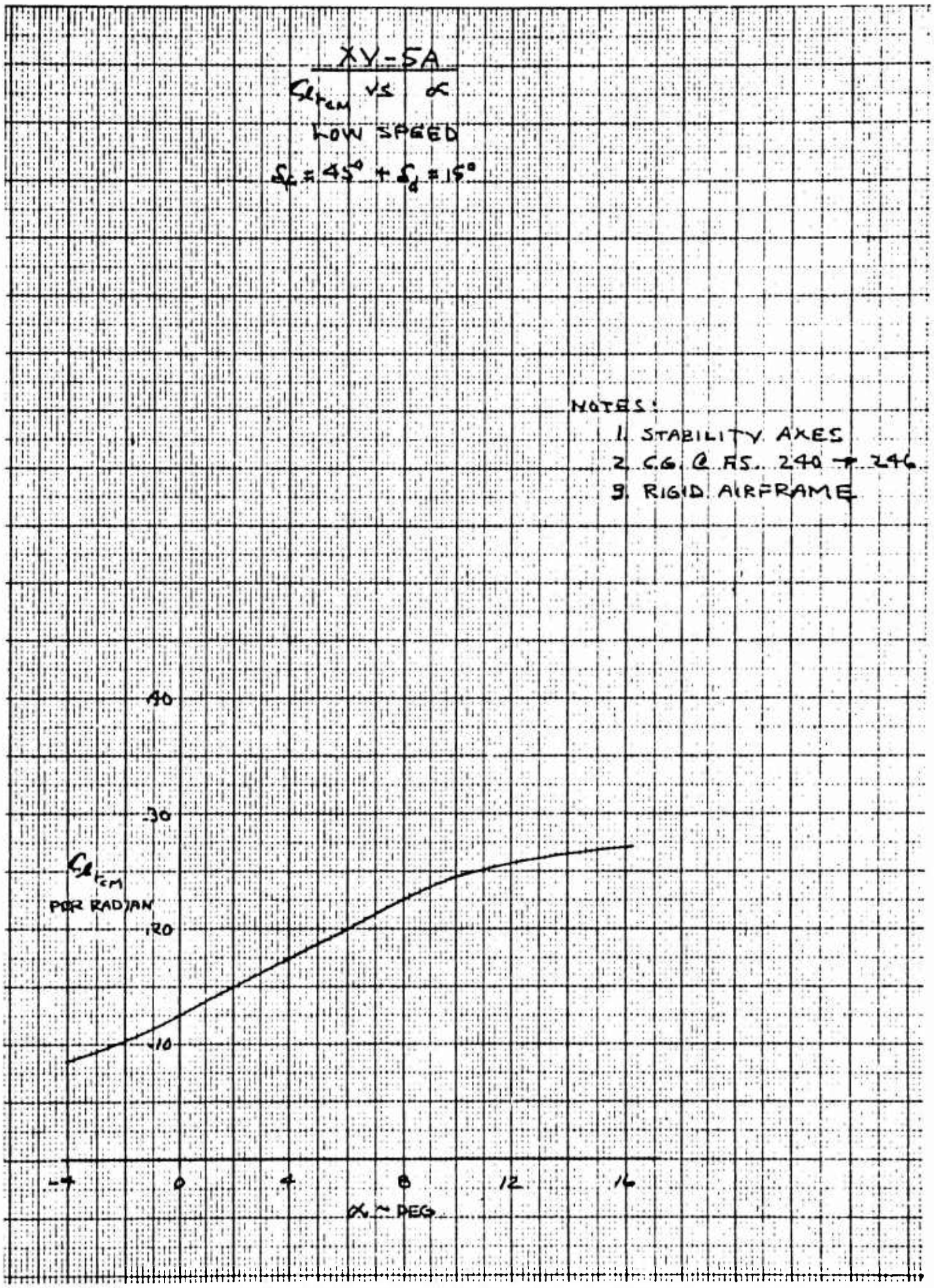

Figure 3.17 Rate of Change of Rolling Moment Coefficient with Yawing Velocity, $C_{l_{r_{CM}}}$, vs Angle of Attack.

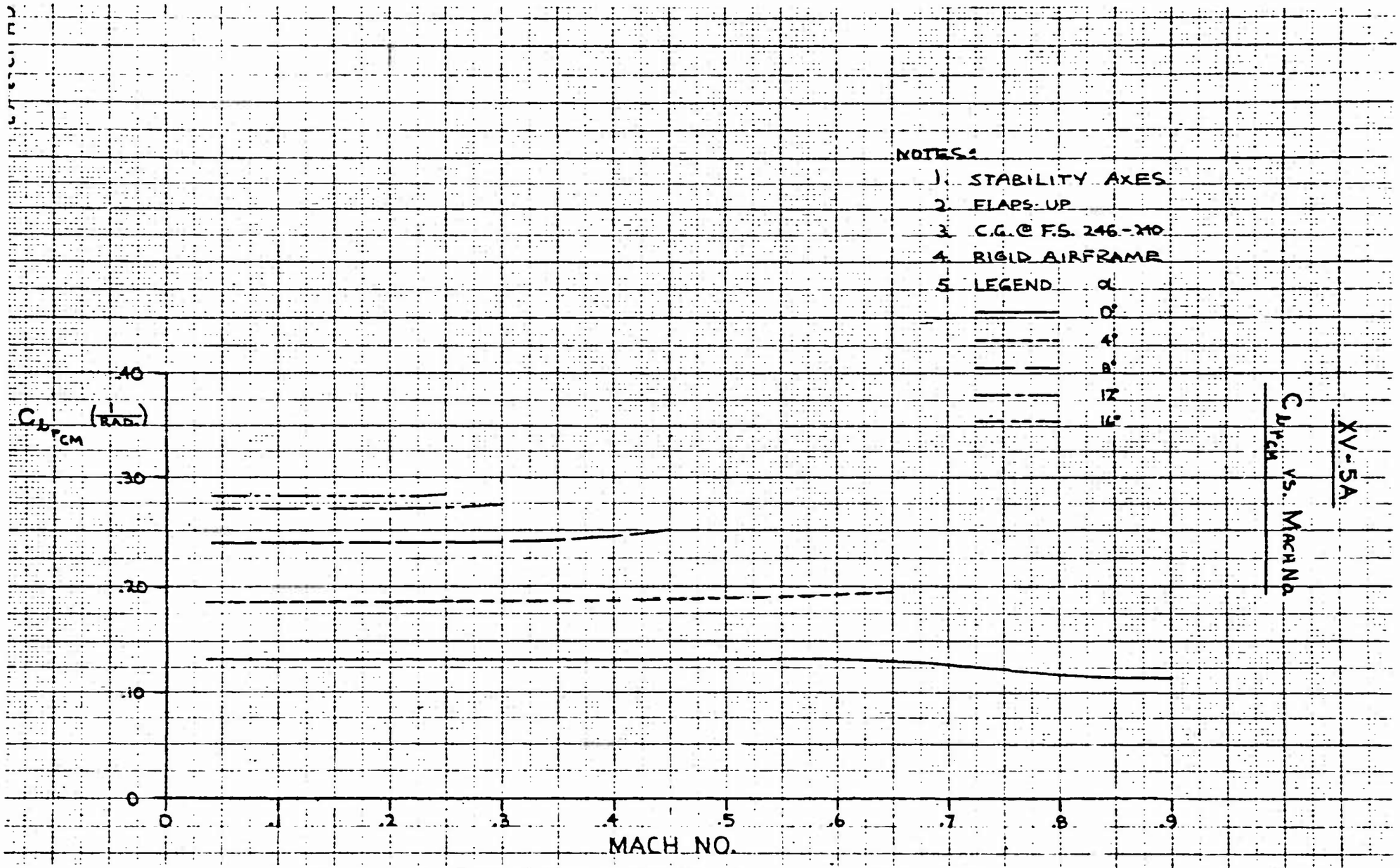

Figure 3.18 Rate of Change of Rolling Moment Coefficient with Yawing Velocity, $C_{l_{r_{CM}}}$, vs Mach No.

XV-5A

$C_{Y_{P_{CM}}}$ VS α

LOW SPEED

$\zeta_f = 95°$ $\delta_f = 15°$

NOTE:
1. RIGID AIRFRAME
2. STABILITY AXES
3. C.G. AT F.S. 240 + 246

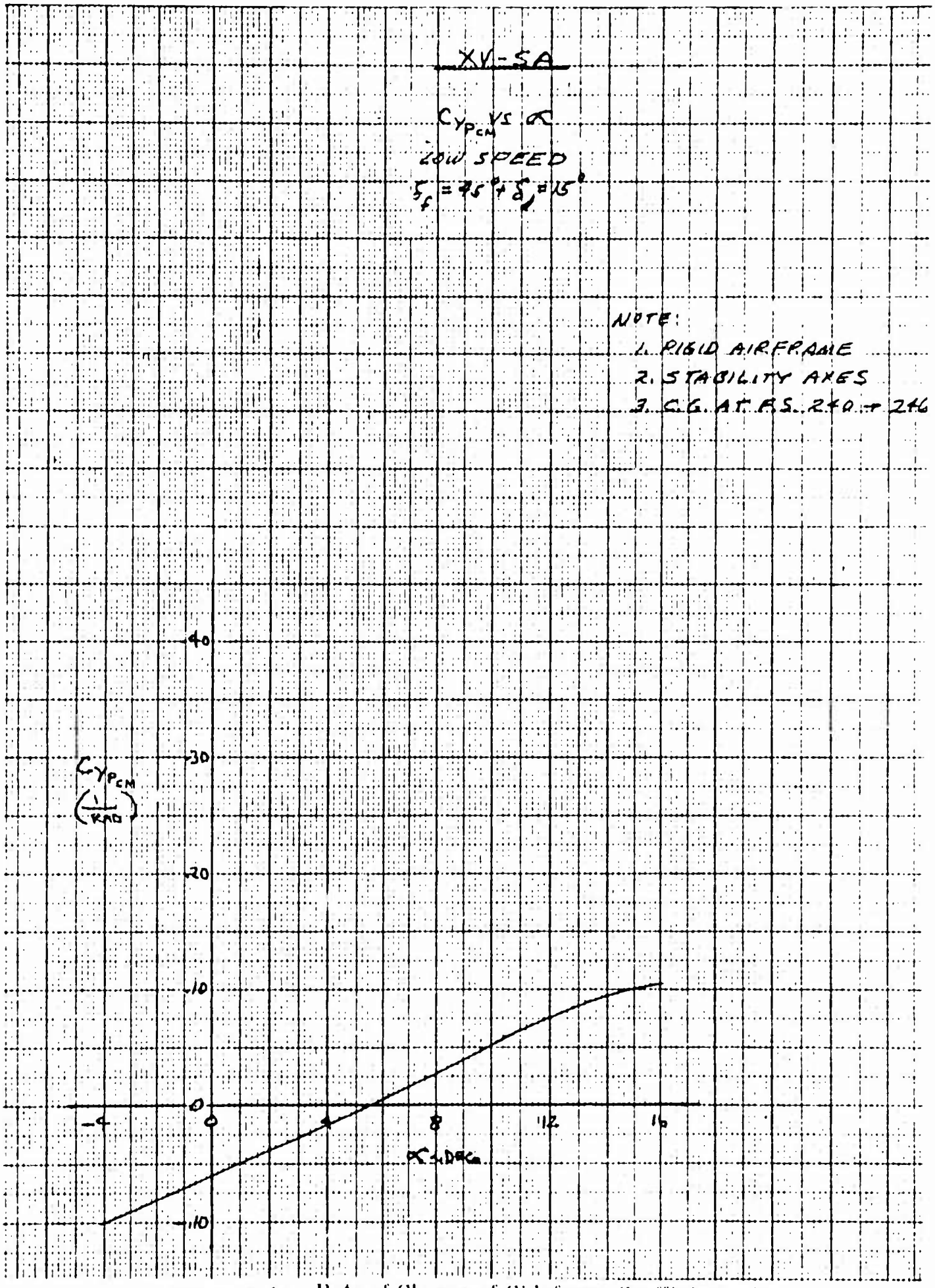

Figure 3.19 Rate of Change of Sideforce Coefficient with Rolling Velocity, $C_{y_{P_{CM}}}$, vs Angle of Attack.

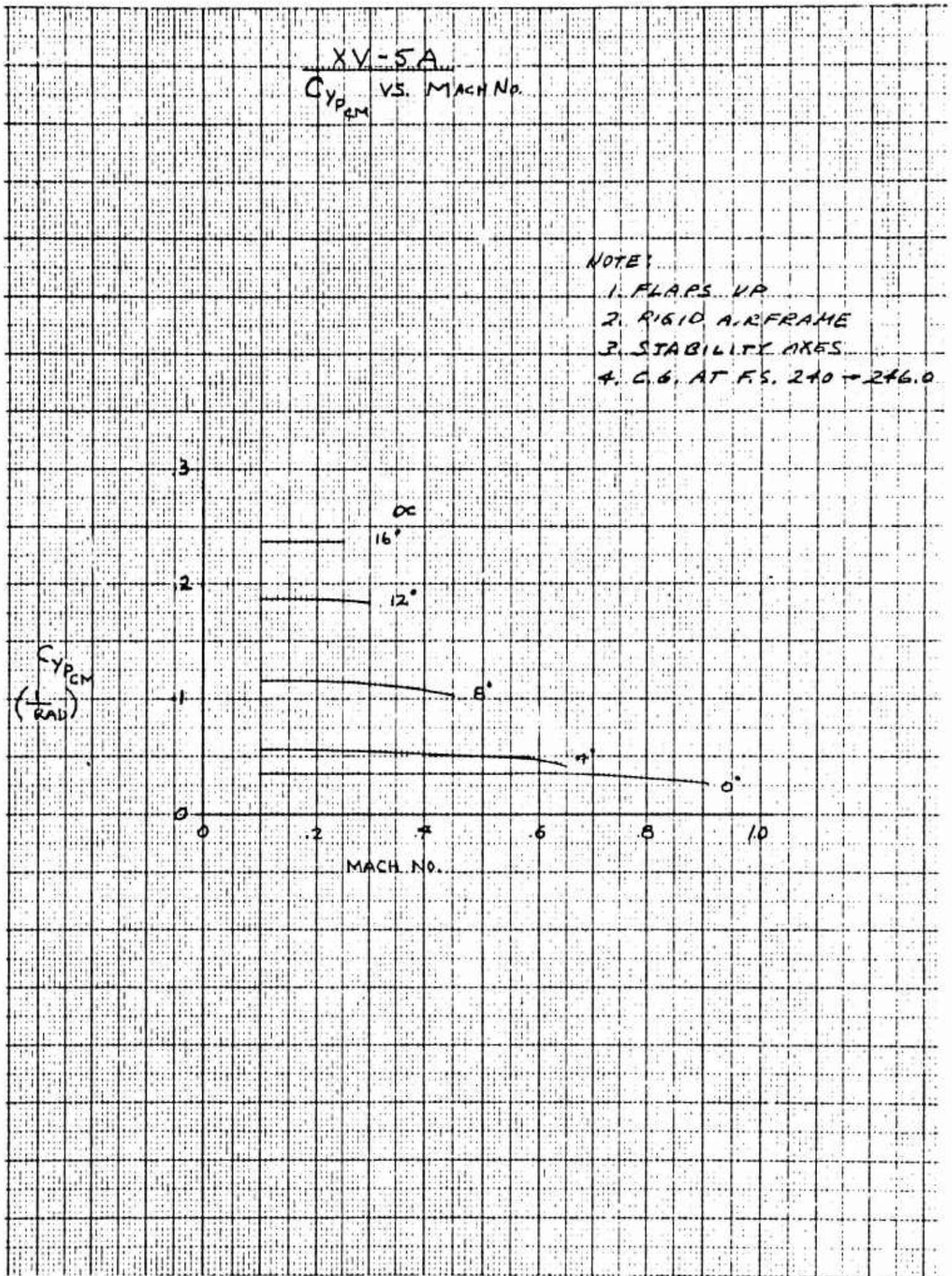

Figure 3.20 Rate of Change of Sideforce Coefficient with Rolling Velocity, $C_{y_{p_{CM}}}$, vs Mach No.

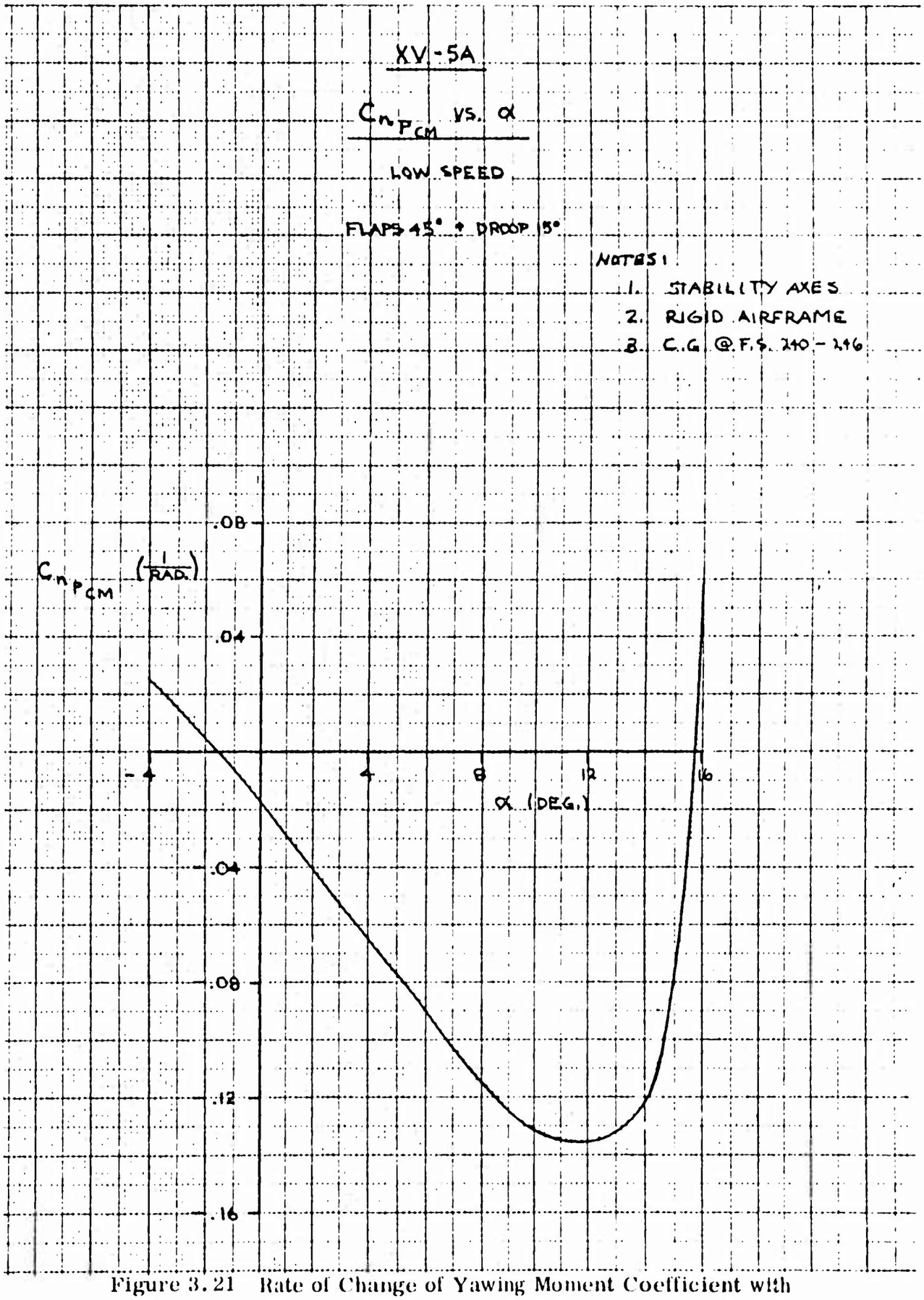

Figure 3.21 Rate of Change of Yawing Moment Coefficient with Rolling Velocity, $C_{n_{P_{CM}}}$, vs Angle of Attack.

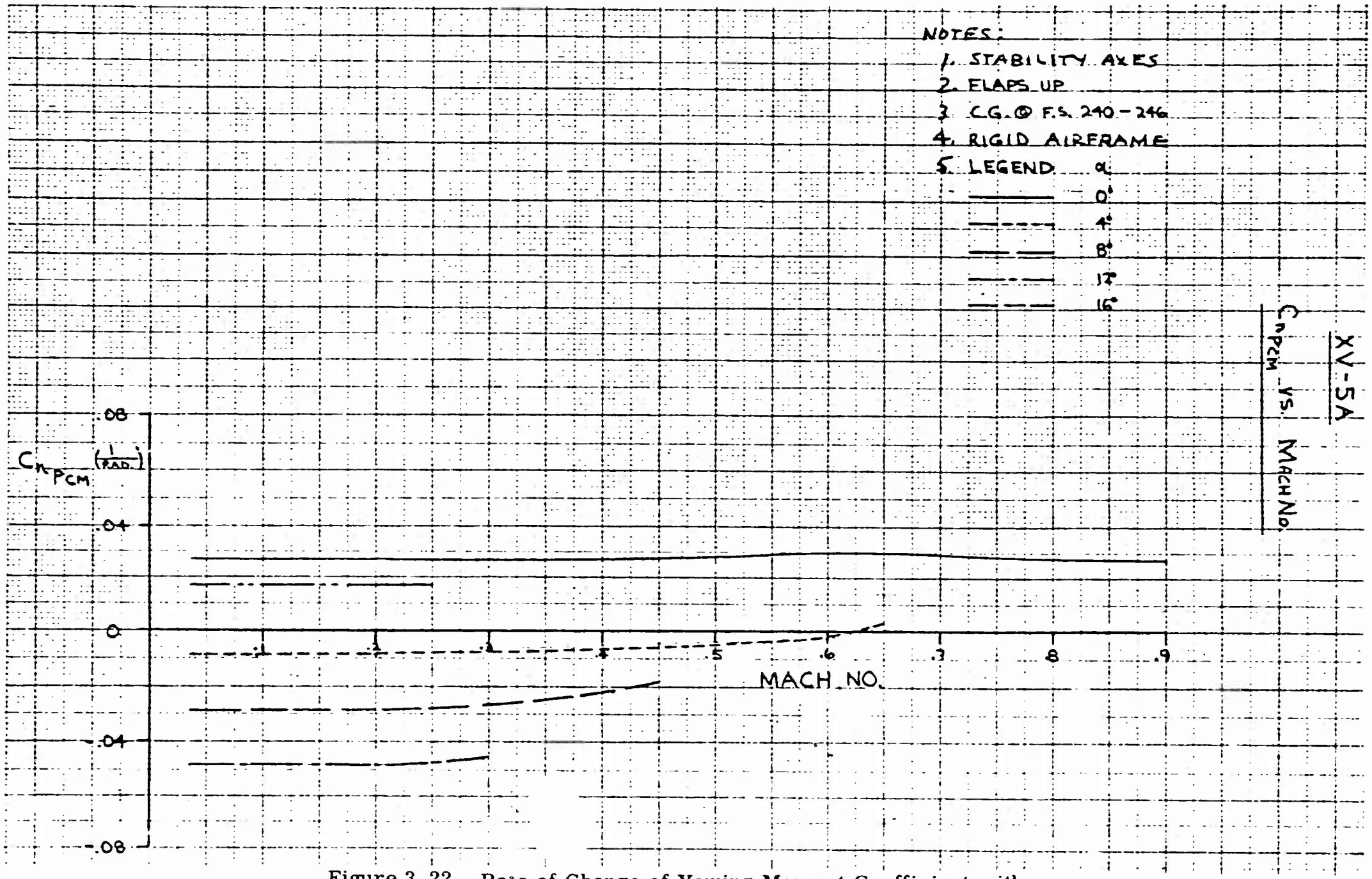

Figure 3.22 Rate of Change of Yawing Moment Coefficient with Rolling Velocity, $C_{n_{p_{CM}}}$, vs Mach No.

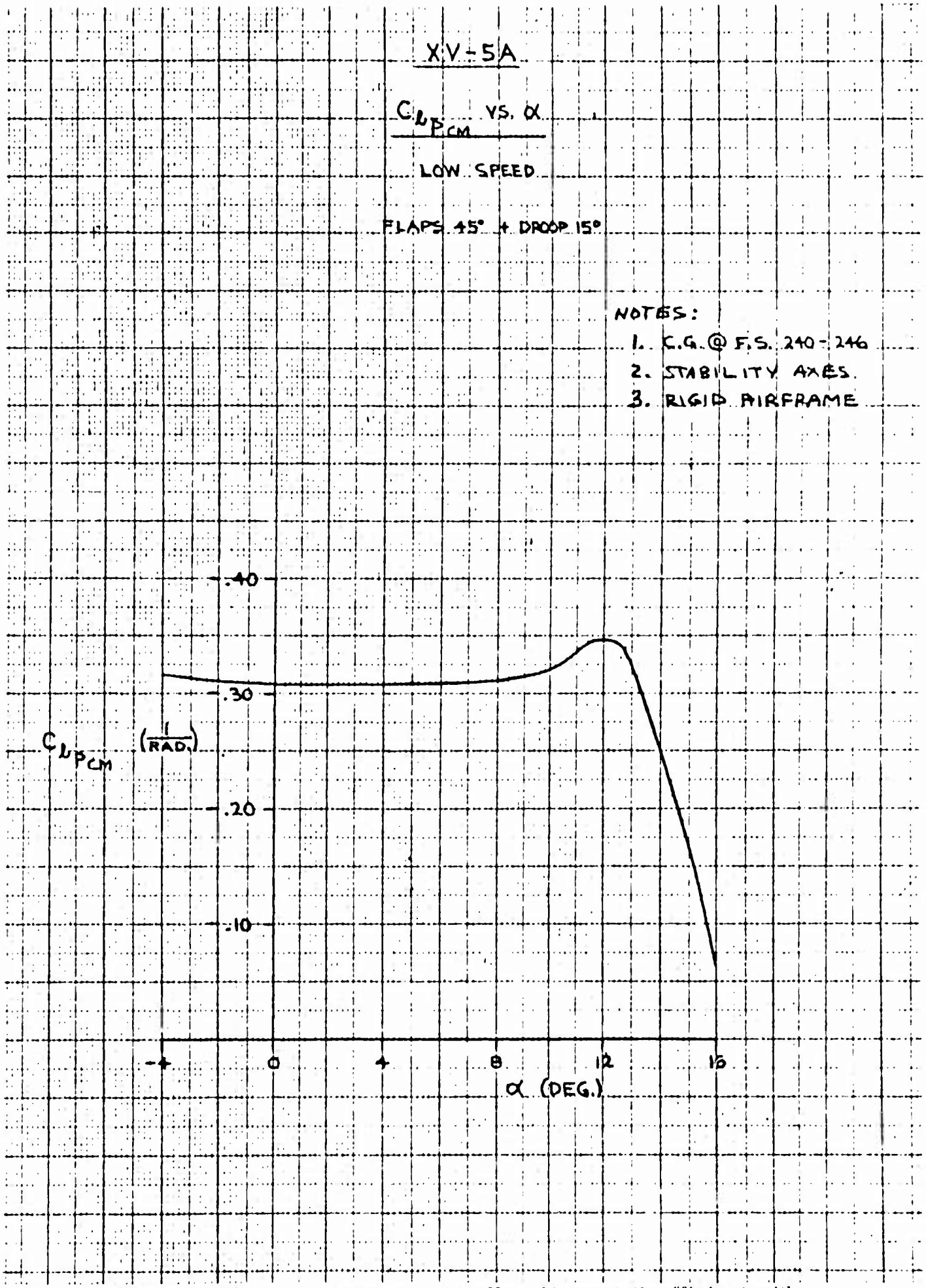

Figure 3.23 Rate of Change of Rolling Moment Coefficient with Rolling Velocity, $C_{\ell_{P_{CM}}}$, vs Angle of Attack.

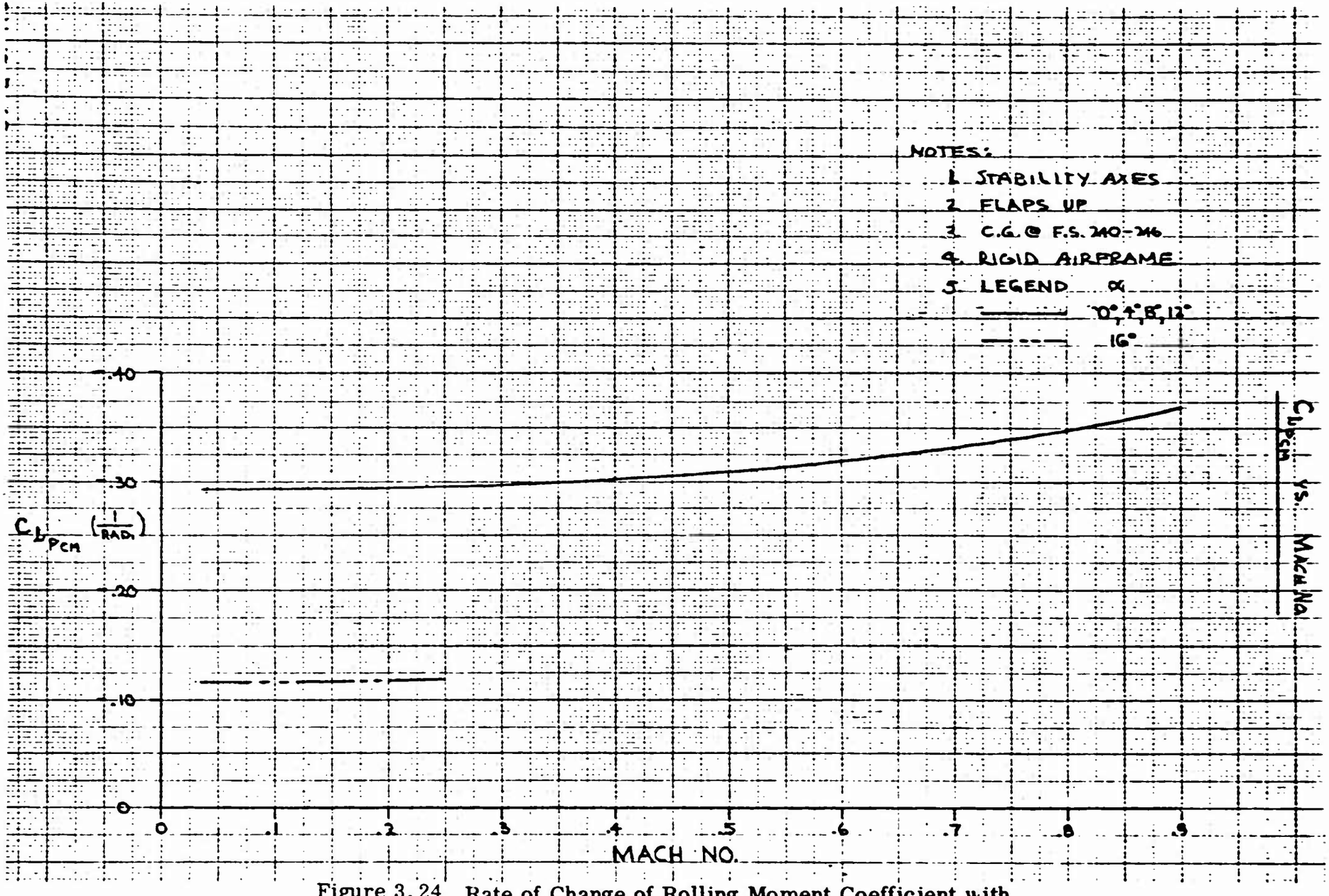

Figure 3.24 Rate of Change of Rolling Moment Coefficient with Rolling Velocity, $C_{\ell_{P_{CM}}}$, vs Mach No.

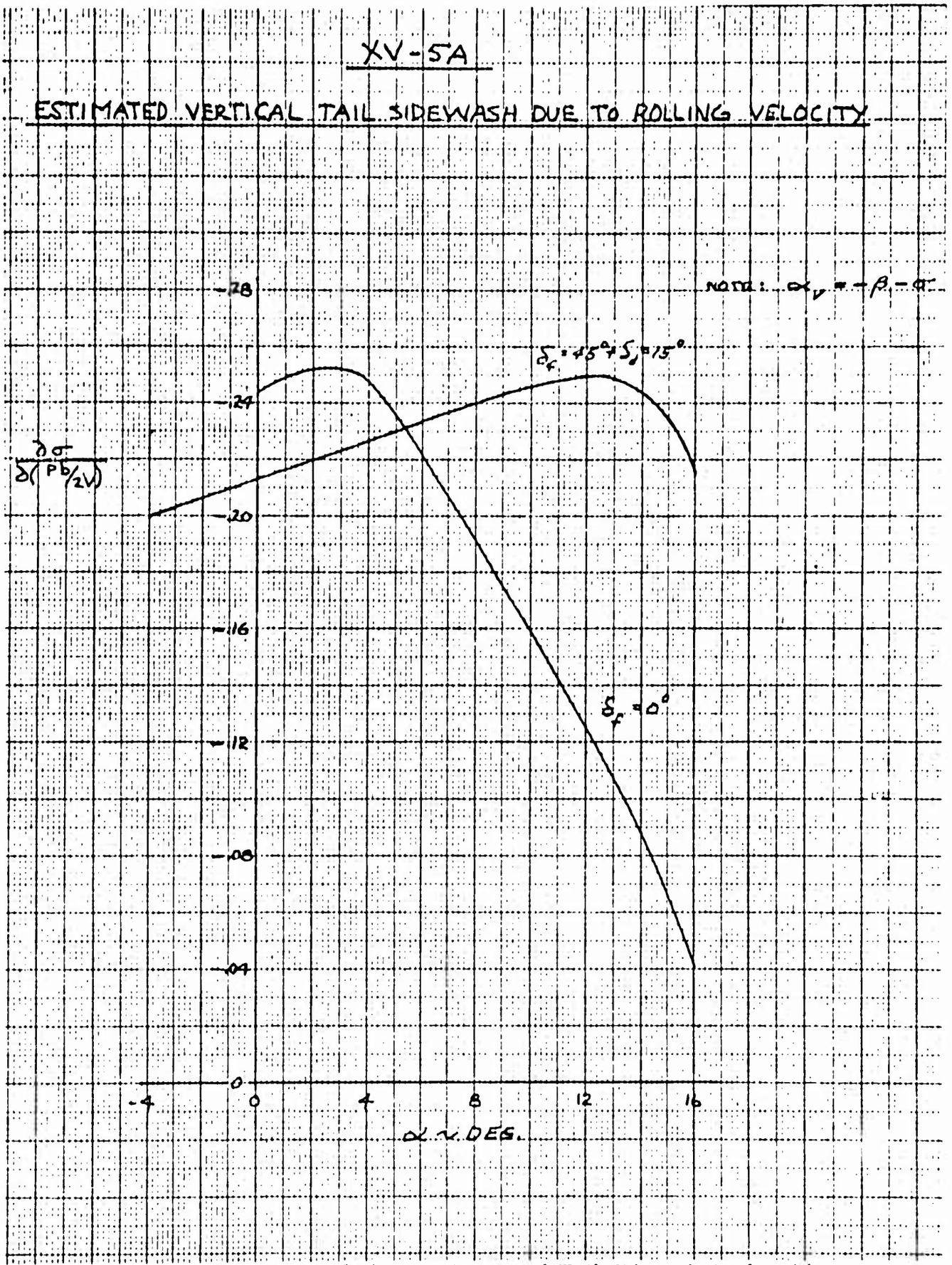

Firgure 3.25 Rate of Change of Vertical Tail Sidewash Angle with Rolling Velocity, $\frac{\partial \sigma}{\partial (pb/2V)}$, vs Angle of Attack.

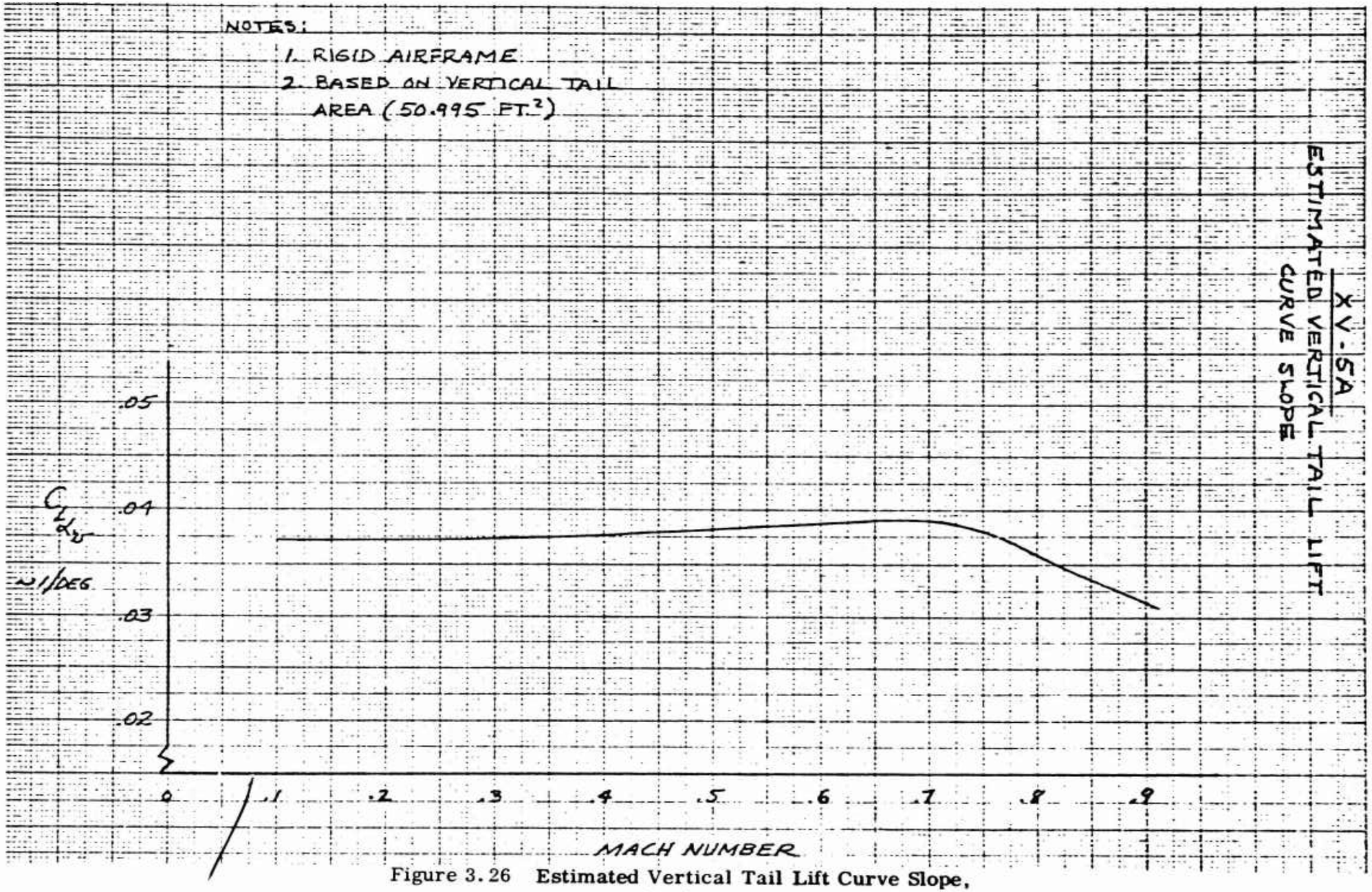

Figure 3.26 Estimated Vertical Tail Lift Curve Slope, $C_{L_{\alpha_v}}$, vs Mach No.

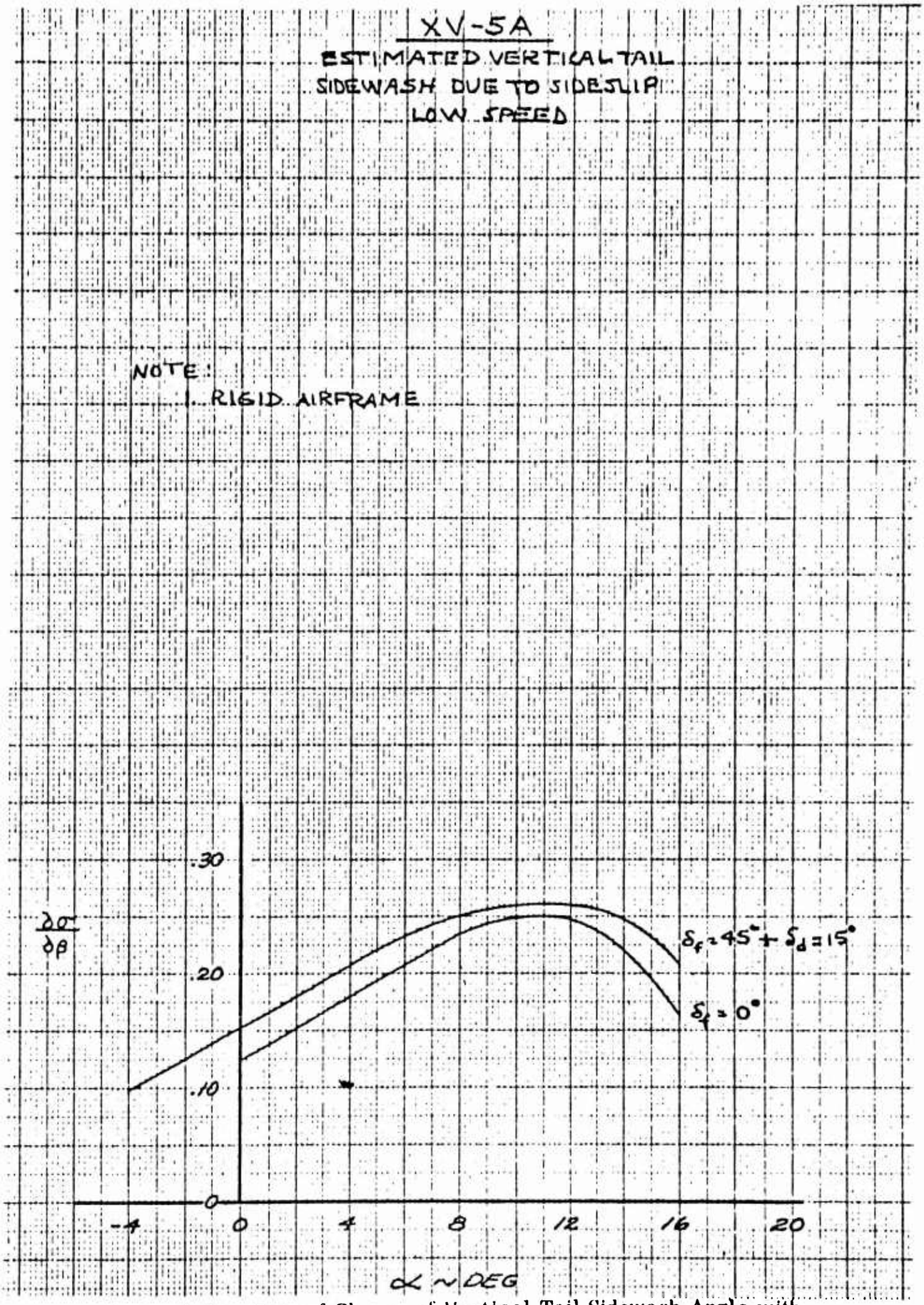

Figure 3.27 Rate of Change of Vertical Tail Sidewash Angle with Sideslip Angle, $\frac{\partial \sigma}{\partial \beta}$, vs Angle of Attack.

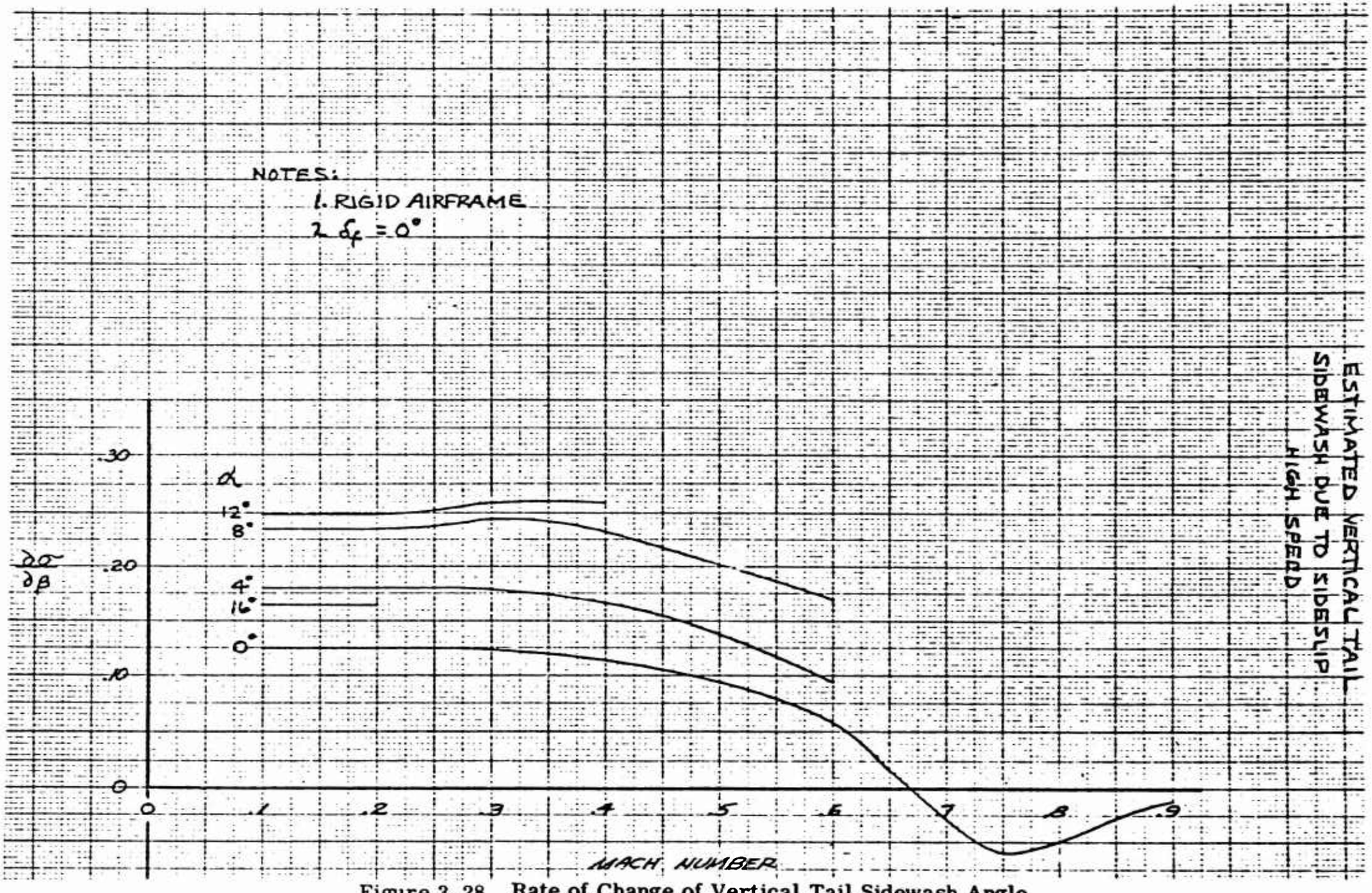

Figure 3.28 Rate of Change of Vertical Tail Sidewash Angle with Sideslip Angle, $\frac{\partial\sigma}{\partial\beta}$, vs Mach No.

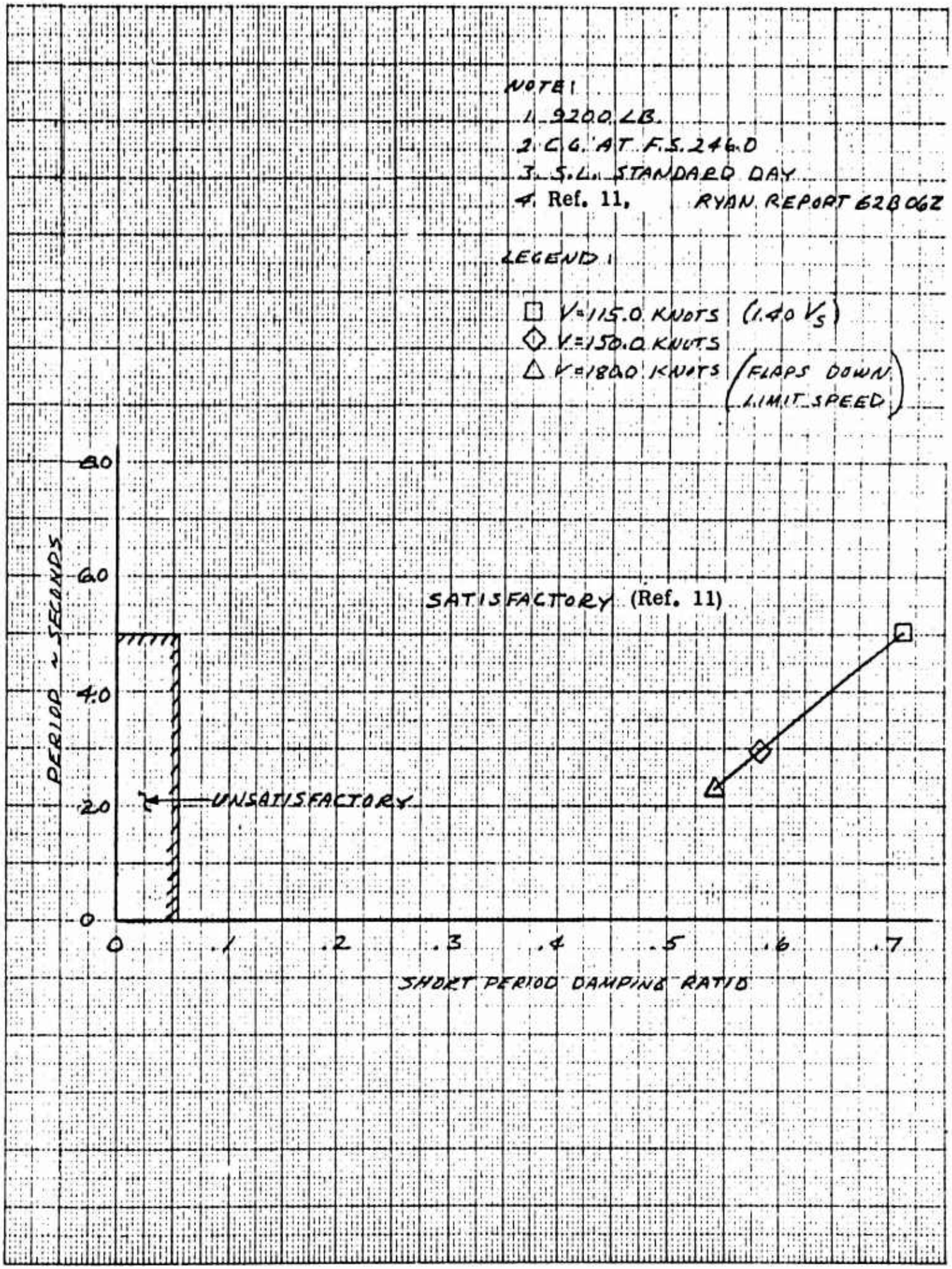

Figure 3.29 Longitudinal Dynamic Stability - Short Period Mode. $\delta_f = 45° + \delta_d = 15°$.

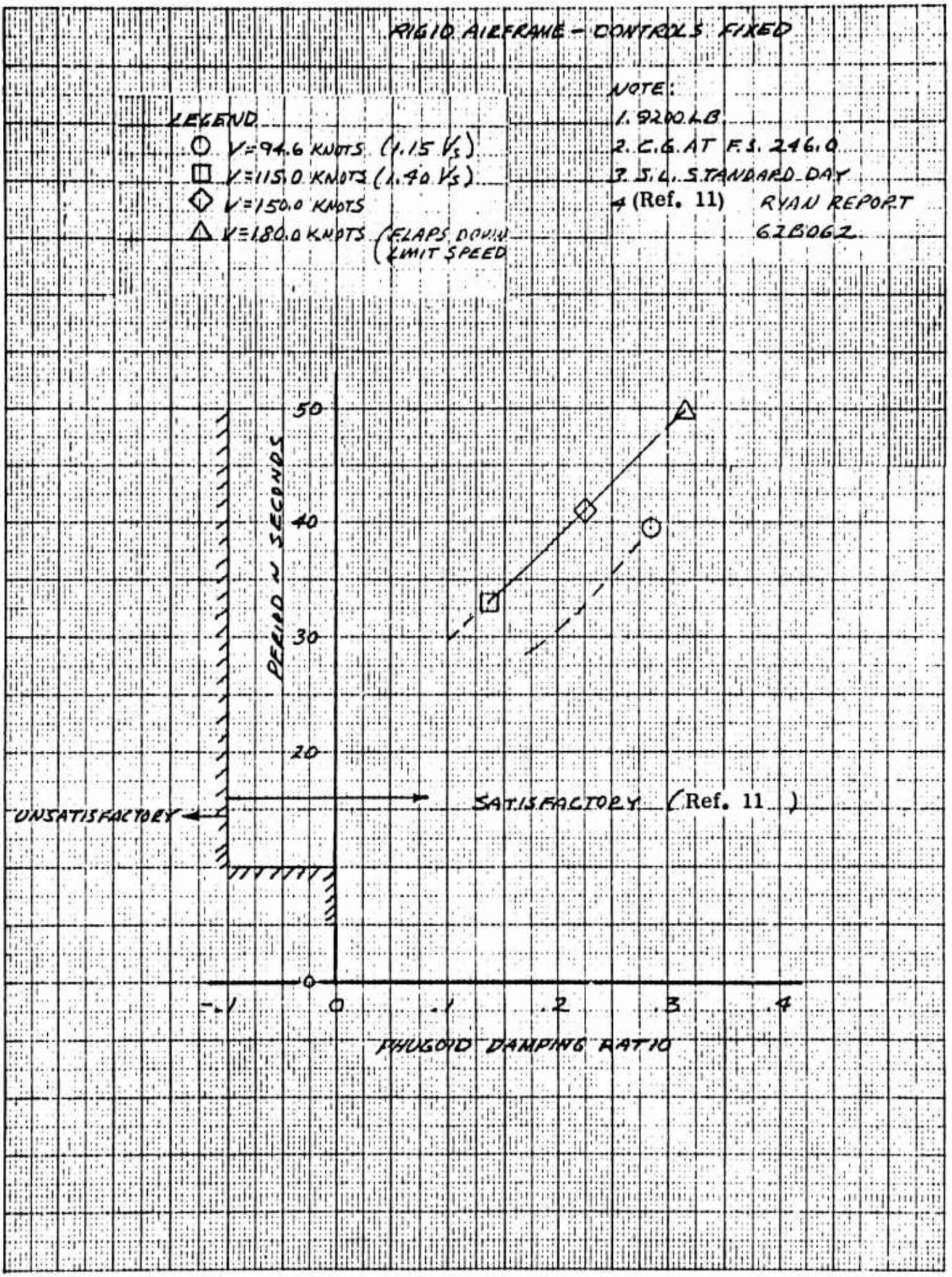

Figure 3.30 Longitudinal Dynamic Stability - Phugoid Mode.
$\delta_f = 45° + \delta_d = 15°$.

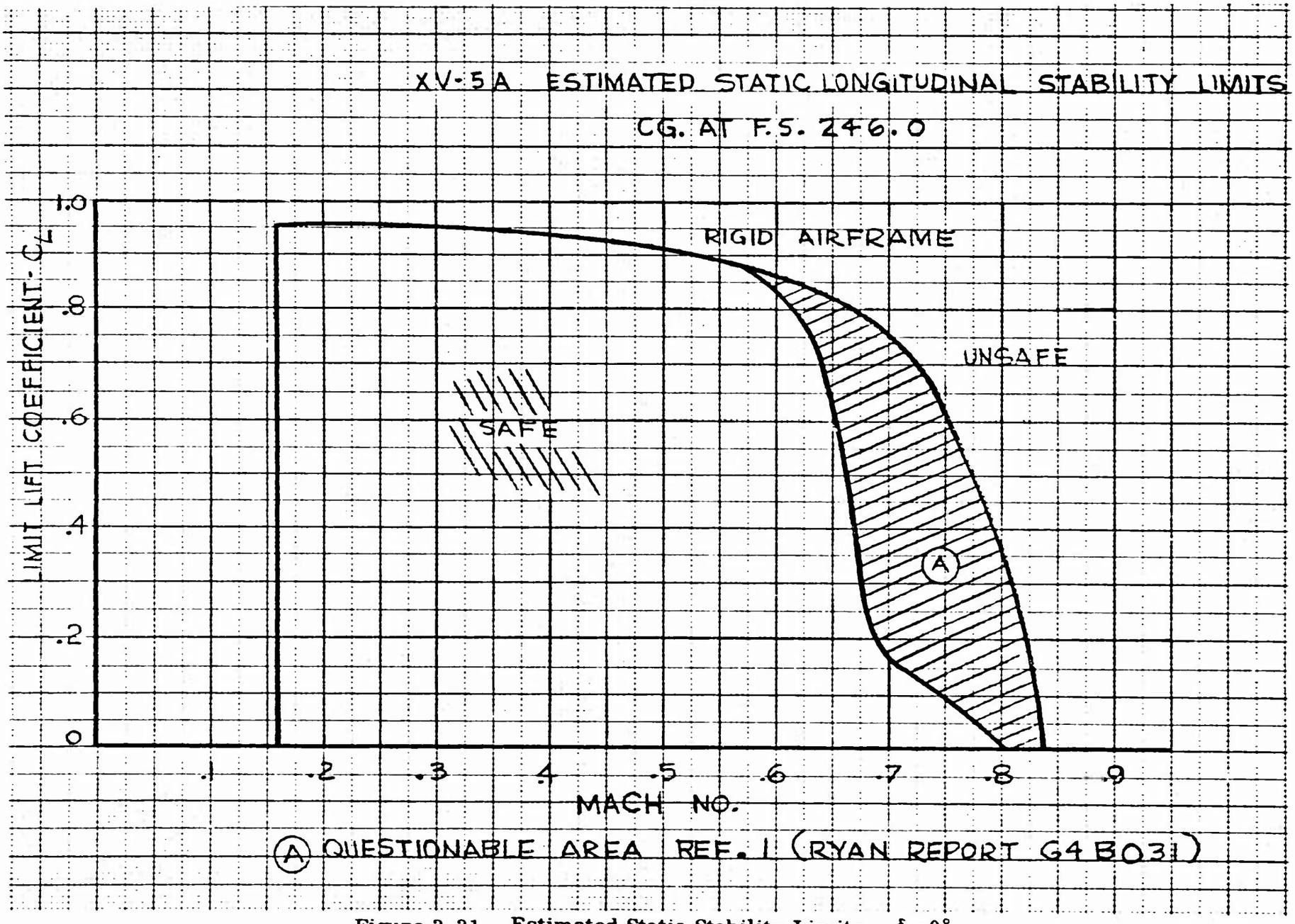

Figure 3.31 Estimated Static Stability Limits. $\delta_f = 0°$

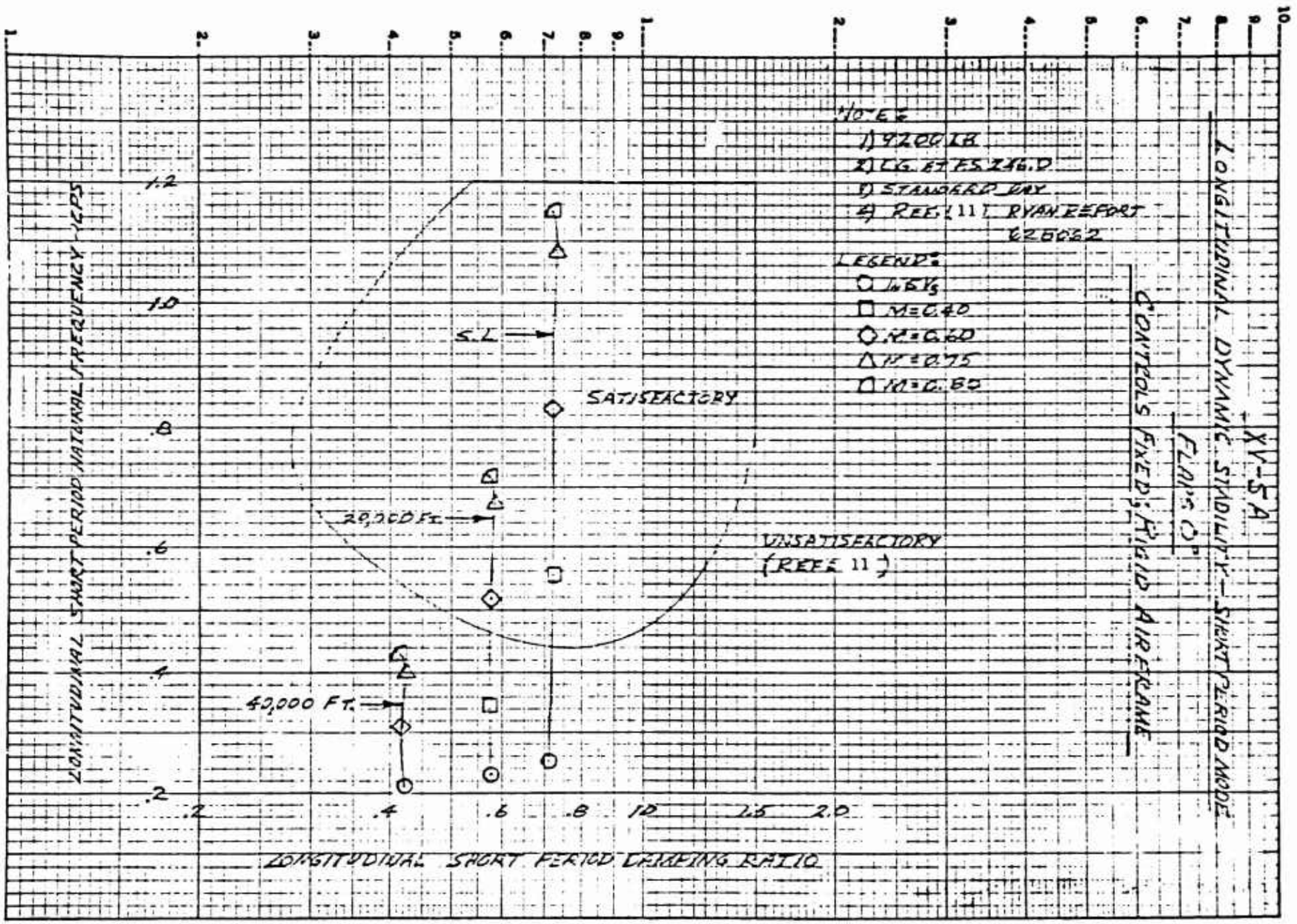

Figure 3.32 Longitudinal Dynamic Stability - Short Period Mode. $\delta_f = 0°$.

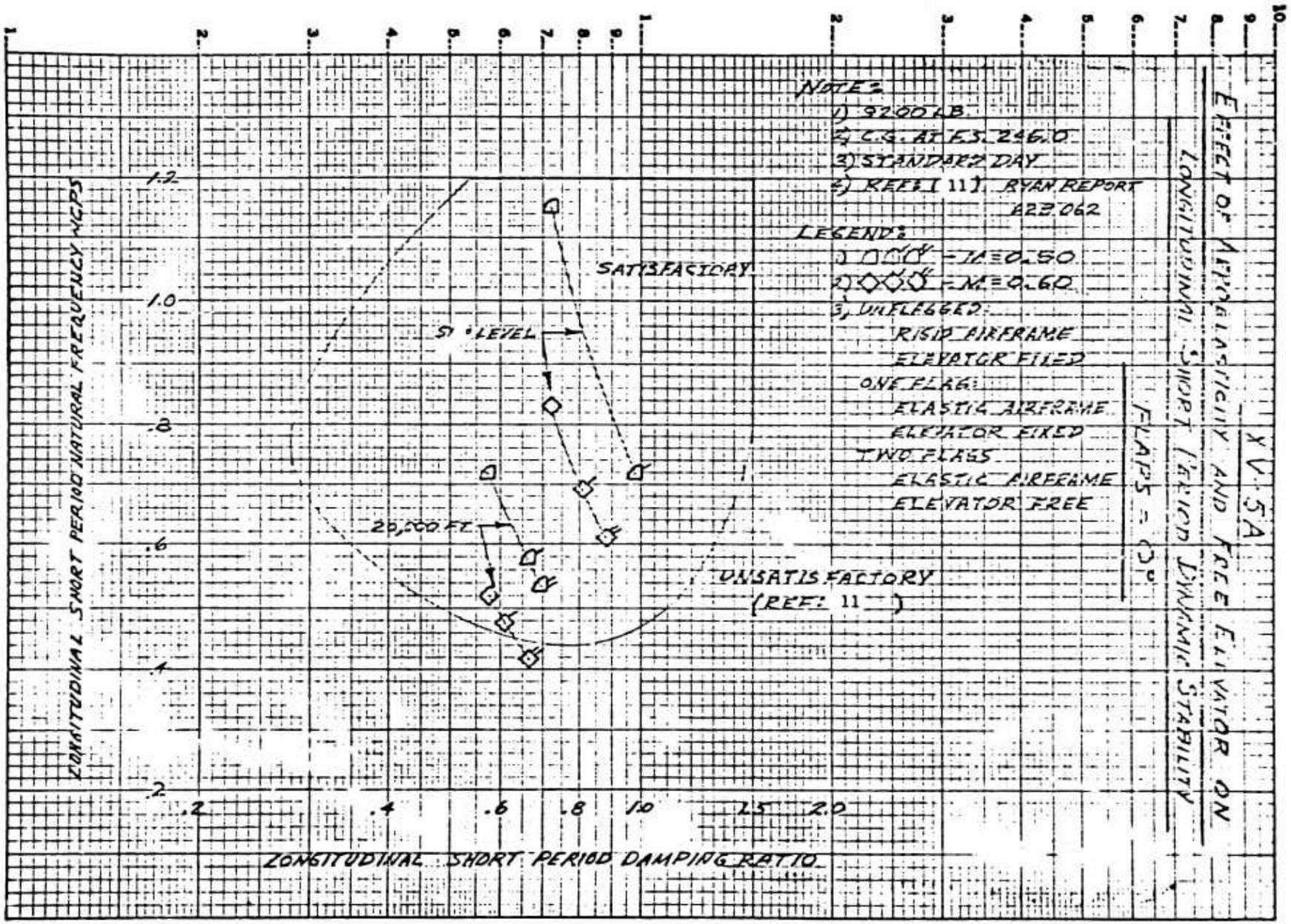

Figure 3.33 Effect of Aeroelasticity and Free Elevator on Longitudinal Short Period Dynamic Stability. $\delta_f = 0°$.

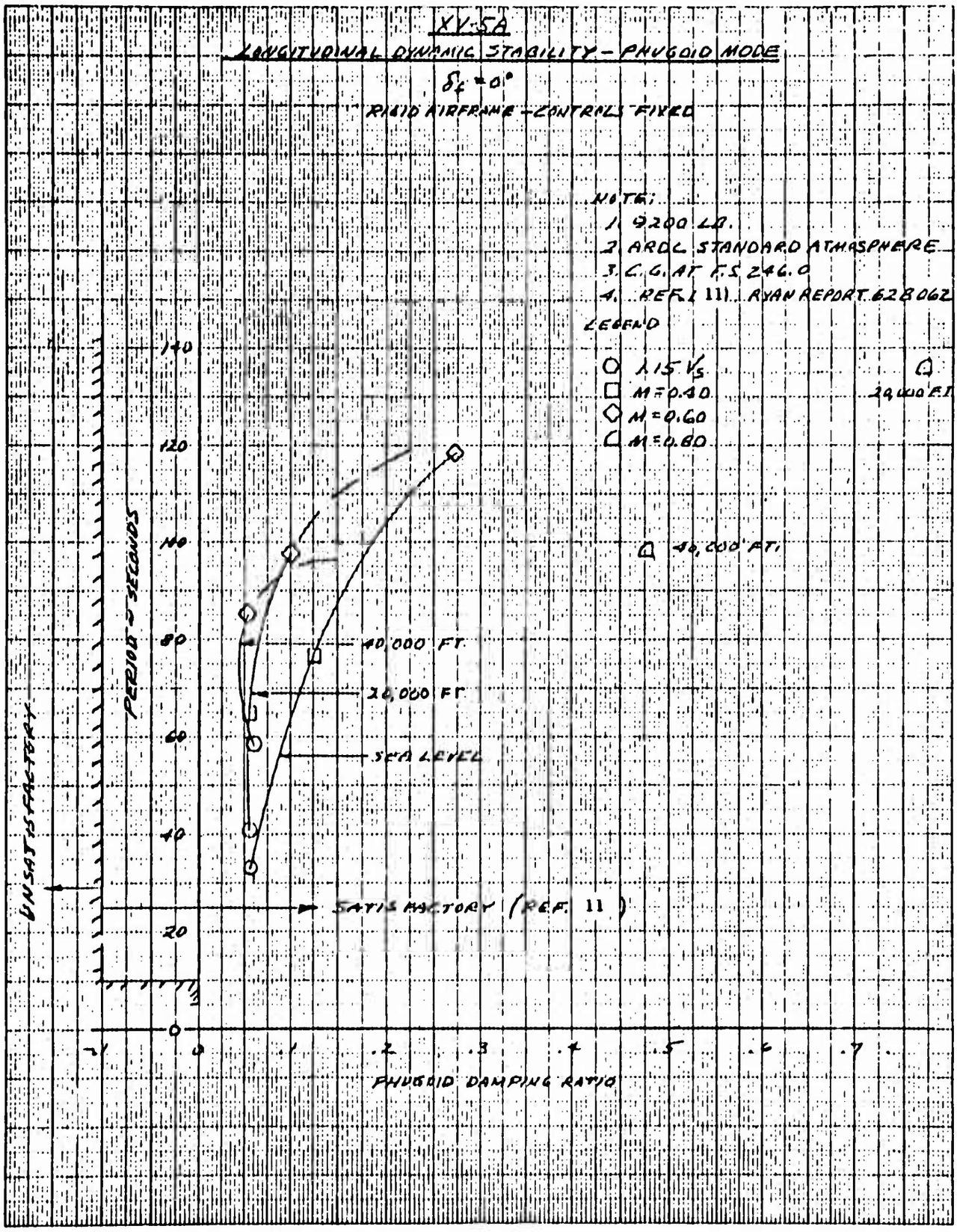

Figure 3.34 Longitudinal Dynamic Stability - Phugoid Mode. $\delta_f = 0°$.

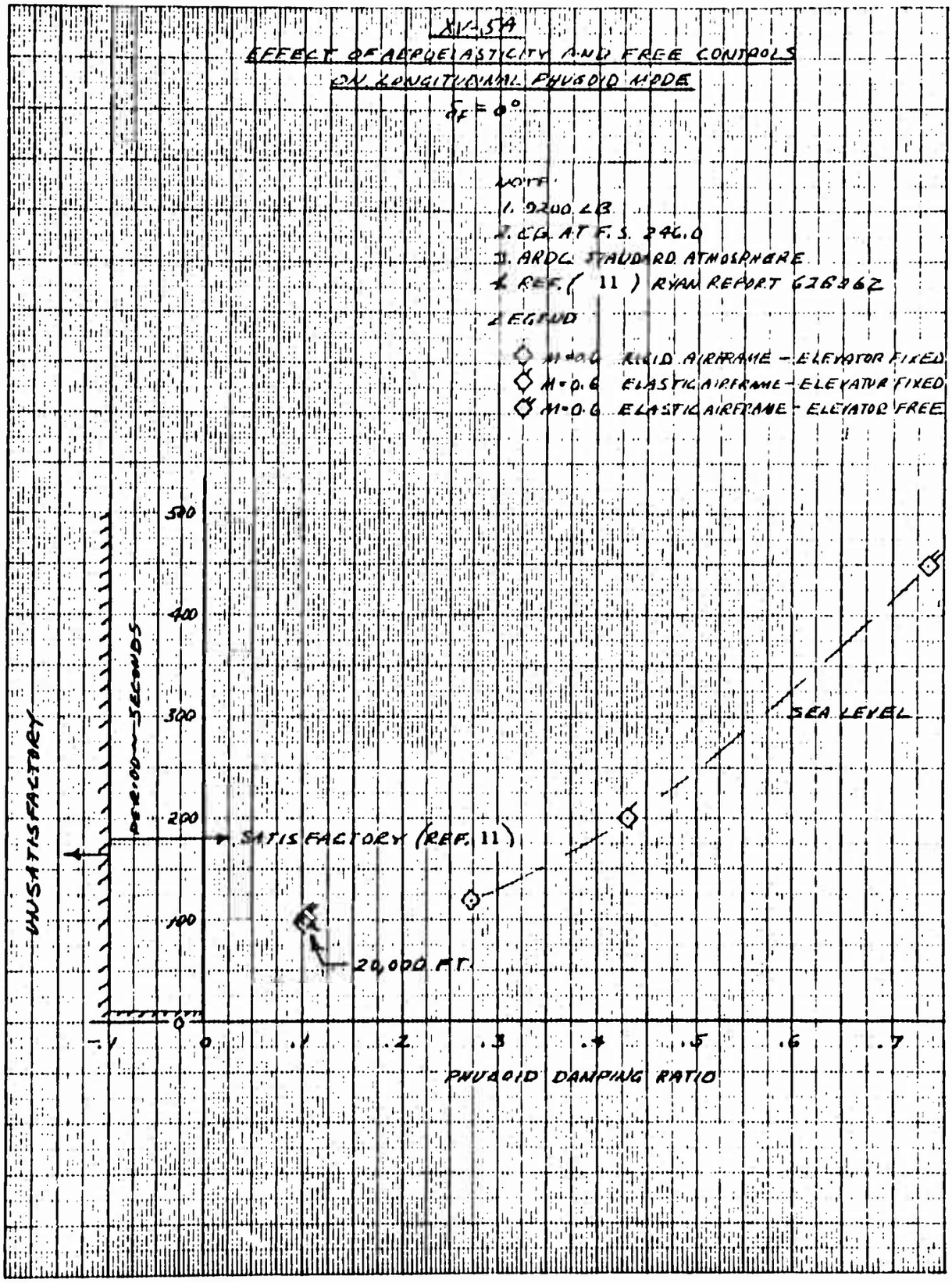

Figure 3.35 Effect of Aeroelasticity and Free Controls on Longitudinal Phugoid Mode. $\delta_f = 0°$.

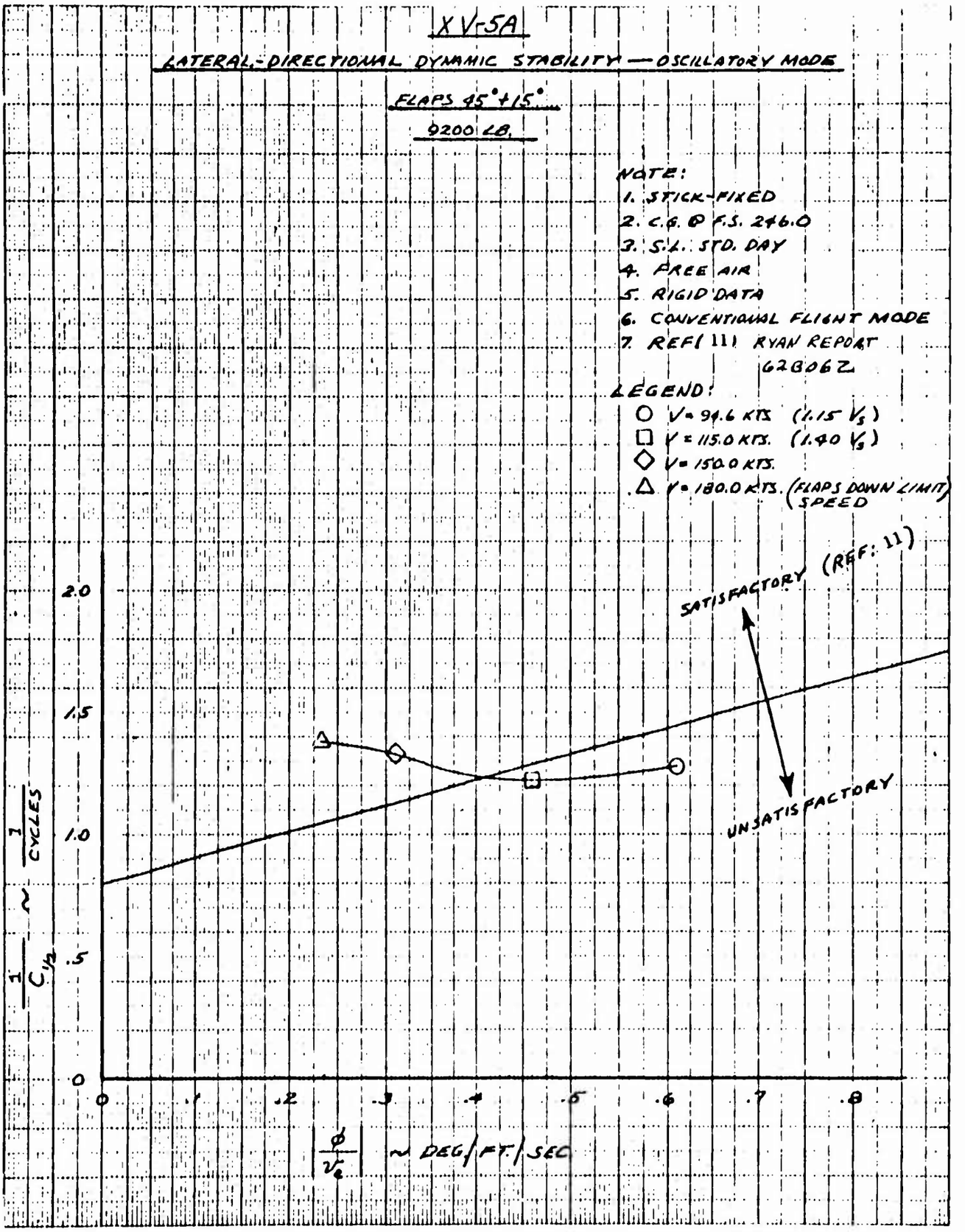

Figure 3.36 Lateral-Directional Dynamic Stability - Oscillatory Mode. δ_f 45° + δ_d 15°.

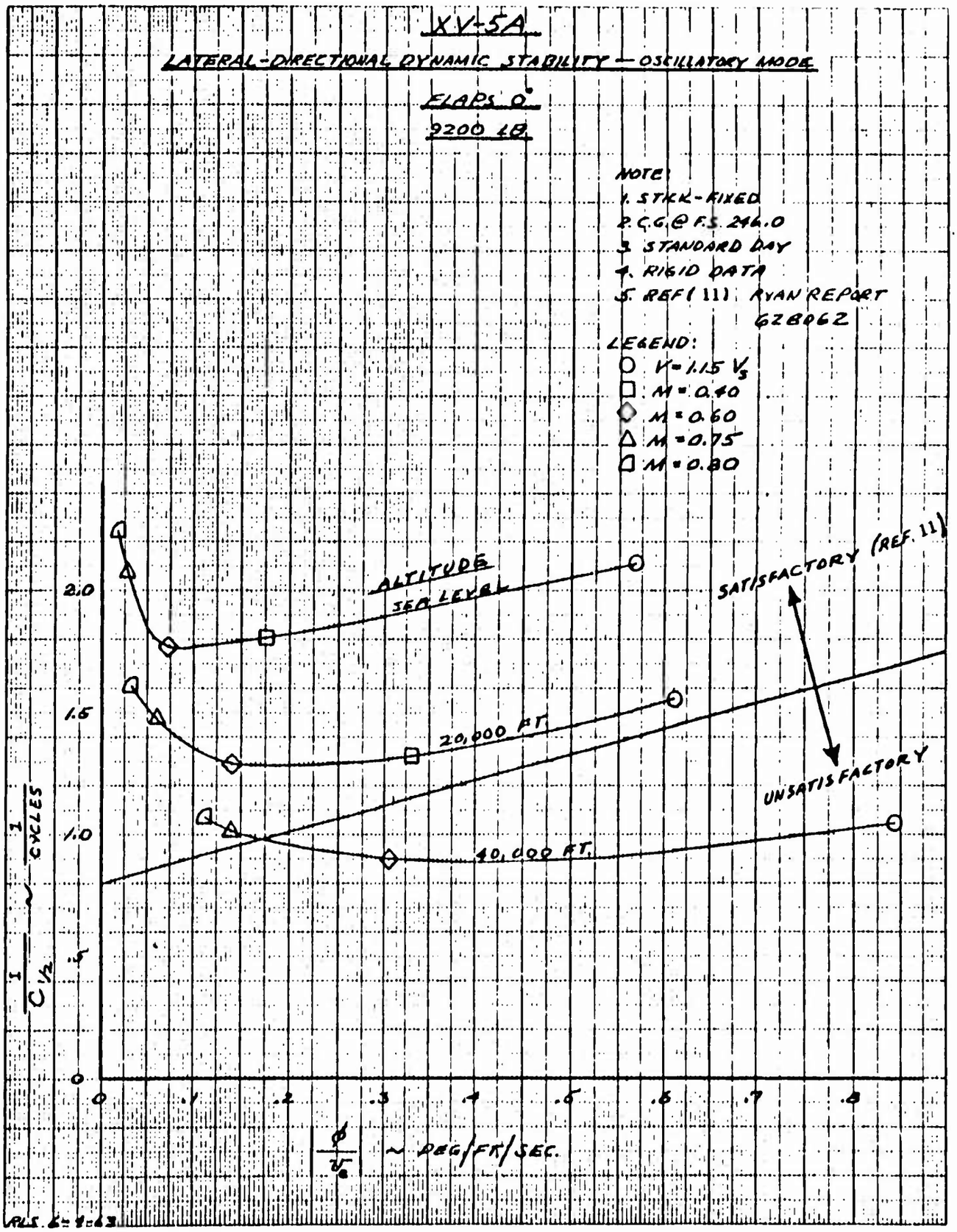

Figure 3.37 Lateral-Directional Dynamic Stability - Oscillatory Mode. $\delta_f = 0°$.

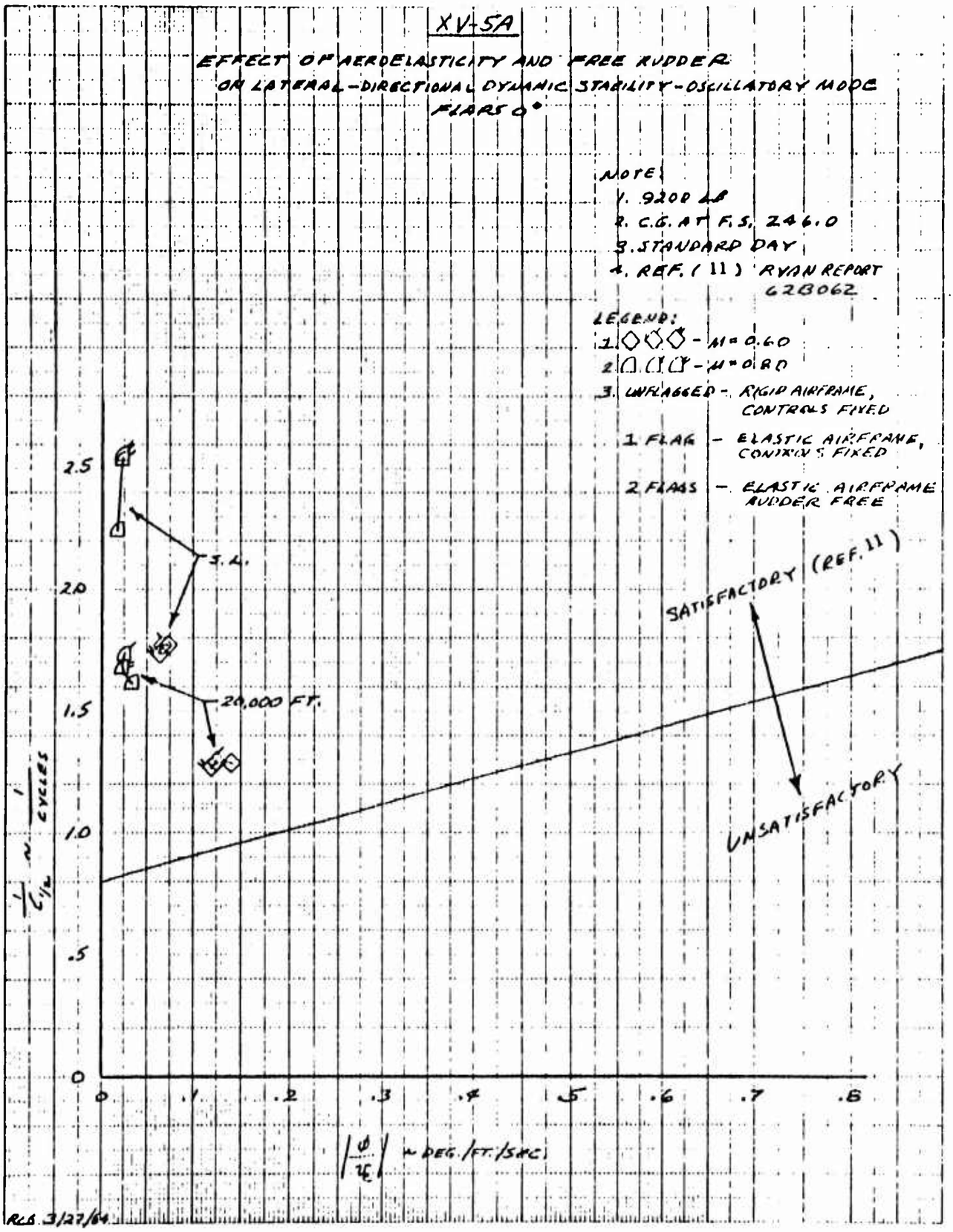

Figure 3.38 Effect of Aeroelasticity and Free Rudder on Laterai-Directional Dynamic Stability - Oscillatory Mode. $\delta_f = 0°$.

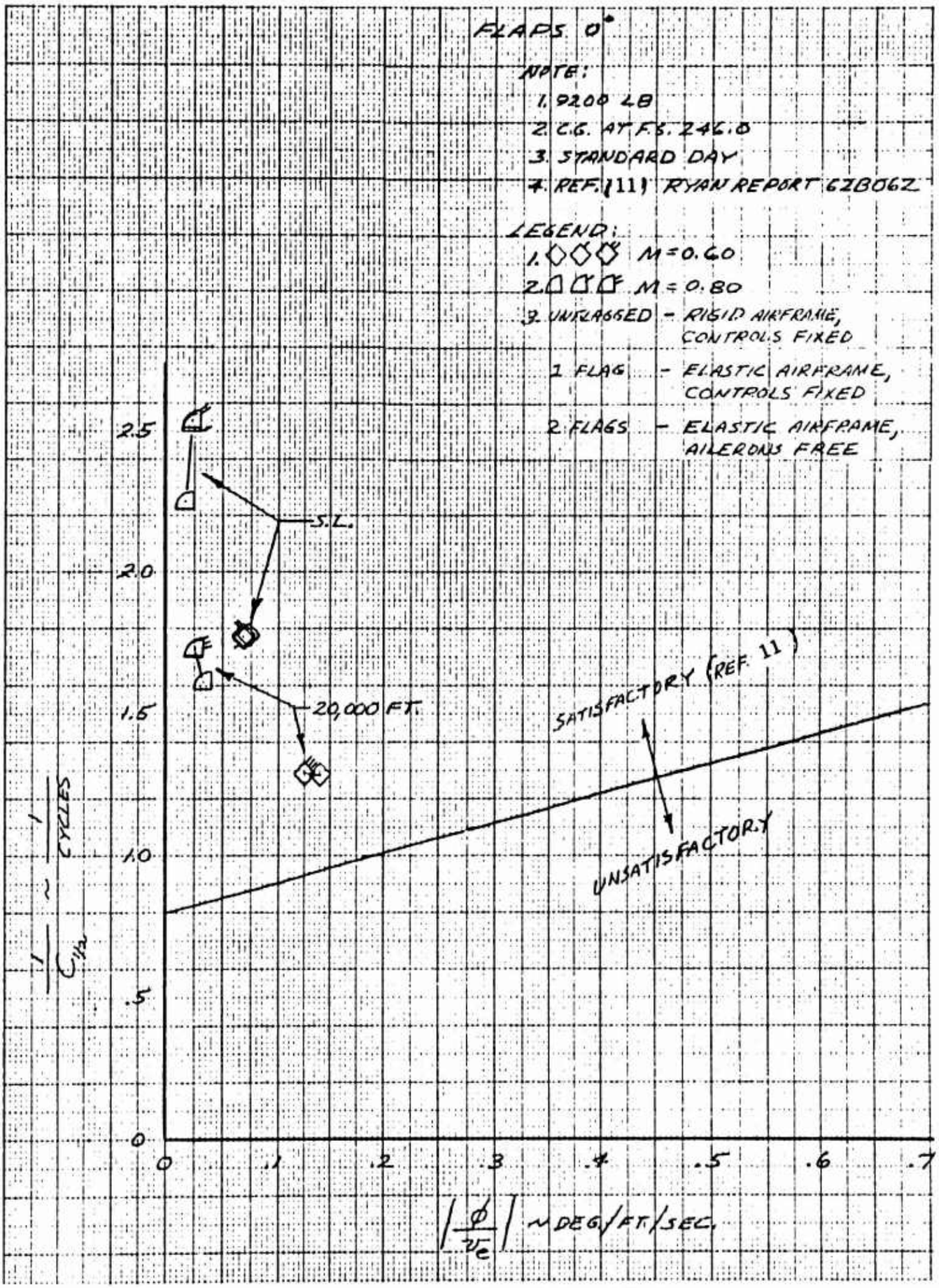

Figure 3.39 Effect of Aeroelasticity and Free Ailerons on Lateral-Directional Dynamic Stability - Oscillatory Mode. δ_f 0°.

TABLE 3.1

Elastic Ratios Model Minus Tail (Elastic Wing-Rigid Body)

ARDC Standard Atmosphere

Elastic Ratio	M=0.30 S. L.	M=0.60 S. L.	M=0.80 S. L.	M=0.30 20,000 FT.	M=0.60 20,000 FT.	M=0.80 20,000 FT.
$^{*}\alpha_{OL}/\alpha_{OL}$	0.984	0.935	0.805	0.993	0.970	0.915
$^{*}C_{m_{OL}}/C_{m_{OL}}$	0.980	0.923	0.955	0.990	0.965	0.979
$^{*}C_{L_{\alpha}}/C_{L_{\alpha}}$	1.003	1.011	1.019	1.001	1.005	1.009
$^{*}C_{m_{\alpha}}/C_{m_{\alpha}}$ (CG at F.S. 240.0)	0.996	0.985	0.984	0.998	0.993	0.993
$^{*}C_{m_{\alpha}}/C_{m_{\alpha}}$ (CG at F.S. 246.0)	0.999	0.995	0.994	0.999	0.998	0.997
$^{*}C_{\ell_p}/C_{\ell_p}$	0.997	0.985	0.974	0.999	0.994	0.988
$^{*}C_{\ell_{\delta_a}}/C_{\ell_{\delta_a}}$	0.964	0.850	0.732	0.982	0.931	0.875

TABLE 3.2

Elastic Ratios Empennage (Elastic Empennage-Elastic Body)

ARDC Standard Atmosphere

Elastic Ratio	M=0.30 S.L.	M-0.60 S.L.	M=0.80 S.L.	M=0.30 20,000 FT.	M=0.60 20,000 FT.	M=0.80 20,000 FT.
$*C_{L_\alpha}/C_{L_\alpha}$ HT (VT, B)	0.966	0.865	0.745	0.984	0.933	0.864
$*C_{L_{\delta_e}}/C_{L_{\delta_e}}$ HT (VT, B)	0.936	0.777	0.647	0.970	0.887	0.806
$*C_{y_\beta}/C_{y_\beta}$ VT (HT, B)	0.974	0.898	0.868	0.988	0.950	0.935
$*C_{y_p}/C_{y_p}$ VT (HT, B)	0.959	0.845	0.787	0.981	0.924	0.894
$*C_{n_p}/C_{n_p}$ VT (HT, B)	0.960	0.845	0.788	0.981	0.925	0.907
$*C_{y_{\delta_r}}/C_{y_{\delta_r}}$ VT (HT, B)	0.954	0.836	0.795	0.979	0.920	0.898
$*C_{n_{\delta_r}}/C_{n_{\delta_r}}$ VT (HT, B)	0.961	0.858	0.820	0.982	0.931	0.911
$*C_{\ell_{\delta_r}}/C_{\ell_{\delta_r}}$ VT (HT, B)	0.950	0.822	0.781	0.977	0.913	0.891

NOTE: HT (VT, B) - horizontal tail in the presence of the vertical tail and body

VT (HT, B) - vertical tail in the presence of the horizontal tail and body

TABLE 3.3

Elastic Airframe Longitudinal Stability Derivatives

ARDC Standard Atmosphere
$\delta_f = 0°$; cg at F.S. 246.0

NOTE: All values per radian except as noted.

	M=0.6 S.L.	M=0.8 S.L.	M=0.6 20,000 FT.	M=0.8 20,000 FT.
$*\alpha_{OL_{M-T}}$ ~ DEG.	-1.40	-0.89	-1.46	-1.01
$*C_{m_{OL_{M-T}}}$	-0.042	-0.052	-0.044	-0.053
$*C_{L_{\alpha_{M-T}}}$	3.26	3.27	3.24	3.24
$*C_{m_{\alpha_{M-T}}}$	0.538	0.540	0.541	0.544
$*C_{L_{\delta_e}}$	-0.206	-0.138	-0.237	-0.1735
$*C_{m_{\delta_e}}$	-0.466	-0.318	-0.532	-0.397
$*C_{L_{\alpha_{CM}}}$	3.57	3.55	3.57	3.55
$*C_{m_{\alpha_{CM}}}$	-0.1205	-0.0435	-0.169	-0.132
$*C_{L_{q_{CM}}}$	2.72	2.52	2.88	2.81
$*C_{m_{q_{CM}}}$	-5.41	-4.96	-5.78	-5.66
$*C_{L_{\dot{\alpha}_{CM}}}$	0.853	0.795	0.923	0.923
$*C_{m_{\dot{\alpha}_{CM}}}$	-1.867	-1.74	-2.02	-2.02
$*C_{L_{u_{CM}}}$	0	-0.148	0	-0.192
$*C_{m_{u_{CM}}}$	0	-0.00085	0	-0.0022
$*C_{D_{u_{CM}}}$	0	0.063	0	0.062
$*C_{D_{\alpha_{CM}}}$	0.065	0.0788	0.1303	0.1303

TABLE 3.4

Elastic Airframe Lateral-Directional Stability Derivatives

ARDC Standard Atmosphere
$\delta_f=0°$, cg at F.S. 246.0
Trimmed Level Flight at 9200 Pounds

NOTE: All values per radian

	M=0.60 S.L.	M=0.80 S.L.	M=0.60 20,000 FT.	M=0.80 20,000 FT.
$*C_{y_{\beta_{CM}}}$	-0.927	-0.808	-0.950	-0.830
$*C_{n_{\beta_{CM}}}$	0.1345	0.0573	0.149	0.0715
$*C_{\ell_{\beta_{CM}}}$	-0.0423	0.003	-0.0475	-0.002
$*C_{y_{r_{CM}}}$	0.522	0.426	0.550	0.460
$*C_{n_{r_{CM}}}$	-0.328	-0.279	-0.348	-0.301
$*C_{\ell_{r_{CM}}}$	0.122	0.108	0.128	0.115
$*C_{y_{p_{CM}}}$	-0.027	-0.020	-0.032	-0.026
$*C_{n_{p_{CM}}}$	0.024	0.021	0.027	0.025
$*C_{\ell_{p_{CM}}}$	-0.313	-0.337	-0.317	-0.343
$*C_{y_{\delta_r}}$	0.0895	0.0550	0.0985	0.0620
$*C_{n_{\delta_r}}$	-0.058	-0.037	-0.063	-0.041
$*C_{\ell_{\delta_r}}$	0.012	0.007	0.013	0.008
$*C_{\ell_{\delta_a}}$	0.0365	0.0198	0.040	0.0236

TABLE 3.5

Estimated Control Surface Hinge Moment Derivatives

Elevator			Rudder		
Mach No.	0.6	0.8	Mach No.	0.6	0.8
$C_{h_{e_{\delta_e}}}$	-0.400	-0.513	$C_{h_{r_{\delta_r}}}$	-0.350	-0.364
$C_{h_{e_{\dot{\delta}_e}}}$	-4.617	-4.648	$C_{h_{r_{\dot{\delta}_r}}}$	-4.740	-4.625
$C_{h_{e_\alpha}}$	-0.0355	-0.031	$C_{h_{r_\beta}}$	-0.047	-0.063
$C_{h_{e_{\dot{\alpha}}}}$	-0.857	-0.777	$C_{h_{r_{\dot{\beta}}}}$	0.078	-0.104
$C_{h_{e_q}}$	-2.170	-1.920	$C_{h_{r_r}}$	1.333	2.070
$C_{h_{e_{\dot{q}}}}$	0	0	$C_{h_{r_{\dot{r}}}}$	0	0
$C_{h_{e_u}}$	$\cong 0$	$\cong 0$	$C_{h_{r_p}}$	$\cong 0$	$\cong 0$
			$C_{h_{r_{\dot{p}}}}$	0	0

Aileron Tab					
Mach No.	0.6	0.8	Mach No.	0.6	0.8
$C_{h_{t_{\delta_t}}}$	-0.320	-0.298	$C_{h_{t_{\delta_a}}}$	0.132	0.132
$C_{h_{t_{\dot{\delta}_t}}}$	-4.070	-4.070	$C_{h_{t_{\dot{\delta}_a}}}$	0.910	0.910
$C_{h_{t_\alpha}}$	0.0344	0.0344	$C_{h_{t_r}}$	$\cong 0$	$\cong 0$
$C_{h_{t_\beta}}$	-0.0048	-0.0048	$C_{h_{t_{\dot{r}}}}$	0	0
$C_{h_{t_{\dot{\beta}}}}$	0	0	$C_{h_{t_p}}$	-3.180	-3.180
			$C_{h_{t_{\dot{p}}}}$	0	0

NOTE: 1) Rigid Control System
2) cg at F.S. 246.0

TABLE 3.6

Miscellaneous XV-5A Constants

I_{x_B}	=	4,252 slug-ft^2	Mass moment of inertia about the body X axis at 9200 lb.
I_{y_B}	=	15,139 slug-ft^2	Mass moment of inertia about the body Y axis at 9200 lb.
I_{z_B}	=	17,418 slug-ft^2	Mass moment of inertia about the body Z axis at 9200 lb.
I_{xz}	=	919 slug-ft^2	Product of inertia at 9200 lb.
I_e	=	0.176 slug-ft^2	Elevator mass moment of inertia about the hinge line.
I_r	=	0.260 slug-ft^2	Rudder mass moment of inertia about the hinge line.
I_t	=	0.004 slug-ft^2	Aileron tab mass moment of inertia about the tab hinge line.
Z_T	=	0	Moment arm of thrust axis about the C.G. at F.S. 246.0.
i_T	=	6.5°	Thrust incidence angle with respect to the body X axis.
$\frac{d\,\delta_a}{d\,\delta_t}$	=	-2.0 deg./deg.	Aileron to aileron tab gearing.

TABLE 3.7

Results of Longitudinal Dynamic Stability Investigations

9200 Pounds
cg at F.S. 246.0
ARDC Standard Atmosphere
Rigid Airframe
Controls Fixed

$\delta_f = 0°$

M	Altitude ~ft.	Roots of Characteristic Equation	ω_n ~rad/sec	ξ	$T_{1/2}$ or T_2 ~sec	P ~sec
0.177	S. L.	-1.120 ± j 1.111	1.578	0.710	0.619	5.75
		-0.0107 ± j 0.191	0.192	0.056	64.8	32.9
0.40	S. L.	-2.511 ± j 2.407	3.478	0.722	0.276	2.61
		-0.0103 ± j 0.0821	0.083	0.125	67.3	76.5
0.60	S. L.	-3.762 ± j 3.608	5.213	0.722	0.184	1.74
		-0.0150 ± j 0.0531	0.055	0.272	46.0	118.3
0.75	S. L.	-4.974 ± j 4.621	6.790	0.733	0.139	1.36
		-0.104	-	-	6.66	-
		-0.0064	-	-	108.2	-
0.80	S. L.	-5.207 ± j 4.981	7.206	0.723	0.133	1.26
		-0.177	-	-	3.91	-
		-0.0305	-	-	22.7	-
0.261	20,000	-0.822 ± j 1.172	1.431	0.574	0.843	5.35
		-0.0083 ± j 0.153	0.154	.054	83.7	41.0
0.40	20,000	-1.244 ± j 1.765	2.159	0.576	0.557	3.56
		-0.0055 ± j 0.0970	0.098	.056	125.0	64.8
0.60	20,000	-1.865 ± j 2.652	3.243	0.575	0.372	2.37
		-0.0065 ± j 0.0645	0.065	0.100	106.0	97.4

NOTE: T_2 is indicated by a negative value.

TABLE 3.7 (Continued)

M	Altitude ~ft.	Roots of Characteristic Equation	ω_n ~rad/sec	ξ	$T_{1/2}$ or T_2 ~sec	P ~sec
0.75	20,000	-2.469 ± j 3.412	4.212	0.586	0.281	1.84
		-0.0521	-	-	13.3	-
		-0.0032	-	-	216.5	-
0.80	20,000	-2.583 ± j 3.683	4.498	0.574	0.268	1.70
		-0.0560 ± j 0.0463	0.073	0.770	12.4	135.7
0.411	40,000	-0.559 ± j 1.204	1.327	0.421	1.241	5.22
		-0.0064 ± j 0.108	0.0109	0.059	108.3	58.2
0.60	40,000	-0.808 ± j 1.761	1.937	0.417	0.858	3.56
		-0.0039 ± j 0.0738	0.074	0.053	177.7	85.2
0.75	40,000	-1.070 ± j 2.271	2.510	0.426	0.648	2.76
		-0.0351	-	-	19.7	-
		+0.0125	-	-	-55.4	-
0.80	40,000	-1.114 ± j 2.452	2.693	0.414	0.622	2.56
		-0.0347 ± j 0.0641	0.073	0.476	20.0	98.0

$\delta_f = 45° + \delta_d = 15°$

V ~KTS						
94.6	S. L.	-0.0474 ± j 0.159	0.166	0.285	14.6	39.5
		-1.468	-	-	0.472	-
		-0.755	-	-	0.918	-
115.0	S. L.	-1.269 ± j 1.250	1.781	0.713	0.546	5.02
		-0.0262 ± j 0.190	0.192	0.136	26.4	33.0
150.0	S. L.	-1.522 ± j 2.120	2.610	0.583	0.455	2.96
		-0.0352 ± j 0.153	0.157	0.224	19.7	41.0
180.0	S. L.	-1.763 ± j 2.741	3.259	0.541	0.393	2.29
		-0.0418 ± j 0.126	0.133	0.315	16.6	49.8

NOTE: T_2 is indicated by a negative value.

TABLE 3.8

Results of Longitudinal Dynamic Stability Investigations

9200 Pounds
cg at F.S. 246.0
ARDC Standard Atmosphere
Elastic Airframe
Controls Fixed

$\delta_f = 0°$

M	Altitude ~ ft.	Roots of Characteristic Equation	ω_n ~rad/sec	ξ	$T_{1/2}$ or T_2 ~sec	P ~sec
0.6	S.L.	-3.487 ± j 2.555	4.323	0.807	0.199	2.46
		-0.0150 ± j 0.0314	0.035	0.431	46.2	200.0
0.8	S.L.	-4.406 ± j 0.931	4.503	0.978	0.157	6.75
		-0.222			3.12	
		+0.0185			-37.5	
0.6	20,000	-1.806 ± j 2.362	2.973	0.607	0.384	2.66
		-0.0065 ± j 0.0644	0.065	0.100	106.6	97.5
0.8	20,000	-2.380 ± j 2.717	3.612	0.659	0.291	2.31
		-0.138			5.02	
		+0.0330			-21.0	

NOTE: T_2 is indicated by a negative value.

TABLE 3.9

Results of Longitudinal Dynamic Stability Investigations

9200 Pounds
cg at F.S. 246.0
ARDC Standard Atmosphere
Elastic Airframe
Elevator Free

$\delta_f = 0°$

M	Altitude ~ft.	Roots of Characteristic Equation	ω_n ~rad/sec	ξ	$T_{1/2}$ or T_2 ~ sec	P ~ sec
0.6	S. L.	-3.372 ± j 1.822	3.832	0.880	0.206	3.45
		-0.0151 ± j 0.0140	0.021	0.734	45.9	448.6
		-77.4 ± j 100.70	126.9	0.610	0.009	0.063
0.8	S. L.	-5.669			0.122	
		-2.996			0.231	
		-0.220			3.150	
		+0.0163			-42.5	
		-103.7 ± j 161.0	191.0	0.543	0.007	0.039
0.6	20,000	-1.742 ± j 1.955	2.619	0.665	0.398	3.21
		-0.0064 ± 0.0625	0.063	0.102	108.3	100.5
		-38.3 ± j 77.0	86.0	0.446	0.018	0.082
0.8	20,000	-2.335 ± j 2.410	3.355	0.696	0.297	2.60
		-0.139			4.99	
		+0.0336			-20.6	
		-51.3 ± j 119.3	159.0	0.322	0.013	0.053

NOTE: T_2 is indicated by a negative value.

TABLE 3.10

Results of Lateral-Directional Dynamic Stability Investigations

9200 Pounds
cg at F.S. 246.0
ARDC Standard Atmosphere
Rigid Airframe
Controls Fixed

$\delta_f = 0°$

M	Altitude ~ft.	Roots of Characteristic Equation	ω_n ~rad/sec	ξ	$T_{1/2}$ or T_2 ~sec	P ~sec	$1/C_{1/2}$ ~1/ cycles	ϕ/v_e ~deg/ ft/sec
0.177	S.L.	-0.514 ± j 2.211	2.270	0.227	1.348	2.84	2.108	0.568
		-1.992			0.348			
		-0.0260			26.7			
0.40	S.L.	-0.789 ± j 3.963	4.041	0.195	0.878	1.59	1.806	0.176
		-4.566			0.152			
		-0.0078			88.8			
0.60	S.L.	-1.188 ± j 6.086	6.201	0.192	0.583	1.033	1.770	0.072
		-7.077			0.098			
		+0.0066			-105.0			
0.75	S.L.	-1.405 ± j 6.138	6.297	0.223	0.493	1.022	2.075	0.028
		-9.244			0.075			
		+0.0061			-113.5			
0.80	S.L.	-1.509 ± j 6.087	6.272	0.241	0.459	1.033	2.247	0.018
		-10.053			0.069			
		+0.0094			-73.8			
0.261	20,000	-0.379 ± j 2.239	2.271	0.167	1.827	2.80	1.536	0.611
		-1.448			0.478			
		-0.0191			36.3			

NOTE: T_2 is indicated by a negative value

TABLE 3.10 (Continued)

M	Altitude ~ ft.	Roots of Characteristic Equation	ω_n ~rad/sec	ξ	$T_{1/2}$ or T_2 ~ sec	P ~ sec	$1/C_{1/2}$ ~1/ cycles	ϕ/v_e ~deg/ ft/sec
0.40	20,000	-0.433 ± j 2.974	3.006	0.144	1.600	2.11	1.320	0.330
		-2.305			0.300			
		-0.0063			110.0			
0.60	20,000	-0.603 ± j 4.254	4.296	0.140	1.149	1.48	1.286	0.139
		-3.563			0.194			
		+0.0029			-239.0			
0.75	20,000	-0.699 ± j 4.281	4.338	0.161	0.991	1.46	1.481	0.061
		-4.637			0.150			
		+0.0063			-110.0			
0.80	20,000	-0.761 ± j 4.287	4.354	0.175	0.911	1.46	1.609	0.033
		-5.031			0.138			
		+0.0096			-72.2			
0.411	40,000	-0.307 ± j 2.663	2.681	0.115	2.257	2.36	1.045	0.842
		-0.943			0.735			
		-0.052			13.3			
0.60	40,000	-0.299 ± j 3.011	3.026	0.099	2.317	2.08	0.901	0.306
		-1.572			0.440			
		+0.0028			-247.0			
0.75	40,000	-0.327 ± j 2.933	2.951	0.111	2.117	2.14	1.012	0.138
		-2.040			0.340			
		+0.0083			-83.5			
0.80	40,000	-0.350 ± j 2.968	2.989	0.117	1.981	2.11	1.068	0.113
		-2.216			0.313			
		+0.0095			-73.0			

NOTE: T_2 is indicated by a negative value.

TABLE 3.10 (Continued)

$\delta_f = 45° + \delta_d = 15°$

V ~ KTS	Altitude ~ft.	Roots of Characteristic Equation	ω_n ~rad/sec	ξ	$T_{1/2}$ or T_2 ~ sec	P ~sec	$1/C_{1/2}$ ~ 1/ cycles	ϕ/v_e ~ deg/ ft/sec
94.6		-0.267 ± j 1.896	1.915	0.140	2.595	3.32	1.277	0.610
		-1.918			0.361			
		-0.0264			26.2			
115.0		-0.270 ± j 2.004	2.022	0.134	2.567	3.14	1.221	0.459
		-2.234			0.310			
		-0.0292			23.7			
150.0		-0.336 ± j 2.280	2.305	0.146	2.065	2.76	1.335	0.310
		-2.806			0.247			
		-0.0317			21.8			
180.0		-0.393 ± j 2.582	2.612	0.151	1.763	2.44	1.380	0.232
		-3.345			0.207			
		-0.0279			24.8			

NOTE: T_2 is indicated by a negative value.

TABLE 3.11

Results of Lateral-Directional Dynamic Stability Investigations

9200 Pounds
cg at F.S. 246.0
ARDC Standard Atmosphere
Elastic Airframe
Controls Fixed

$\delta_f = 0°$

M	Altitude ~ft.	Roots of Characteristic Equation	ω_n ~rad/sec	ξ	$T_{1/2}$ or T_2 ~sec	P ~sec	$1/C_{1/2}$ ~1/ cycles	ϕ/v_e ~deg/ ft/sec
0.60	0	-1.093 ± j 5.597	5.702	0.192	0.634	1.120	1.770	0.067
		-6.944			0.100			
		+0.0028			-247.0			
0.80	0	-1.375 ± j 4.913	5.101	0.269	0.504	1.278	2.536	0.023
		-9.683			0.072			
		+0.0124			-55.8			
0.60	20,000	-0.563 ± j 3.961	4.001	0.141	1.231	1.585	1.289	0.125
		-3.514			0.197			
		+0.0028			-247.0			
0.80	20,000	-0.710 ± j 3.719	3.786	0.187	0.977	1.690	1.730	0.025
		-4.925			0.141			
		+0.0118			-58.7			

NOTE: T_2 is indicated by a negative value.

TABLE 3.12

Results of Lateral-Directional Dynamic Stability Investigations

9200 Pounds
cg at F.S. 246.0
ARDC Standard Atmosphere
Elastic Airframe
Rudder Free

$\delta_f = 0°$

M	Altitude ~ft.	Roots of Characteristic Equation	ω_n ~rad/sec	ξ	$T_{1/2}$ or T_2 ~ sec	P ~ sec	$1/C_{1/2}$ ~1/ cycles	ϕ/v_e ~ deg/ ft/sec
0.60	0	-1.109 ± j 5.766	5.872	0.189	0.625	1.090	1.743	0.064
		-6.947			0.100			
		+0.0030			-231.0			
		-35.96 ± j 66.38	75.4	.477	0.019	0.094		
0.80	0	-1.374 ± j 4.909	5.098	0.270	0.504	1.280	2.538	0.023
		-9.690			0.072			
		+0.0120			-57.7			
		-46.73 ± j 91.42	102.7	.455	0.015	0.068		
0.60	20,000	-0.573 ± j 4.078	4.118	0.139	1.210	1.540	1.272	0.119
		-3.515			0.197			
		+0.0029			-239.0			
		-17.78 ± j 47.96	51.1	.348	0.039	0.131		
0.80	20,000	-0.721 ± j 3.904	3.967	0.182	0.961	1.608	1.676	0.022
		-4.930			0.141			
		+0.0114			-60.7			
		-23.12 ± j 65.61	69.6	.332	0.030	0.096		

NOTE: T_2 is indicated by a negative value.

TABLE 3.13

Results of Lateral-Directional Dynamic Stability Investigations

9200 Pounds
cg at F.S. 246.0
ARDC Standard Atmosphere
Elastic Airframe
Ailerons Free

$\delta_f = 0°$

M	Altitude ~ ft.	Roots of Characteristic Equation	ω_n ~ rad/sec	ξ	$T_{1/2}$ or T_2 ~ sec	P ~sec	$1/C_{1/2}$ ~ 1/ cycles	ϕ/v_e ~deg/ ft/sec
0.60	S. L.	-1.095 ± j 5.597	5.703	0.192	0.633	1.120	1.773	0.0673
		-6.814			0.102			
		+0.0031			-224.0			
		-50.19 ± j 171.1	105.6	.476	0.014	0.037		
0.8	S. L.	-1.376 ± j 4.914	5.103	0.270	0.504	1.280	2.538	0.0233
		-9.587			0.072			
		+0.0127			-54.6			
		-66.78 ± j 223.1	139.0	.481	0.010	0.028		
0.6	20,000	-0.565 ± j 3.961	4.001	0.141	1.227	1.585	1.293	0.125
		-3.443			0.201			
		+0.0031			-224.0			
		-24.82 ± j 118.2	59.6	.417	0.028	0.053		
0.8	20,000	-0.710 ± j 3.720	3.787	0.188	0.976	1.688	1.731	0.0251
		-4.868			0.142			
		+0.0121			-57.3			
		-33.06 ± j 154.4	78.7	.420	0.021	0.041		

NOTE: T_2 is indicated by a negative value.

4.0 LIFT FAN MODE CHARACTERISTICS

4.1 WING FAN LIFT DAMPING IN VERTICAL FLIGHT

Estimated lift damping in hovering vertical flight arising from the change in fan thrust due to axial inflow velocity is shown in Figure 4-1. The variation of lift was calculated from the 1/6 scale model coefficients of Figure 4.31 of Reference 1. Also shown in Figure 4.1 is the estimated lift change due to axial velocity given in Reference 13. The nonlinear nature of the 1/6 scale data is believed to occur because the fan damping is relatively small compared with the vertical drag of the fuselage-wing-tail and data scatter permitted only an approximate determination of the character of lift change with tunnel speed.

4.2 WING FAN CONTRIBUTION TO ROLL AND YAW DAMPING

The estimated contribution of the wing fans to roll and yaw damping in transition flight were made inherent in the equations of motion developed for the Flight Simulator without recourse to stability derivatives. This was accomplished by simulating the left and right fans separately such that the local angle of attack of each fan could be determined as functions of angular rates of the aircraft.

For example, the rolling and yawing moments arising from the angular rates were expressed as

$$L = C^{s}_{N_L} \; q^{s}_{L} \; \frac{A_f}{2} \; y_F - C^{s}_{N_R} \; q^{s}_{R} \; \frac{A_F}{2} \; y_F$$

$$N = C^{s}_{X_L} \; q^{s}_{L} \; \frac{A_F}{2} \; y_F - C^{s}_{X_R} \; q^{s}_{r} \; \frac{A_F}{2} \; y_F$$

and

$$\alpha_L = \tan^{-1} \frac{w_{A/C} - \dot{\varphi} y_F}{u_{A/C} + \dot{\psi} y_F}$$

$$\alpha_R = \tan^{-1} \frac{w_{A/C} + \dot{\phi} y_F}{u_{A/C} - \dot{\psi} y_F}$$

A roll rate will, therefore, result in a differential change in angle of attack for the left and right hand wings and the change in normal force coefficient with angle of attack produces a rolling moment about the plane of symmetry. An example is illustrated in Figure 4.2 for several values of vector angle and flight speed for a constant level of total fan thrust. Also shown in Figure 4.2 is the damping due to the estimated theoretical lift damping given in Reference 13. These results indicate that the fans alone account for less than 25% of the total wing and fan damping as estimated by the above procedure.

A change in yaw rate will produce similar changes in longitudinal force resulting in a damping moment in yaw. Consider the case of zero airplane angle of attack ($w_{A/C} = 0$) and zero roll rate. A yaw rate now will produce no differential change in angle of attack but changes in the left and right hand thrust coefficient, T_c^s, and q^s arise because of the relative change in velocity of the two fans. The product of the longitudinal coefficient, which varies with T_c^s, and q^s results in a yawing moment. This yawing moment is due to the momentum drag of the fans which is a linear function of velocity and therefore independent of flight speed but dependent on the fan thrust level.

From simple momentum theory it can be shown that the fan momentum drag variation with velocity is expressed by:

$$\frac{dD}{du} = (\rho A_F T_{ooo})^{1/2}$$

where T_{ooo} is the static thrust per fan

A_F is the area of one fan

The yawing moment of both fans is

$$N = -2y_F^2 \frac{dD}{du} \dot{\Psi}$$

or

$$\frac{dN}{d\dot{\Psi}} = -2y_F^2 \frac{dD}{du}$$

The theoretical value of dD/du based upon momentum theory for a fan thrust of 5000 pounds is 14.7 lb/ft/sec. From test data, dD/du was found to be 9.8 lb/ft/sec. for the same thrust level. Therefore,

$$\frac{dN}{d\dot{\Psi}} = -2y_F^2 \frac{\left(\frac{dD}{du}\right)_{TEST}}{\left(\frac{dD}{du}\right)_{THEORY}} \times \left(\frac{dD}{du}\right)_{THEORY}$$

$$= -2y_F^2 \frac{9.8}{14.7} \sqrt{\rho A_F \frac{\left(T_{ooo}\right)_{2\ FANS}}{2}} = -5.10 \left(T_{ooo_{2\ FANS}}\right)^{1/2}$$

Figure 4.3 shows the yaw damping derivative calculated for a range of fan thrust along with a value determined from the differential variation in longitudinal force coefficient.

4.3 PITCH DAMPING CONTRIBUTION OF NOSE FAN

Wind tunnel test data of Reference 14 indicated that the incremental nose fan normal force coefficient due to axial flow with respect to the model could be approximated by

$$\Delta C_{N_{NF}}^{s} = 6.25 \left(1 - T_c^{s}\right)_{NF}$$

This expression was modified empirically to obtain values of the coefficient at angles of attack other than ±90° as follows:

$$\Delta C_{N_{NF}}^{s} = 6.25 \left(1 - T_c^{s}\right)_{NF} \text{Sin } \alpha_{NF}$$

where

$$\alpha_{NF} = \tan^{-1} \frac{w_{A/C} - \dot{\theta} \chi_{NF}}{u_{A/C}}$$

The damping moment of the nose fan is given by

$$M = \Delta C_{N_{NF}}^{s} q_{NF}^{s} A_{NF} \chi_{NF}$$

where the incremental normal force coefficient varies with either airplane angle of attack or with airplane pitch rate. The damping moment was evaluated for zero airplane angle of attack and for various values of pitch rate over a range of transition flight speeds as shown in Figure 4.4. The pitching moment calculated for the theoretical lift damping given in Reference 15 is also shown in Figure 4.4. The damping moment based on test data is less than the theoretical value for speeds less than those associated with $\beta_V \cong 25°$ and greater than the theoretical for speeds higher than this condition.

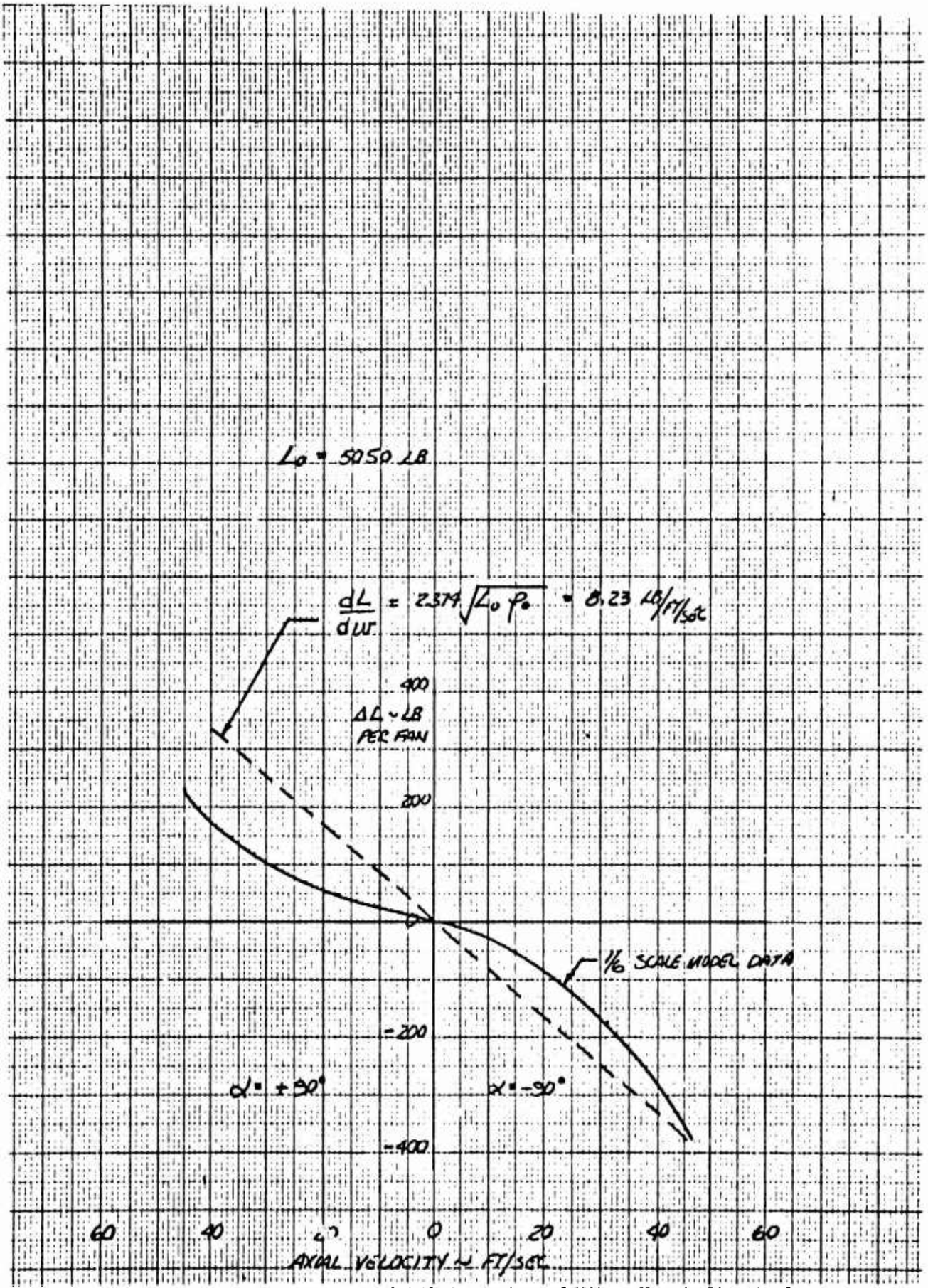

Figure 4.1 Estimated Lift Damping of Wing Fan in Vertical Flight.

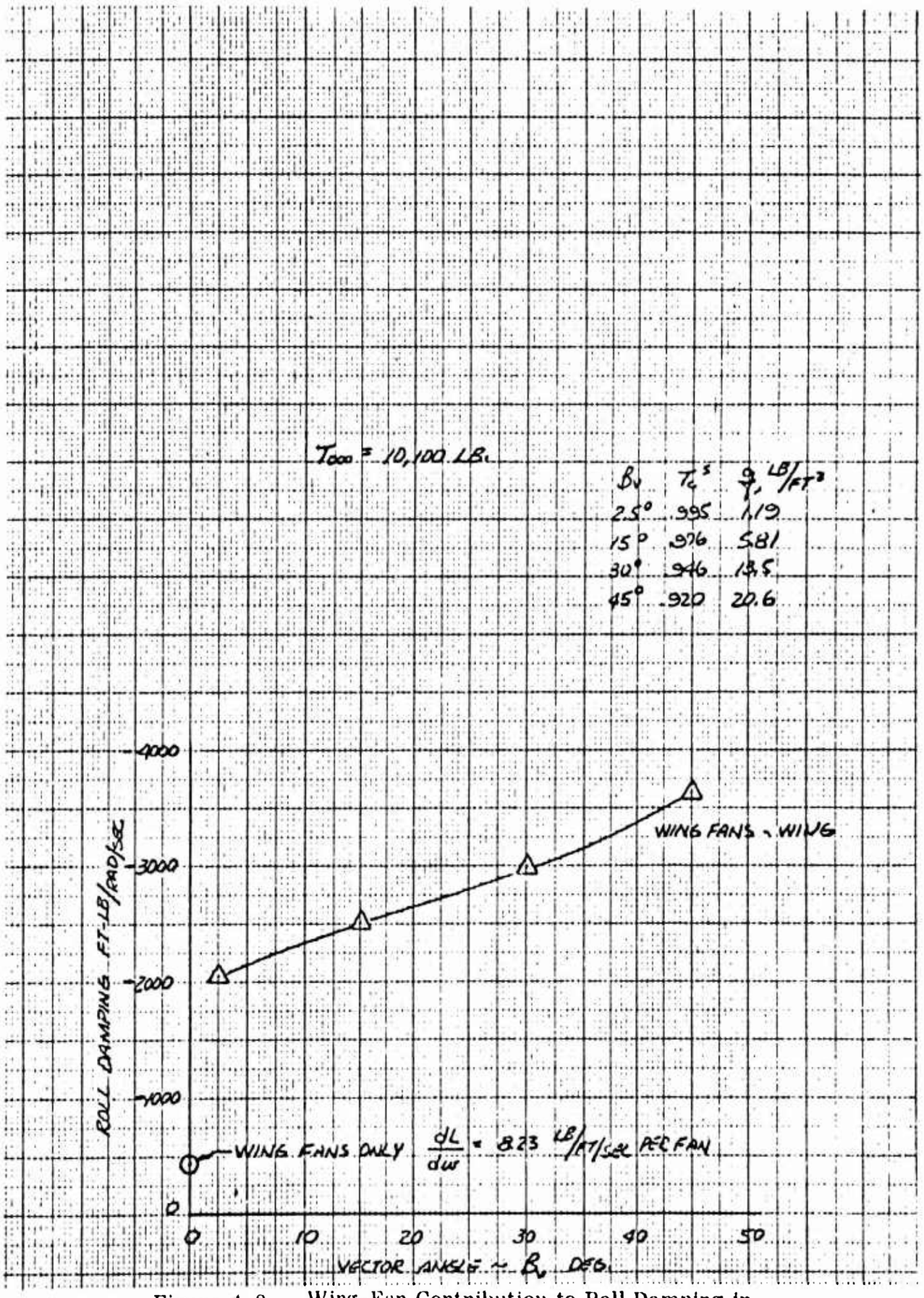

Figure 4.2 Wing-Fan Contribution to Roll Damping in Transition Flight.

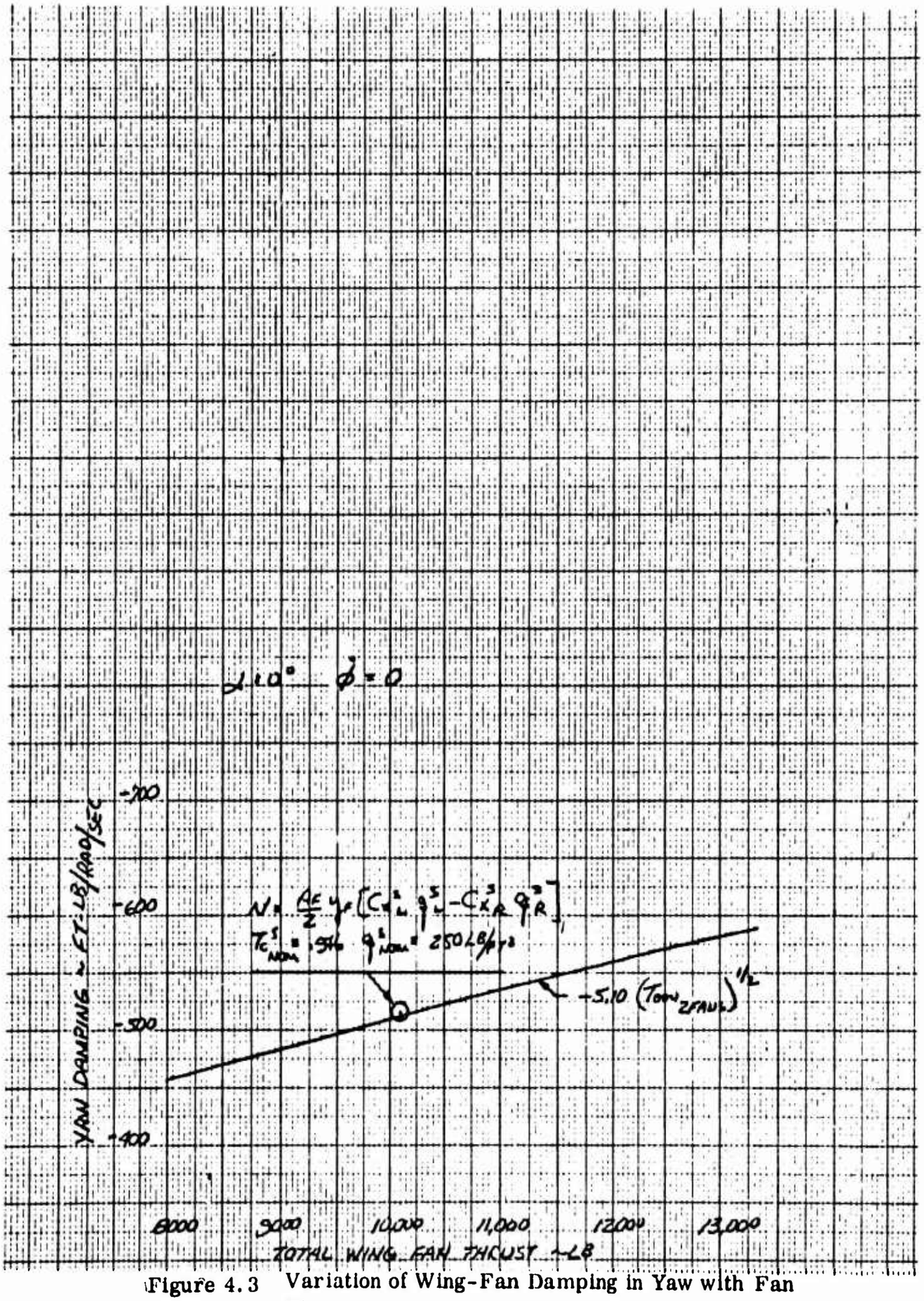

Figure 4.3 Variation of Wing-Fan Damping in Yaw with Fan Thrust.

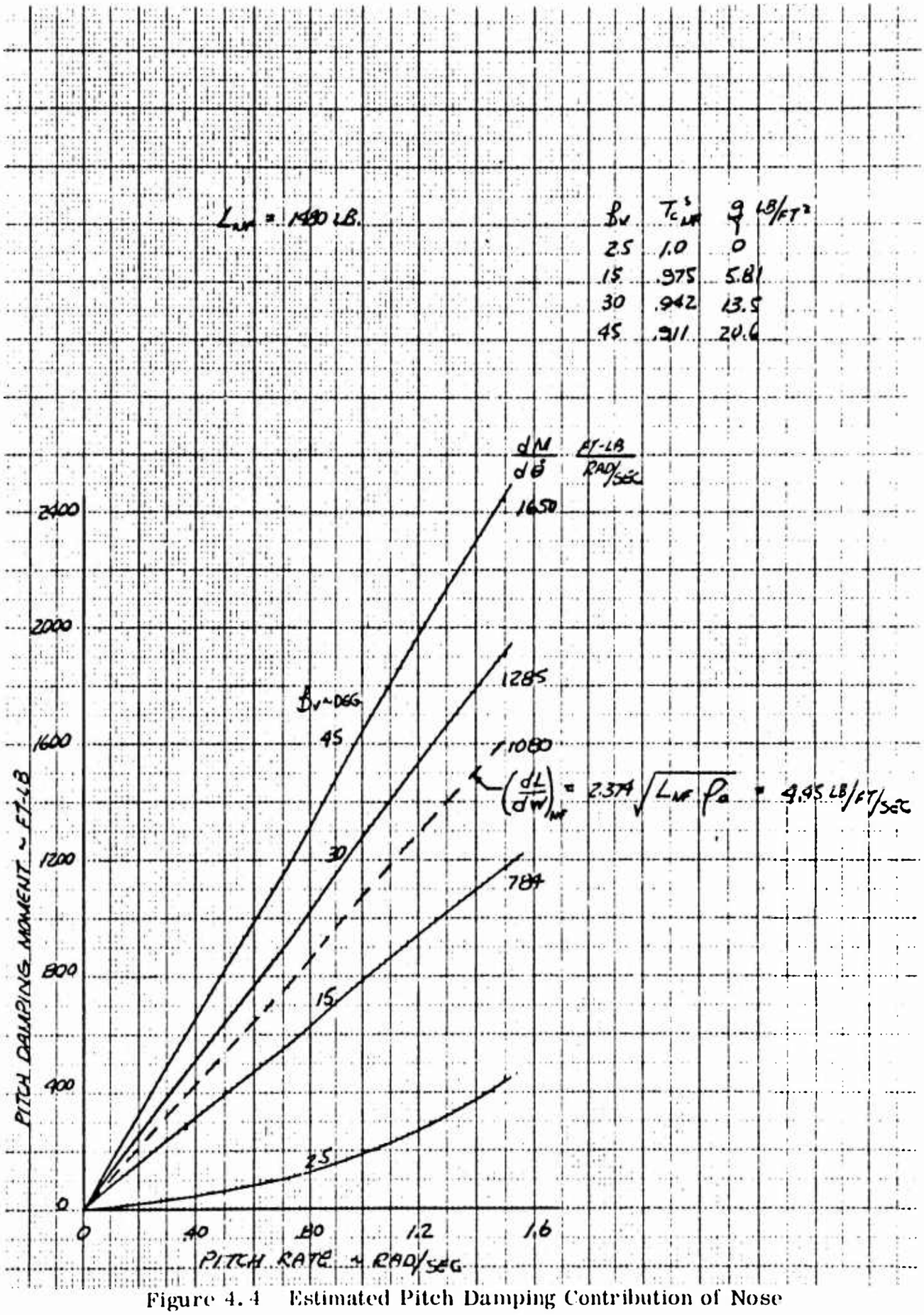

Figure 4.4 Estimated Pitch Damping Contribution of Nose Fan.

5.0 CONCLUSIONS

In the conventional, clean airplane configuration, the longitudinal short period mode meets the damping requirements of the XV-5A Flying Qualities Specification throughout the flight envelope. However, the natural frequency of the short period mode is less than required by the specification at 40,000 feet and for speeds less than M = .75 at 30,000 feet, M = 0.60 at 20,000 feet and M = 0.30 at sea level. While the low natural frequency may be undesirable for a fighter-type aircraft, this characteristic, where it exists, should not affect the utility of the aircraft for its intended purpose or require any unusual piloting techniques.

Freeing the controls reduces to a slight degree the speed-altitude range, wherein the short period requirements of the Flying Qualities Specifications are satisfied because of a small reduction in natural frequency and increase in damping ratio.

Although longitudinal static and dynamic stability are satisfactory in straight and level flight for speeds up to Mach 0.8 at altitudes up to about 40,000 feet, neutral static stability may be encountered above Mach 0.7 at lift coefficients corresponding to high normal load factors. Deterioration in high speed, static longitudinal stability with increasing lift coefficient is gradual except near Mach 0.8 where an abrupt pitch-up is anticipated at the higher attainable load factors at high altitude.

The longitudinal dynamic stability characteristics in the conventional flight landing configuration are satisfactory for flight testing at all flight conditions. Static longitudinal stability becomes marginal at high angles of attack, but the flight characteristics are satisfactory, primarily due to high pitch damping.

The characteristics of the lateral-directional oscillation, or dutch roll mode, in the clean airplane configuration meet the requirements of the XV-5A Flying Qualities Specification at all speeds from 15% above the stall speed to Mach 0.8 at altitudes below about 25,000 feet. At altitudes from 25,000 to 40,000 feet, the requirements are satisfied for speeds above approximately Mach 0.7. At speeds below about Mach 0.6, at altitudes above 25,000 feet, the relative magnitude of the rolling motion

to sideslipping in the dutch roll mode increases with little change in damping as a result of increasing dihedral effect at high-angles of attack. This characteristic is common at high altitude and low speed for aircraft without artificial damping, and is not expected to affect the utility of the aircraft for research purposes.

Aeroelastic and controls free considerations had no significant effect on the dutch roll characteristics for any of the flight conditions investigated.

The dutch roll characteristics in the conventional flight landing configuration meet the requirements of the Flying Qualities Specification at all speeds above approximately 120 knots at sea level. The dutch roll damping is estimated to be only slightly less than the requirement between 95 and 120 knots.

The static and dynamic stability characteristics above Mach 0.8 up to the structural speed limit of Mach 0.9 are unsatisfactory, due to rising static longitudinal instability, rapid loss in pitch damping and rapid loss of control power about all three axes.

Pitch-yaw coupling may result in exceeding the vertical and lateral limit load factors during rapid, 360 degree rolling maneuvers at high speeds with rudder and elevator fixed. Prolonged rolling maneuvers with lateral control displacements up to one-half of full throw at dynamic pressures less than 250 to 300 pounds per square foot only produce small variations in load factor. The effects of pitch-yaw coupling at all flight conditions have not been investigated at the present time.

Deterioration of high speed static longitudinal stability, with increasing lift coefficient and pitch-yaw coupling, requires that extreme caution be exercised during initial flight test investigations of high speed maneuvering characteristics, particularly at high altitudes or high normal load factors. A center of gravity location forward of Fuselage Station 243.0 is recommended for initial flight tests from the standpoint of longitudinal static and dynamic stability characteristics.

The contributions of the wing fans to roll, yaw and vertical lift damping and the contributions of the nose fan to pitch damping are small, even at low speeds, compared with the damping attributed to the normal aircraft surfaces.

6.0 APPENDIX

6.1 REFERENCES

1. Estimated Static Stability and Control Characteristics, General Electric Co., Report No. 146, 1964.

2. Report of Preliminary Systems Analysis and Simulation, General Electric Co., Report No. 127

3. Toll, Thomas A., and Queijo, M.J , "Approximate Relations and Charts for Low-Speed Stability Derivatives of Swept Wings". NACA Technical Note. TN 1581, Langley Memorial Aeronautical Laboratory, Langley Field, Va., May 1948.

4. Northrop Aircraft, Inc., "Dynamics of the Airframe", Burear of Aeronautics Report AE-61-4II, September 1952.

5. Calculated Installed Power Plant Performance, General Electric Co., Report No 150, September 1964.

6. Malthan, L V. et al . "USAF Stability and Control Handbook", Douglas Aircraft Co., October 1960.

7. Decker, J. et al.. "USAF Stability and Control Handbook", M-03671, 1956 (Title Unclassified).

8. Wiggins, W W.. "Wind-Tunnel Investigation of Sweep on Rolling Derivatives at Angles of Attack up to 13° and at High Subsonic Mach Numbers, Including a Semi-Empirical Method of Estimating the Rolling Derivatives". NACA RM L54C26, 1954.

9. Perkins, C.D. and Hage, R.E.: "Airplane Performance Stability and Control"; John Wiley and Sons, Inc., Copyright 1949.

10. Structural Design Loads, General Electric Co., Report No 143, 1964

11. XV-5A Flying Qualities Specification Appendix to General Electric Co., Report No. 118A, April 22, 1963

12. Letko, William and Riley, Donald R.. Effect of an Unswept Wing on the Contribution of Unswept-Tail Configuration to Low Speed Static and Rolling Stability Derivative. NACA TN2175, August 1950.

13. Anon X353-5B Propulsion System Specification, VZ-11 Lift Fan Flight Research Aircraft Program, General Electric Specification No 112, 15 January 1962.

14. Parks, W.C. and Schattschneider, D.G.: Wind Tunnel Test Report, One-Sixth Scale Powered Lift-Fan Model U.S. Army XV-5A Lift-Fan Research Aircraft; Ryan Report No. 63B092, 11 September 1963

15. Anon: X-376 Pitch Fan Specification, VZ-11 Lift-Fan Flight Research Aircraft Program, General Electric Specification No. 113, 1 March 1962.

16. Toll, Thomas A., and Schnieter, Leslie E.: Approximate Relations for Hinge-Moment Parameters of Control Surfaces on Swept Wings at Low Mach Numbers; NACA TN1711, October, 1948.

17. Dads, Jules B., Jr.: Estimation of Low Speed Lift and Hinge-Moment Parameters for Full-Span Trailing-Edge Flaps on Lifting Surfaces With and Without Sweepback, NACA TN2288, February 1951.

6.2 SYMBOLS AND NOMENCLATURE

General Symbols

A	Aspect ratio, b^2/S. Unsubscripted symbol refers to wing.
A	Total Fan Area, $\frac{2\pi D^2}{4}$, ft^2.
a_o	Speed of sound, ft./sec.
b	Span, ft. Unsubscripted symbol refers to wing.
$\bar{c}$	Mean aerodynamic chord, ft. Unsubscripted symbol refers to wing.
$C_{1/2}$	Cycles to damp to one half amplitude.
C_D	Drag coefficient, D/qS.
C_h	Hinge moment coefficient, $HM/qS_{ref}\bar{c}_{ref}$.
C_L	Lift coefficient, L/qS.
C_ℓ	Rolling moment coefficient, R/qSb.
C_m	Pitching moment coefficient, $M/qS\bar{c}$.
C_N^s	Normal force coefficient, NORMAL FORCE/q^sA_F.
C_n	Yawing moment coefficient, N/qSb
C_X^s	Axial force coefficient, X/q^sA_F.
C_Y	Sideforce coefficient, Y/q^sA_F.
D	Drag force, lb. or fan diameter, ft.
HM	Hinge moment, ft.-lb.
j	Complex multiplier, $\sqrt{-1}$
L	Lift force, lb. or rolling moment, ft.-lb.

ℓ Distance from the center of gravity to the aerodynamic center of the horizontal or vertical tail along the stability X axis.

M Pitching moment, ft.-lb. or Mach number.

N Yawing moment, ft.-lb.

P Period of an oscillatory motion, sec.

p Angular velocity about the airplane X axis, radians/sec.

q Angular velocity about the airplane Y axis, radians/sec. or dynamic pressure, lb./ft^2.

q_o Freestream dynamic pressure ($1/2\,\rho\,V^2$), lb./ft^2.

q^s Slipstream dynamic pressure, ($q_o + T_{ooo}/A_F$), lb./ft^2.

R Rolling moment, ft-lb.

r Angular velocity about the airplane Z axis, radians/sec.

S Reference area, ft^2. Unsubscripted symbol refers to wing. Control surface areas are aft of the hinge line.

T Static fan thrust or turbojet installed net thrust, lb.

T_{ooo} Wing fan static normal force with $\beta_v = 0^\circ$, $\beta_s = 0^\circ$, V = 0, lb.

$T_{1/2}$ Time to damp to one half amplitude, sec.

T_2 Time to double the amplitude for an unstable oscillation, sec.

u Velocity along the airplane X axis, ft./sec.

U_o Freestream velocity along the flight path, ft./sec.

V Freestream velocity along the flight path, ft./sec.

v Velocity along the airplane Y axis, ft./sec.

w Velocity along the airplane Z axis, ft./sec.

x Distance from the airplane center of gravity along the airplane X axis, ft.

x_t Distance from the aileron hinge line to the 0.25 MAC of the aileron tab, ft.

y Distance from the plane of symmetry along the airplane Y axis, ft.

Y Sideforce, lb.

Z Distance from the center of gravity along the airplane Z axis, ft.

Greek Symbols

α Angle of attack, degrees or radians.

β Sideslip angle, degrees or radians.

β Wing fan exit louver angle, degrees. Measured between louver aft surface tangent plane and a plane parallel to fan axis, positive trailing edge aft.

β_s Exit louver stagger angle, measured between any even numbered louver and the adjacent odd numbered louver, i.e., $\beta_s = \beta_2 - \beta_1$ where β_2 is the most forward and alternate louver.

β_v Exit louver vector angle determined from the average angle formed by adjacent louvers, i.e., $\beta_v = \frac{\beta_2 + \beta_1}{2}$

δ Flap or control surface deflection, degrees or radians. Trailing edge down positive; rudder deflection positive trailing edge left.

ϵ Downwash angle at the horizontal tail, degrees.

η_t Dynamic pressure ratio at the horizontal tail, q_t/q_o.

ρ Air mass density, slug/ft^3

σ Sidewash angle at the vertical tail, degrees; ($\alpha_v = -\beta - \sigma$).

ξ Fraction of critical damping, e.g., damping ratio.

ϕ Airplane euler roll angle, degrees or radians.

θ Airplane euler pitch angle, degrees or radians.

ψ Airplane euler yaw angle, degrees or radians.

Λ Sweep angle of the wing quarter chord line.

ω_n Natural frequency of oscillation, radians/sec.

Γ Outboard wing panel dihedral, radians.

Subscripts

a Aileron.

A/C Complete airplane.

ac Aerodynamic center.

CM Complete model.

d Ailerons, drooped as flaps.

e Elevator or equivalent airspeed.

F Wing fans.

f Wing, inboard trailing edge flaps.

L Left hand.

M-T Model minus tail.

NF Nose fan.

NOM Nominal.

0 Zero angle of attack, zero velocity or free stream.

OL Zero lift.

0α Zero angle of attack.

R Right hand.

r Rudder.

s Wing stall or stagger.

TR Trimmed flight ($C_m = 0$).

t Horizontal tail or aileron tab.

v Vertical tail or vector.

Superscripts

s Slipstream notation.

* Elastic airframe.

Abbreviations

ARDC Air Force Research and Development Command.

B. L. Butt line.

C. G. Center of gravity.

C. P. S. Cycles per second.

DEG. Degree.

F. S. Fuselage station.

FWD Forward.

MAC Mean aerodynamic chord.

max Maximum.

RAD. Radian.

S. L. Sea level.

W. L. Water line.

Derivatives

C_{D_u}	$\frac{U_0}{2}\frac{\partial C_D}{\partial u}$	
C_{D_α}	$\partial C_D/\partial \alpha$	1/RAD
$C_{h_{e_q}}$	$\partial C_{h_e}/\partial\left(\frac{q\bar{c}_e}{2U_0}\right)$	1/RAD
$C_{h_{e_{\dot{q}}}}$	$\partial C_{h_e}/\partial\left(\frac{\dot{q}\bar{c}_e}{2U_0}\right)$	1/RAD/SEC
$C_{h_{e_u}}$	$\partial C_{h_e}/\partial u$	1/FT/SEC
$C_{h_{e_{\delta_e}}}$	$\partial C_{h_e}/\partial \delta_e$	1/RAD
$C_{h_{e_{\dot{\delta}_e}}}$	$\partial C_{h_e}/\partial\left(\frac{\dot{\delta}_e\bar{c}_e}{2U_0}\right)$	1/RAD
$C_{h_{e_\alpha}}$	$\partial C_{h_e}/\partial \alpha$	1/RAD
$C_{h_{e_{\dot{\alpha}}}}$	$\partial C_{h_e}/\partial\left(\frac{\dot{\alpha}\bar{c}_e}{2U_0}\right)$	1/RAD
$C_{h_{e_{\alpha_t}}}$	$\partial C_{h_e}/\partial \alpha_t$	1/RAD
$C_{h_{r_p}}$	$\partial C_{h_r}/\partial\left(\frac{p\bar{c}_r}{2U_0}\right)$	1/RAD

$C_{h_{r_{\dot{p}}}}$	$\partial C_{h_r} / \partial \left(\frac{\dot{p} \bar{c}_r}{2U_0} \right)$	1/RAD/SEC
$C_{h_{r_r}}$	$\partial C_{h_r} / \partial \left(\frac{r \bar{c}_r}{2U_0} \right)$	1/RAD
$C_{h_{r_{\dot{r}}}}$	$\partial C_{h_r} / \partial \left(\frac{\dot{r} \bar{c}_r}{2U_0} \right)$	1/RAD/SEC
$C_{h_{r_{\alpha_v}}}$	$\partial C_{h_r} / \partial \alpha_v$	1/RAD
$C_{h_{r_\beta}}$	$\partial C_{h_r} / \partial \beta$	1/RAD
$C_{h_{r_{\dot{\beta}}}}$	$\partial C_{h_r} / \partial \left(\frac{\dot{\beta} \bar{c}_r}{2U_0} \right)$	1/RAD
$C_{h_{r_{\delta_r}}}$	$\partial C_{h_r} / \partial \delta_r$	1/RAD
$C_{h_{r_{\dot{\delta}_r}}}$	$\partial C_{h_r} / \partial \left(\frac{\dot{\delta}_r \bar{c}_r}{2U_0} \right)$	1/RAD
$C_{h_{t_r}}$	$\partial C_{h_t} / \partial \left(\frac{r \bar{c}_t}{2U_0} \right)$	1/RAD
$C_{h_{t_{\dot{r}}}}$	$\partial C_{h_t} / \partial \left(\frac{\dot{r} \bar{c}_t}{2U_0} \right)$	1/RAD/SEC
$C_{h_{t_p}}$	$\partial C_{h_t} / \partial \left(\frac{p \bar{c}_t}{2U_0} \right)$	1/RAD
$C_{h_{t_{\dot{p}}}}$	$\partial C_{h_t} / \partial \left(\frac{\dot{p} \bar{c}_t}{2U_0} \right)$	1/RAD/SEC

$C_{h_{t_\alpha}}$	$\partial C_{h_t} / \partial \alpha$	1/RAD
$C_{h_{t_\beta}}$	$\partial C_{h_t} / \partial \beta$	1/RAD
$C_{h_{t_{\dot\beta}}}$	$\partial C_{h_t} / \partial \left(\frac{\dot\beta \bar{c}_t}{2 U_0} \right)$	1/RAD
$C_{h_{t_{\delta_a}}}$	$\partial C_{h_t} / \partial \left(\delta_{a_L} - \delta_{a_R} \right)$	1/RAD
$C_{h_{t_{\dot\delta_a}}}$	$\partial C_{h_t} / \partial \left(\frac{\left(\dot\delta_{a_L} - \dot\delta_{a_R} \right) \bar{c}_t}{2 U_0} \right)$	1/RAD
$C_{h_{t_{\delta_t}}}$	$\partial C_{h_t} / \partial \left(\delta_{t_L} - \delta_{t_R} \right)$	1/RAD
$C_{h_{t_{\dot\delta_t}}}$	$\partial C_{h_t} / \partial \left(\frac{\left(\dot\delta_{t_L} - \dot\delta_{t_R} \right) \bar{c}_t}{2 U_0} \right)$	1/RAD
C_{L_q}	$\partial C_L / \partial \left(\frac{q \bar{c}}{2 U_0} \right)$	1/RAD
C_{L_u}	$\frac{U_0}{2} \frac{\partial C_L}{\partial u}$	
C_{L_α}	$\partial C_L / \partial \alpha$	1/RAD
$C_{L_{\dot\alpha}}$	$\partial C_L / \partial \left(\frac{\dot\alpha \bar{c}}{2 U_0} \right)$	1/RAD
$C_{L_{\alpha_t}}$	$\partial C_L / \partial \alpha_t$	(Based on horizontal tail area) 1/RAD

$C_{L_{\alpha_v}}$	$\partial C_L / \partial \alpha_v$	(Vertical tail lift based on vertical 1/RAD tail area)
$C_{L_{\delta_e}}$	$\partial C_L / \partial \delta_e$	1/RAD
C_{ℓ_p}	$\partial C_\ell / \partial \left(\frac{pb}{2U_0} \right)$	1/RAD
C_{ℓ_r}	$\partial C_\ell / \partial \left(\frac{rb}{2U_0} \right)$	1/RAD
C_{ℓ_β}	$\partial C_\ell / \partial \beta$	1/RAD
$C_{\ell_{\delta_a}}$	$\partial C_\ell / \partial \left(\delta_{a_L} - \delta_{a_R} \right)$	1/RAD
$C_{\ell_{\delta_r}}$	$\partial C_\ell / \partial \delta_r$	1/RAD
C_{m_q}	$\partial C_m / \partial \left(\frac{q\bar{c}}{2U_0} \right)$	1/RAD
C_{m_u}	$\frac{U_0}{2} \frac{\partial C_m}{\partial u}$	
C_{m_α}	$\partial C_m / \partial \alpha$	1/RAD
$C_{m_{\dot{\alpha}}}$	$\partial C_m / \partial \left(\frac{\dot{\alpha} \bar{c}}{2U_0} \right)$	1/RAD
$C_{m_{\delta_e}}$	$\partial C_m / \partial \delta_e$	1/RAD
C_{n_p}	$\partial C_n / \partial \left(\frac{pb}{2U_0} \right)$	1/RAD
C_{n_r}	$\partial C_n / \partial \left(\frac{rb}{2U_0} \right)$	1/RAD

C_{n_β}	$\partial C_n / \partial \beta$	1/RAD
$C_{n_{\delta_r}}$	$\partial C_n / \partial \delta_r$	1/RAD
C_{y_p}	$\partial C_y / \partial \left(\frac{pb}{2U_0} \right)$	1/RAD
C_{y_r}	$\partial C_y / \partial \left(\frac{rb}{2U_0} \right)$	1/RAD
C_{y_β}	$\partial C_y / \partial \beta$	1/RAD
$C_{y_{\delta_r}}$	$\partial C_y / \partial \delta_r$	1/RAD

6.3 PHYSICAL CHARACTERISTICS

6.3.1 Wing Geometry

Dimensions based on a vertical projection onto a horizontal plane.

Gross area	260.321 sq ft
Aspect ratio	3.419
Taper ratio	
Inboard panel	.752
Outboard panel	.394
Span	29.833 ft
Chord length	
Root (BL 0.00)	145.000 in.
At break of quarter chord line (BL 100.75)	109.005 in.
Tip (BL 179.00)	43.000 in.
MAC	112.919
Airfoil section	
BL 170.05	NACA 0012-64 a = 0.8 (modified), C_{l_i} = 0.2
See tabulated ordinates for other sections, Table 6.3.7	
Dihedral	
Inboard panel	0.000 deg
Outboard panel (from BL 107.000)	4.000 deg
Sweep	
Leading edge - inboard panel	19.660 deg
Leading edge - outboard panel	36.881 deg
Quarter chord line - inboard panel	15.000 deg
Quarter chord line - outboard panel	28.343 deg

64B104

Trailing edge - inboard panel	0.000	deg
Trailing edge - outboard panel	-5.399	deg
Geometric twist, see page 113-A		
Fuselage Station of root chord leading edge (BL 0.00)	180.050	
Fuselage Station of .25 MAC	239.380	
BL of semi-span MAC	75.353	

6.3.2 Aileron Geometry

Gross area (aft of hinge line, per side)	10.057	sq ft
Aspect ratio	4.041	
Taper ratio	.836	
Span (per side, perpendicular to BL 0.00)	6.375	ft
Span-wise location	.573 to 1.000	b/2
Chord length (aft of hinge line, parallel to BL 0.00)		
BL 102.50	20.622	in.
BL 179.00	17.239	in.
MAC	18.981	in.
Fuselage Station of hinge line		
BL 103.61	304.370	
BL 168.43	301.060	
Fuselage Station of .25 MAC	307.249	
BL of panel MAC	139.610	
Deflection limits (from zero degree position)		
with zero degrees droop	+15 -19	deg
with +15.0 deg droop (differentially coupled)	+27 - 8	deg

Type of balance - Internally sealed pressure balance.

Control - Full hydraulic power

Aileron servo, feel tab
(Serves as trim tab on left aileron)

Area (aft of hinge line, per side)	0.974 sq ft
Aspect ratio	5.545
Taper ratio	.938
Span (per side, perpendicular to BL 0.00)	2.324 ft
Span-wise location	.573 to .728 b/2
Chord length (aft of hinge line, parallel to BL 0.00)	
BL 102.50 (25% of local aileron chord)	5.156 in
BL 130.24 (25% of local aileron chord)	4.870 in.
MAC	5.029 in.
Fuselage Station of hinge line	
BL 102.50	319.894
BL 130.24	317.525
Fuselage Station of .25 MAC	319.942
BL of panel MAC	116.387
Deflection limits (tab gear ratio -.5 to 1.0 per deg. of aileron deflection from zero degrees)	
Right side	-13.5 to +9.5 deg
Left side (includes ±3.0 deg. for trim)	-16.5 to +12.5 deg

Type of balance - Radius nose, unsealed

64B10

6.3.3 Flap Geometry

Area (per side)	12.684 sq ft
Aspect ratio	3.246
Taper ratio	1.000
Span (per side, perpendicular to BL 0.00)	6.417 ft
Span-wise location	.138 to .568 b/2
Chord length	
BL 24.75	23.721 in.
BL 101.75	23.721 in.
MAC	23.721 in.
Fuselage Station of hinge line	308.150
WL of hinge line	92.580
Fuselage Station of .25 MAC	307.259
BL of panel MAC	63.250
Deflection limits	0.0 to +45.0 deg
Type of flap - single slotted with a NACA 634-021 modified airfoil section (see tabulated data for ordinates, Table 6.3.8)	

6.3.4 Fan Geometry

Rotor area (per wing fan, including hub)	21.305 sq ft
Rotor diameter	5.208 ft
Fuselage Station of fan center line	256.000
BL of fan center line	61.000
Vane deflection limits	
Simple vector	-7.5 to +50.0 deg
Simple stagger	13.0 to 37.0 deg

6.3.5 Horizontal Tail Geometry

Dimensions based on a vertical projection onto a horizontal plane.

Gross area	52.864 sq ft
Aspect ratio	3.288
Taper ratio	.466
Span	13.183 ft
Chord length	
Root (BL 0.00)	65.640 in.
Tip (BL 79.10)	30.600 in.
MAC	50.245 in.
Airfoil section	NACA 64A012
Dihedral	0.000 deg
Sweep	
Leading edge	19.519 deg
Quarter chord line	13.697 deg
Trailing edge	-5.058 deg
Incidence limits at root chord relative to fuselage reference plane (WL 100.00)	+20.0 to -5.0 deg
Fuselage Station root chord leading edge (WL 206.00)	468.560
Fuselage Station of .25 MAC (WL 206.00)	493.439
BL of panel MAC	34.749
Fuselage Station of horizontal tail pivot point (WL 201.25)	496.700
Tail length coefficient - Distance between wing .25 MAC and horizontal tail .25 MAC parallel to fuselage reference plane (WL 100.00) divided by the wing MAC	2.250

Elevator

Area (aft of hinge line, per side)	5.985	sq ft
Aspect ratio	5.001	
Taper ratio	.638	
Span (per side, perpendicular to BL 0.00)	5.471	ft
Span-wise location	.054 to .884 b/2	
Chord length (aft of hinge line, parallel to BL 0.00)		
BL 4.26	16.033	in.
BL 69.91	10.224	in.
MAC	13.343	in.
Fuselage Station of elevator hinge line (WL 206.00)	517.790	
Fuselage Station of .25 MAC (WL 206.00)	521.126	
BL of panel MAC	34.664	
Deflection limits	±25.0	deg
Type of balance - Internally sealed pressure balance		

6.3.6 Vertical Tail Geometry

Dimensions based on a horizontal projection onto a vertical plane.

Gross area (excluding dorsal)	50.995	sq ft
Aspect ratio	1.178	
Taper ratio	.520	
Span	7.750	ft
Chord length (parallel to WL 100.00)		
Root (WL 113.00)	103.920	in.
Tip (WL 206.00)	54.000	in.
MAC	81.590	in.

Airfoil section		
WL 113.00	NACA 64A (012) - 016.5	
WL 206.00	NACA 64A (012) -013	
Sweep		
Leading edge	35.435	deg
Quarter chord line	30.000	deg
Trailing edge	9.918	deg
Fuselage Station of root chord leading edge (WL 113.00)	408.450	
Fuselage Station of .25 MAC	458.451	
WL of MAC	154.600	
Tail length coefficient - Distance between wing .25 MAC and vertical tail .25 MAC parallel to fuselage reference plane (WL 100.00) divided by the wing MAC	1.940	
Rudder		
Area (aft of hinge line)	6.395	sq ft
Aspect ratio	4.228	
Taper ratio	.674	
Span (parallel with hinge line)	5.200	ft
Chord (aft of hinge line, perpendicular with hinge line)		
Root (18% of local vertical tail chord)	17.634	in.
Tip (18% of local vertical tail chord)	11.882	in.
MAC	14.945	in.
Sweep of rudder hinge line	15.184	deg
Fuselage Station of root chord at hinge line	496.132	
WL of root chord at hinge line	122.072	

Fuselage Station of tip chord at hinge line	512.475	
WL of tip chord at hinge line	182.293	
Fuselage Station of .25 MAC	507.378	
WL of .25 MAC	149.248	
Deflection limits	±25.0	deg
Type of balance - Internally sealed pressure balance		

Rudder trim tab

Area (aft of hinge line)	.714	sq ft
Aspect ratio	6.057	
Taper ratio	.870	
Span (parallel to rudder hinge line)	2.080	ft
Chord (aft of hinge line, perpendicular to rudder hinge line)		
Root (25% of local rudder chord)	4.408	in.
Tip (25% of local rudder chord)	3.833	in.
MAC	4.128	in.
Sweep of rudder trim tab hinge line	11.451	deg
Fuselage Station of root chord at hinge line	508.896	
WL of root chord at hinge line	118.608	
Fuselage Station of tip chord at hinge line	513.768	
WL of tip chord at hinge line	143.147	
Fuselage Station of .25 MAC	512.271	
WL of .25 MAC	130.322	
Deflection limits	±10.0	deg
Type of balance - Radius nose, unsealed		

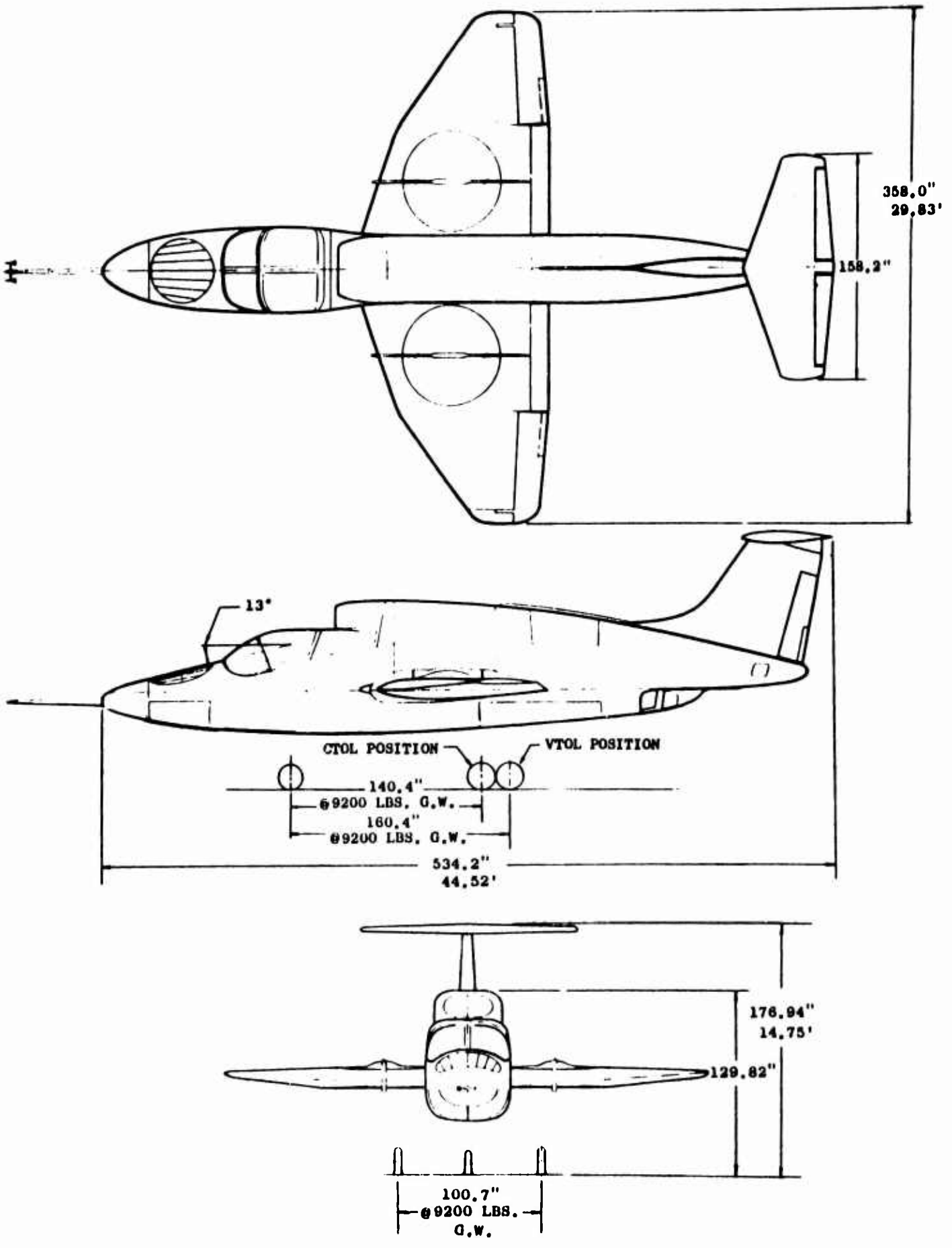

Three View - XV-5A

6.3.7 Wing Airfoil Ordinates

(Station and Ordinates Given in Percent of Local Chord)

BL = 25.000[1]

Station	Ordinate, Upper Surface	Ordinate, Lower Surface
0.961	1.132	-0.977
3.806	2.109	-1.712
8.426	3.113	-2.396
14.645	4.068	-2.962
22.222	4.971	-3.642
30.866	5.695	-3.851
40.246	6.203	-4.079
50.000	6.395	-4.197
59.754	6.136	-4.189
69.134	5.438	-3.844
77.778	4.446	-3.153
85.355	3.136	-2.183
91.574	1.837	-1.286
96.194	0.845	-0.588
99.039	0.206	-0.154

BL = 40.000[1]

Station	Ordinate, Upper Surface[2]	Ordinate, Lower Surface
0.961	1.285	-1.086
3.806	2.356	-2.047
8.426	3.350	-2.677
14.645	4.284	-3.236
22.222	5.171	-3.828
30.866	5.944	-4.246
40.246	6.418	-4.409
50.000	6.530	-4.498
59.754	6.204	-4.422
69.134	5.462	-3.993
77.778	4.437	-3.225
85.355	3.106	-2.218
91.574	1.820	-1.292
96.194	0.818	-0.584
99.039	0.198	-0.145

BL = 51.364[1]

Station	Ordinate, Upper Surface[2]	Ordinate, Lower Surface
0.961	1.313	-1.152
3.806	2.518	-2.289
8.426	3.600	-2.992
14.645	4.566	-3.624
22.222	5.455	-4.266
30.866	6.158	-4.563
40.246	6.561	-4.686
50.000	6.629	-4.737
59.754	6.245	-4.603
69.134	5.479	-4.105
77.778	4.421	-3.284
85.355	3.079	-2.250
91.574	1.800	-3.310
96.194	.805	-0.584
99.039	.192	-0.142

BL = 59.100[1]

Station	Ordinate, Upper Surface[2]	Ordinate, Lower Surface
0.961	1.323	-1.170
3.806	2.579	-2.386
8.426	3.780	-3.280
14.645	4.786	-3.995
22.222	5.626	-4.552
30.866	6.296	-4.786
40.246	6.667	-4.883
50.000	6.883	-4.907
59.754	6.279	-4.730
69.134	5.492	-4.189
77.778	4.420	-3.325
85.355	3.067	-2.276
91.574	1.795	-1.320
96.194	0.807	-0.589
99.039	0.196	-0.145

Notes: (1) Leading edge radius = 1.25 in. (2) Excluding door fairing.

(Station and Ordinates Given in Percent of Local Chord)

BL = 75.000[1]

Station	Ordinate, Upper Surface[2]	Ordinate, Lower Surface
0.961	1.238	-1.150
3.806	2.656	-2.588
8.426	4.199	-3.976
14.645	5.262	-4.796
22.222	6.006	-5.135
30.866	6.573	-5.262
40.246	6.860	-5.312
50.000	6.810	-5.278
59.754	6.336	-4.999
69.134	5.515	-4.365
77.778	4.390	-3.414
85.355	3.042	-2.331
91.574	1.776	-1.350
96.194	0.798	-0.609
99.039	0.203	-0.152

BL = 85.000[1]

Station	Ordinate, Upper Surface[2]	Ordinate, Lower Surface
0.961	1.352	-1.264
3.806	2.835	-2.787
8.426	4.379	-4.296
14.645	5.539	-5.264
22.222	6.228	-5.487
30.866	6.738	-5.556
40.246	6.996	-5.583
50.000	6.865	-5.504
59.754	6.350	-5.173
69.134	5.513	-4.479
77.778	4.361	-3.463
85.355	2.992	-2.355
91.574	1.762	-1.369
96.194	0.802	-0.628
99.039	0.200	-0.157

BL = 90.000[1]

Station	Ordinate, Upper Surface[2]	Ordinate, Lower Surface
0.961	1.374	-1.294
3.806	2.916	-2.850
8.426	4.467	-4.388
14.645	5.660	-5.487
22.222	6.329	-5.682
30.866	6.817	-5.735
40.246	7.034	-5.739
50.000	6.896	-5.638
59.754	6.364	-5.265
69.134	5.513	-4.538
77.778	4.343	-3.501
85.355	2.978	-2.375
91.574	1.746	-1.400
96.194	0.797	-0.638
99.039	0.196	-0.163

BL = 100.75[1]

Station	Ordinate, Upper Surface	Ordinate, Lower Surface
0.961	1.410	-1.363
3.806	3.052	-2.847
8.426	4.693	-4.267
14.645	6.029	-5.436
22.222	6.706	-6.108
30.866	7.105	-6.141
40.246	7.254	-6.101
50.000	7.050	-5.927
59.754	6.465	-5.436
69.134	5.575	-4.629
77.778	4.360	-3.543
85.355	2.977	-2.393
91.574	1.744	-1.400
96.194	0.793	-0.640
99.039	0.204	-0.166

Notes: (1) Leading edge radius = 1.25 in.
(2) Excluding door fairing.

64B104

(Station and Ordinates Given in Percent of Local Chord)

BL = 105.000(3)

Station	Ordinate, Upper Surface	Ordinate, Lower Surface
0.961	1.409	-1.409
3.806	3.065	-2.866
8.426	4.737	-4.208
14.645	6.031	-5.274
22.222	6.803	-6.150
30.866	7.150	-6.465
40.246	7.236	-6.436
50.000	6.969	-6.217
59.754	6.379	-5.646
69.134	5.503	-4.741
77.778	4.341	-3.551
85.355	2.970	-2.399
91.574	1.742	-1.413
96.194	0.828	-0.676
99.039	0.247	-0.209

BL = 110.000(3)

Station	Ordinate, Upper Surface	Ordinate, Lower Surface
0.961	1.451	-1.402
3.806	3.121	-2.824
8.426	4.780	-4.118
14.645	6.143	-5.205
22.222	6.914	-6.015
30.866	7.215	-6.489
40.246	7.235	-6.568
50.000	6.963	-6.301
59.754	6.385	-5.634
69.134	5.521	-4.671
77.778	4.365	-3.506
85.355	2.992	-2.370
91.574	1.768	-1.402
96.194	0.829	-0.661
99.039	.256	-0.217

BL = 112.154(3)

Station	Ordinate, Upper Surface	Ordinate, Lower Surface
0.961	1.471	-1.391
3.806	3.174	-2.797
8.426	4.821	-4.088
14.645	6.157	-5.163
22.222	6.921	-5.962
30.866	7.212	-6.439
40.246	7.222	-6.529
50.000	6.946	-6.253
59.754	6.378	-5.620
69.134	5.515	-4.651
77.778	4.354	-3.485
85.355	2.988	-2.360
91.574	1.768	-1.396
96.194	0.798	-0.637
99.039	0.251	-0.221

BL = 140.000(3)

Station	Ordinate, Upper Surface	Ordinate, Lower Surface
0.961	1.558	-1.387
3.806	3.202	-2.741
8.426	4.734	-3.885
14.645	5.983	-4.826
22.222	6.778	-5.490
30.866	7.166	-5.884
40.246	7.252	-5.957
50.000	7.015	-5.700
59.754	6.463	-5.115
69.134	5.602	-4.247
77.778	4.444	-3.208
85.355	3.103	-2.222
91.574	1.867	-1.341
96.194	0.894	-0.670
99.039	0.276	-0.223

Note: (3) Ordinates outboard of BL 100.75 are with respect to the dihedral plane.

(Station and Ordinates Given in Percent of Local Chord)

BL = 170.000(3)

Station	Ordinate, Upper Surface	Ordinate, Lower Surface
0.961	1.780	-1.385
3.806	3.324	-2.572
8.426	4.590	-3.403
14.645	5.646	-4.028
22.222	6.667	-4.423
30.866	7.043	-4.669
40.246	7.300	-4.708
50.000	7.142	-4.471
59.754	6.647	-3.996
69.134	5.769	-3.339
77.778	4.610	-2.568
85.355	3.324	-1.860
91.574	2.077	-1.159
96.194	1.049	-0.586
99.039	0.376	-0.218

Note: (3) Ordinates outboard of BL 100.75 are with respect to the dihedral plane.

6.3.8 Wing Flap Airfoil Ordinates

(Station and Ordinates Given in Percent of Local Wing Flap Chord)

Station	Ordinate, Upper Surface	Ordinate, Lower Surface
0.000	0.000	0.000
0.500	1.799	-1.422
0.750	2.384	-1.799
1.250	3.305	-2.217
2.500	5.146	-2.594
5.000	8.033	-2.594
7.500	10.292	-2.552
10.000	12.050	-2.510
15.000	14.686	-2.426
20.000	16.569	-2.343
25.000	17.991	-2.217
30.000	18.744	-2.133
35.000	18.912	-2.050
40.000	18.702	-1.924
45.000	17.949	-1.799
50.000	16.820	-1.673
55.000	15.481	-1.506
60.000	13.807	-1.338
65.000	12.092	-1.171
70.000	10.376	-1.004
75.000	8.661	-0.836
80.000	6.945	-0.666
85.000	5.230	-0.502
90.000	3.514	-0.334
95.000	1.757	-0.167
100.000	0.000	0.000

Notes: (1) Wing flap is a constant airfoil section from BL 24.00 to BL 101.75.
(2) Stations and ordinates are with respect to wing flap plane.
(3) Leading edge radious = 0.63 inches.

XV-5A WING GEOMETRIC TWIST

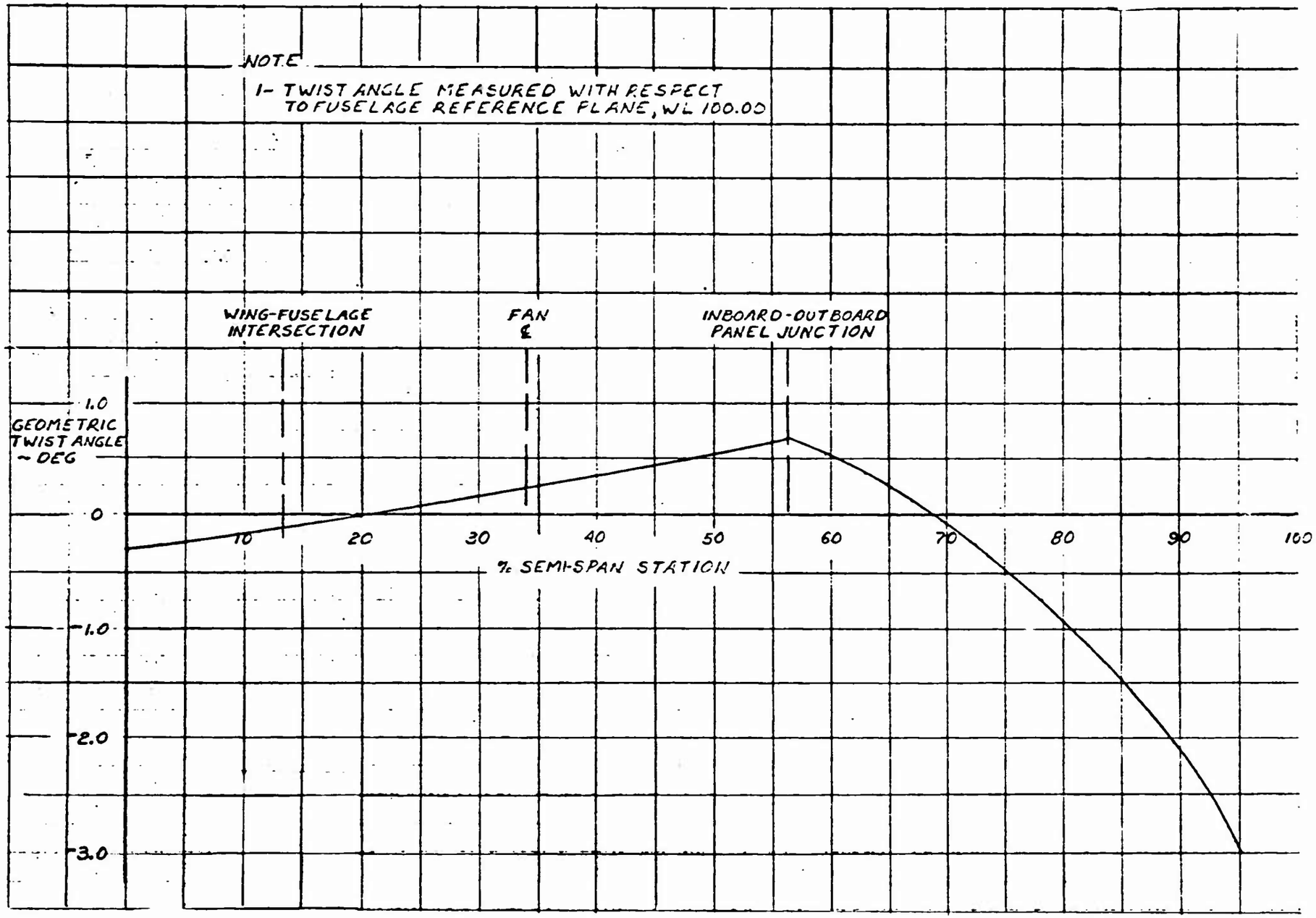

6.4 AIRCRAFT EQUATIONS OF MOTION - CONVENTIONAL FLIGHT MODE

The complete airframe and control surface equations of motion which were used in the analysis of the conventional flight mode dynamic stability are presented in this Appendix for reference purposes. It is particularly desired to present the control surface equations, as the equations representing the airframe with controls fixed are the same as those derived in Reference 4. The controls fixed equations are presented herein only for the sake of completeness. The equations are programmed for solution by digital computer.

The equations of motion are based on small perturbations about a trimmed flight condition. The initial trim condition assumes the aircraft to be in straight, wings level flight with zero sideslip. It is also assumed that the longitudinal and lateral-directional modes are uncoupled and therefore can be treated separately.

The complete equations programmed for the longitudinal mode are:

$$\dot{u} = X_u u + X_{\dot{w}} \dot{w} + X_w w + X_q \dot{\theta} + X_{\delta_e} \delta_e - g (\cos \gamma_0) \theta$$

$$\dot{w} = Z_u u + Z_{\dot{w}} \dot{w} + Z_w w + (U_0 + Z_q) \dot{\theta} + Z_{\delta_e} \delta_e - g (\sin \gamma_0) \theta$$

$$\ddot{\theta} = M_u u + M_{\dot{w}} \dot{w} + M_w w + M_q \dot{\theta} + M_{\delta_e} \delta_e$$

$$\ddot{\delta}_e + \ddot{\theta} = H_{e_u} u + \frac{1}{U_0} H_{e_{\dot{\alpha}}} \dot{w} + \frac{1}{U_0} H_{e_\alpha} w + H_{e_q} q + H_{e_{\dot{q}}} \dot{q} + H_{e_{\dot{\delta}_e}} \dot{\delta}_e + H_{e_{\delta_e}} \delta_e + H_{e_{\delta_c}} \delta_c$$

The first three equations represent the longitudinal motion of the aircraft with the elevator fixed. The dimensional stability derivatives in those equations are as defined in Reference 4, except that the u derivatives of X, Z and M used herein include the engine thrust terms.

The fourth equation represents the additional degree of freedom required for the elevator free case. The elevator dimensional derivatives are defined as:

$$H_{e_u} = K_e C_{h_{e_u}} \qquad H_{e_q} = K_e \frac{\bar{c}_e}{2U_0} C_{h_{e_q}} \qquad H_{e_{\delta_e}} = K_e C_{h_{e_{\delta_e}}}$$

$$H_{e_\alpha} = K_e C_{h_{e_\alpha}} \qquad H_{e_{\dot{q}}} = K_e \frac{\bar{c}_e}{2U_0} C_{h_{e_{\dot{q}}}} \qquad H_{e_{\delta_c}} = K_e C_{h_{e_{\delta_c}}}$$

$$H_{e_{\dot{\alpha}}} = K_e \frac{\bar{c}_e}{2U_0} C_{h_{e_{\dot{\alpha}}}} \qquad H_{e_{\dot{\delta}_e}} = K_e \frac{\bar{c}_e}{2U_0} C_{h_{e_{\dot{\delta}_e}}}$$

Where:

$$K_e = \frac{q_0 (S\bar{c})_e}{I_e}$$

U_0 = freestream velocity at the trimmed flight condition

q_0 = freestream dynamic pressure at the trimmed flight condition

$(S\bar{c})_e$ = elevator area (S) aft of the hinge line and the mean chord ($\bar{c}$) with respect to that area

I_e = elevator mass moment of inertia about the hinge line

The term $H_{e_{\delta_c}}$ represents the elevator stick force for determination of the elevator free transfer functions:

Where:

$$C_{h_{e_{\delta_c}}} = \frac{1}{G_e q_0 (Sc)_e}$$

δ_c = elevator stick force (cockpit control)

G_e = gearing between the elevator and cockpit control in rad./ft.

Solution of the equations of motion for the elevator free, yields a sixth order characteristic equation of motion in the La Place complex operator, "s" as illustrated below. The coefficients of the characteristic

equation are determined by the airframe and elevator aerodynamic derivatives:

$$A_6 s^6 + A_5 s^5 + A_4 s^4 + A_3 s^3 + A_2 s^2 + A_1 s + A_0 = 0$$

The characteristic equation for the elevator fixed case which is obtained by omitting the elevator equation of motion is a fourth order equation. In addition to the usual roots of the characteristic equation representing the "phugoid" and "short period" modes, the elevator free equation yields two additional roots which represent the elevator motion. These latter roots are generally a complex pair indicating an oscillatory motion.

The lateral-directional equations of motion solved by the computer program are:

$$\dot{\beta} = Y_\beta \beta + Y_p \dot{\phi} + Y_r \dot{\psi} + Y_{\delta_a} \delta_a + Y_{\delta_r} \delta_r - \dot{\psi} + \frac{g}{U_0} (\cos \gamma_0) \phi$$

$$+ \frac{g}{U_0} (\sin \gamma_0) \psi$$

$$\ddot{\phi} = L_\beta \beta + L_p \dot{\phi} + L_r \dot{\psi} + L_{\delta_a} \delta_a + L_{\delta_r} \delta_r + \frac{I_{xz}}{I_x} \ddot{\psi}$$

$$\ddot{\psi} = N_\beta \beta + N_p \dot{\phi} + N_r \dot{\psi} + N_{\delta_a} \delta_a + N_{\delta_r} \delta_r + \frac{I_{xz}}{I_z} \ddot{\phi}$$

$$\ddot{\delta}_r + \ddot{\psi} = H_{r_{\delta_r}} \delta_r + H_{r_{\dot{\delta}_r}} \dot{\delta}_r + H_{r_\beta} \beta + H_{r_{\dot{\beta}}} \dot{\beta} + H_{r_r} \dot{\psi} + H_{r_{\dot{r}}} \ddot{\psi} + H_{r_p} \dot{\phi}$$

$$+ H_{r_{\dot{p}}} \ddot{\phi} + H_{r_{\delta_c}} \delta_c$$

$$\ddot{\delta}_a = \left[H_{t_{\delta_t}} + KH_{t_{\delta_a}}\right]\delta_a + \left[H_{t_{\dot{\delta}_t}} + KH_{t_{\dot{\delta}_a}}\right]\dot{\delta}_a + K\left[H_{t_\beta}\beta + H_{t_{\dot{\beta}}}\dot{\beta}\right.$$

$$\left. + H_{t_r}\dot{\psi} + H_{t_{\dot{r}}}\ddot{\psi} + H_{t_p}\dot{\phi} + H_{t_{\dot{p}}}\ddot{\phi} + H_{t_{\delta_c}}\delta_c\right]$$

The first three equations represent the lateral-directional motion of the aircraft with controls fixed, and the fourth and fifth equations are the additional degrees of freedom required for a free rudder and free ailerons respectively. The aileron equation written above in terms of the aileron tab derivatives is specifically applicable to the XV-5A lateral control system. The XV-5A aileron is connected directly to a servo hydraulic actuator, while the cockpit control stick is linked directly to the aileron tab and the command valve of the aileron actuator. Therefore, under normal hydraulic powered operation, the aileron can only be disturbed from its equilibrium position by disturbing the aileron tab. The ratio of aileron deflection to tab deflection is a fixed constant under normal operation and it was assumed in this report that the aileron motion instantaneously follows the tab motion so that:

$$\ddot{\delta}_a = K\ddot{\delta}_t = \frac{d\delta_a}{d\delta_t}\ddot{\delta}_t$$

Therefore, the motion of the aileron can be expressed in terms of the disturbed tab.

The usual aircraft dimensional stability derivatives in the first three equations are defined in Reference 4 and the rudder and aileron tab derivatives are:

$$H_{r_{\delta_r}} = K_r C_{h_{r_{\delta_r}}} \qquad H_{r_{\dot{\beta}}} = K_r \frac{\bar{c}_r}{2U_0} C_{h_{r_{\dot{\beta}}}} \qquad H_{r_p} + K_r \frac{\bar{c}_r}{2U_0} C_{h_{r_p}}$$

$$H_{r_{\dot{\delta}_r}} = K_r \frac{\bar{c}_r}{2U_0} C_{h_{r_{\dot{\delta}_r}}} \qquad H_{r_r} = K_r \frac{\bar{c}_r}{2U_0} C_{h_{r_r}} \qquad H_{r_{\dot{p}}} = K_r \frac{\bar{c}_r}{2U_0} C_{h_{r_{\dot{p}}}}$$

$$H_{r_\beta} = K_r C_{h_{r_\beta}} \qquad H_{r_{\dot{r}}} = K_r \frac{\bar{c}_r}{2U_0} C_{h_{r_{\dot{r}}}} \qquad H_{r_{\delta_c}} = K_r C_{h_{r_{\delta_c}}}$$

$$H_{t_{\delta_t}} = K_t C_{h_{t_{\delta_t}}} \qquad H_{t_\beta} = K_t C_{h_{t_\beta}} \qquad H_{t_p} = K_t \frac{\bar{c}_t}{2U_0} C_{h_{t_p}}$$

$$H_{t_{\dot{\delta}_t}} = K_t \frac{\bar{c}_t}{2U_0} C_{h_{t_{\dot{\delta}_t}}} \qquad H_{t_{\dot{\beta}}} = K_t \frac{\bar{c}_t}{2U_0} C_{h_{t_{\dot{\beta}}}} \qquad H_{t_{\dot{p}}} = K_t \frac{\bar{c}_t}{2U_0} C_{h_{t_{\dot{p}}}}$$

$$H_{t_{\delta_a}} = K_t C_{h_{t_{\delta_a}}} \qquad H_{t_r} = K_t \frac{\bar{c}_t}{2U_0} C_{h_{t_r}} \qquad H_{t_{\delta_c}} = K_t C_{h_{t_{\delta_c}}}$$

$$H_{t_{\dot{\delta}_a}} = K_t \frac{\bar{c}_t}{2U_0} C_{h_{t_{\dot{\delta}_a}}} \qquad H_{t_{\dot{r}}} = K_t \frac{\bar{c}_t}{2U_0} C_{h_{t_{\dot{r}}}}$$

U_0 = free stream velocity at the trimmed flight condition

q_0 = free stream dynamic pressure at the trimmed flight condition

$$K_r = \frac{q_0 (S\bar{c})_r}{I_r}$$

$$K_t = \frac{q_0 (S\bar{c})_t}{I_t}$$

$(S\bar{c})_r$ = rudder area (S) aft of the hinge line and the mean rudder chord ($\bar{c}$) with respect to that area

$(S\bar{c})_t$ = area of one aileron tab (S) aft of the tab hinge line and the mean tab chord with respect to that area

I_r = rudder mass moment of inertia about the hinge line

I_t = mass moment of inertia of one aileron tab about the tab hinge line

The terms $H_{r_{\delta_c}}$ and $H_{t_{\delta_c}}$ are analogous to the $H_{e_{\delta_c}}$ explained previously for the elevator:

$$C_{h_{r_{\delta_c}}} = \frac{1}{G_r q_0 (S\bar{c})_r}$$

$$C_{h_{t_{\delta_c}}} = \frac{1}{G_t q_0 (S\bar{c})_t}$$

G_r = rudder to pedal gearing ~ rad./ft.

G_t = control stick to aileron tab gearing ~ rad./ft.

δ_c = cockpit control force ~ lb.

Solution of the four equations of motion for the rudder or aileron free cases yields a sixth order characteristic equation in the La Place operator "s" of the following form:

$$s\,(A_6 s^6 + A_5 s^5 + A_4 s^4 + A_3 s^3 + A_2 s^2 + A_1 s + A_0) = 0$$

The controls fixed solution, obtained by omitting the rudder and aileron equation, yields a fourth order characteristic equation. In addition to the usual roots of the lateral-directional characteristic equation representing the "dutch roll," spiral and rolling modes, the rudder or the aileron free equation yields two additional roots, generally a complex pair, which represent the rudder or aileron motion.